UNIVERSITY OF ZULULAND

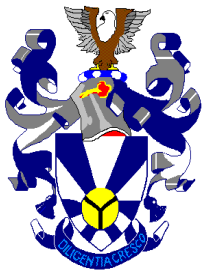

SYNTHESIS AND CHARACTERIZATION OF CADMIUM SELENIDE AND ZINC SELENIDE NANOPARTICLES

DISSERTATION SUBMITTED IN PARTIAL FULFILLMENT OF CHEMISTRY MASTERS DEGREE IN THE FACULTY OF SCIENCE AND AGRICULTURE

By

NKOSINATHI NORMAN DLAMINI

20022314

SUPERVISOR: PROF. N. REVAPRASADU

2012

DECLARATION

I declare, that the work presented in this masters project is, to the best of my knowledge my own work, and it has not been submitted for any degree or examination in any other university and that all the sources I have used or quoted have been acknowledged by complete reference.

Signature of the Student:……

Signature of the Supervisor:……...

ACKNOWLEDGEMENT

I would like to offer my sincerest gratitude to my supervisor, Prof. Neerish Revaprasadu, for his guidance and support throughout my studies with his patience and knowledge whilst allowing me the room to work in my own way.

My appreciation goes to Dr. VSR Rajasekhar Pullabhotla for the guidance he provided to me throughout my work. I continued my studies up to masters level to his encouragement and effort and without him, I would not have thought of continuing with my studies up to this level. He has analysed all my samples using the TEM and HRTEM techniques.

I would like to convey my profound gratitude to my friend, Zamokuhle Zamangwane Ngema for encouraging and convincing me to register my honours. The support she provided throughought my honours degree is appreciated to a great extent. I completed the level of my honours degree through her encouragement and support and without her this thesis, too, would not have been started, completed or written. I also want to thank a number of staff members, colleagues and friends of the University of Zululand, Chemistry Department for all kind of service rendered. A big thank you goes to my classmates, Khethiwe and Nokuthula, the support they provided with physical chemistry lecture notes, without them, I wouldn't make it in physical chemistry exam. Nhlakanipho Mntungwa's prayers and encouragements helped me to press on. I could not rest without recognizing Manelisi Mgabhi, who provided me with accommodation. All my friends and colleagues at house 215 are recognized for their support. My studies would not be

possible without the financial support from the National Research Foundation, a big thank you goes to the NRF for the support.

My immense gratitude goes to Mbatha family, Phiwe and Dumsile for the endless support they provided throughought my studies. Lastly, but not at all the least, I honour the presence of my mother. I greatly appreciate her support and patience through my entire studies.

ABSTRACT

An environmentally friendly synthetic route has been used to synthesize cadmium selenide and zinc selenide nanoparticles. Both aqueous and organically soluble selenide based nanoparticles have been synthesized via mild conditions. The synthesis involved the reduction of selenium powder to produce selenium ions. The complete reduction of selenium is followed by the addition of a metal source MX (M = Cd or Zn and X = Cl or CO). Biocompatible passivating agents such as cysteine or triethanolamine (TEA) induced the solubility of the nanoparticles in water, while the solubility of the nanoparticles in the organic solvents was facilitated by hexadecylamine (HDA).

The evidence for the formation of the nanoparticles with a desired quality was confirmed by using different techniques such as UV-Vis absorption spectroscopy, photoluminescence spectroscopy (PL), X-ray diffraction (XRD), transmission electron microscopy (TEM) and infrared spectroscopy (FT-IR).

Chapter one comprises of the review of nanoparticles outlining their properties, synthesis and applications in biological fields. Chapter two describes the synthesis of water soluble cadmium selenide and zinc selenide nanoparticles at room temperature and at reflux conditions (90 ^{o}C) using biocompatible passivating ligands (cysteine and TEA). The influence of the variation of reaction parameters such as pH, reaction time, concentration, reactant ratio, passivating ligand and temperature on dispersibility, particle size, optical properties and morphology of the nanoparticles were studied. The pH of the solution affected the optical properties of the as-synthesized nanoparticles by shifting the optical

band gaps to higher energies upon increasing the pH of the reaction, which also revealed the decrease in particle size. Water soluble CdSe nanoparticles were obtained using different cadmium sources in which $CdCO_3$ resulted in aggregated nanoparticles, while $CdCl_2$ source yielded clearly defined nanoparticles that were reasonably monodispersed.

Chapter three describes the synthesis of organic soluble ZnSe nanoparticles, using HDA as a capping agent. The reaction parameters such as temperature, reaction time and metal source played a role in altering the optical properties and final morphology of the particles. The reaction carried at 230 ^{o}C with $ZnCl_2$ source resulted in good quality nanoparticles with clearly defined absorption peaks. The increase in reaction time shifted the optical band gaps to lower energies, and hence the increase in the particle size. These findings show that in order to obtain good quality HDA capped ZnSe nanoparticles, the reaction parameters such as temperature, reaction time and metal source need to be strictly controlled.

Keywords: Quantum dots, triethanolamine, cysteine, HDA, $NaBH_4$, selenium, cadmium selenide, zinc selenide and particle size.

List of publications

1. **N.N. Dlamini**, V.S.R. Rajasekhar Pullabhotla and N. Revaprasadu, "*Synthesis of Triethanolamine (TEA) Capped CdSe Nanoparticles.*" Materials Letters 65 **(2011)** 1283-1286.

2. **N.N. Dlamini**, V.S.R. Rajasekhar Pullabhotla and N. Revaprasadu, *"A Simple Route to the Triethanolamine (TEA) and Cysteine Capped ZnSe Nanoparticles."* Journal of Nanoscience and Nanotechnology (**Inpress) 2012**.

TABLE OF CONTENTS

CHAPTER 2

Synthesis of water soluble CdSe and ZnSe nanoparticles

LIST OF FIGURES

LIST OF ABBREVIATIONS

CBD	chemical bath deposition
PL	photoluminescence
UV-VIS	ultra violet and visible
TEM	transmission electron microscopy
HR-TEM	high resolution transmission electron microscopy
XRD	x-ray diffraction
FT-IR	fourier transforms infrared
QDs	quantum dots
QYs	quantum yields
FWHM	full width at half maximum
HOMO	highest occupied molecular orbital
LUMO	lowest unoccupied molecular orbital

Chapter 1

Introduction

1.0 General background

Nanotechnology encompasses the production and application of physical, chemical and biological systems at scales ranging from individual atoms or molecules to submicron dimensions. Nanotechnology is likely to have a profound impact on our economy and society in the early 21st century, comparable to that of semiconductor technology, information technology, and molecular biology. Research in nanotechnology promises breakthroughs in areas such as materials and manufacturing, nanoelectronics [1], medicine and healthcare, energy [2], biotechnology, information technology and national security [3].

Nanometer scale systems are mainly a self assembly of their elemental constituents. Examples include chemical systems, the spontaneous self-assembly of molecular clusters from simple reagents in solution, and biological molecules (e.g. DNA) used as building blocks for the production of three-dimensional nanostructures, or quantum dots. The definition of a nanoparticle is an aggregate of atoms bonded together with a diameter between 1 to 100 nm, typically consisting of 10 to 10^{15} atoms. The discovery of novel materials, processes and phenomena at the nanoscale and the development of new experimental and theoretical techniques for research provide opportunities for the development of innovative nanosystems and nanostructured materials. The properties of materials at the nanoscale are different from the bulk [4-7].

1.1 Electronic properties of semiconducting nanoparticles

Solid materials can be categorized into metals, insulators or semiconductors depending on their capacity to conduct electrical charge and on the separation between the valence and the conduction band. Metals are known to be good conductors of electricity and heat, due to the overlap between the conduction and valence band, hence electrons have got high mobility between the two bands at any temperature.

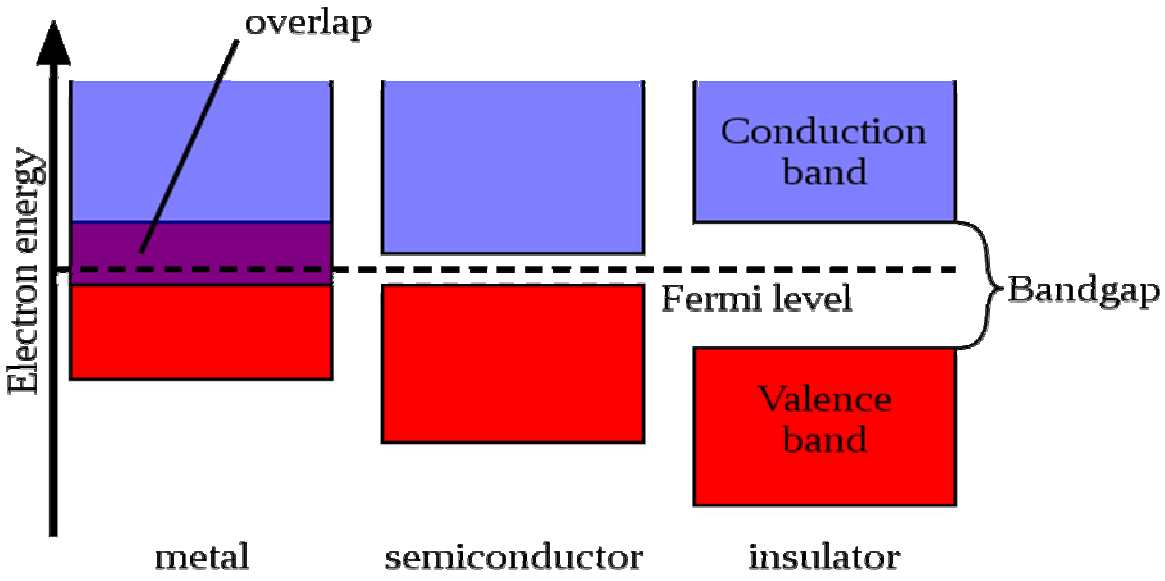

Figure 1.1 The spacial electronic state diagram of solid materials showing electrical conductivity effect (a) metal (b) semiconductor and (c) insulator.

In a semiconducting material, there is a small energy gap between the valence and the conduction band (Figure 1.1). According to the Fermi Direc distribution theorem, all the electrons are found in the valence band at 0 K, but at temperatures above 0 K, electrons can be thermally excited to the conduction band, and therefore, semiconductors can act as conducting materials at elevated temperatures. However, in the case of an insulator all the electrons are

found in the valence band at any temperature due to the wide separation between the valence and the conduction band and therefore, an insulating material cannot conduct electricity at any temperature.

The changes that occur in electronic properties of materials as the length scale is reduced are directly related to the influence of the wave-like property of electrons (quantum effects) and the scarcity of scattering centers. As the size of the system becomes comparable with the de-Broglie wavelength of the electrons, the discrete nature of the energy states becomes apparent once again, although a fully discrete energy spectrum is only observed in systems that are confined in all three dimensions with zero degrees of freedom [8,9]. In certain cases, conducting materials become insulators below a critical length scale, as the energy bands cease to overlap. Owing to their intrinsic wave like nature, electrons can tunnel quantum mechanically between closely adjacent nanostructures, and if a voltage is applied between two nanostructures which aligns the discrete energy level, resonance occurs, which suddenly increases the tunneling current [10]. This phenomenon, known as quantum size effect, causes the continuous band of the solid to split into discrete quantized energy levels and the band gap to increase (Figure 1.2).

Quantum confinement has a profound effect on the optical properties of nanoparticles. The relationship between the electronic and optical properties exists via the following conversion:

$$E = h\nu = hc/\lambda \qquad (1.1)$$

E = band gap energy difference, h = Planck's constant, c = the velocity of light, ν = the frequency of the incident light, and λ = the wavelength of incident light [11].

As the diameter of the particles decreases due to quantum confinement effects, the energy difference of the band gap becomes larger as shown by the inverse proportion between the energy and the wavelength of incidence light. The electronic state diagram of bulk semiconductors and nanoparticles is shown in Figure 1.2. Bulk materials absorb light at longer wavelengths, and as the band gap increases as seen in Figure 1.2 (b), the nanoparticles tend to absorb light at a shorter wavelength (e.g. the ultraviolet and visible light), hence absorbance is affected by the particle size.

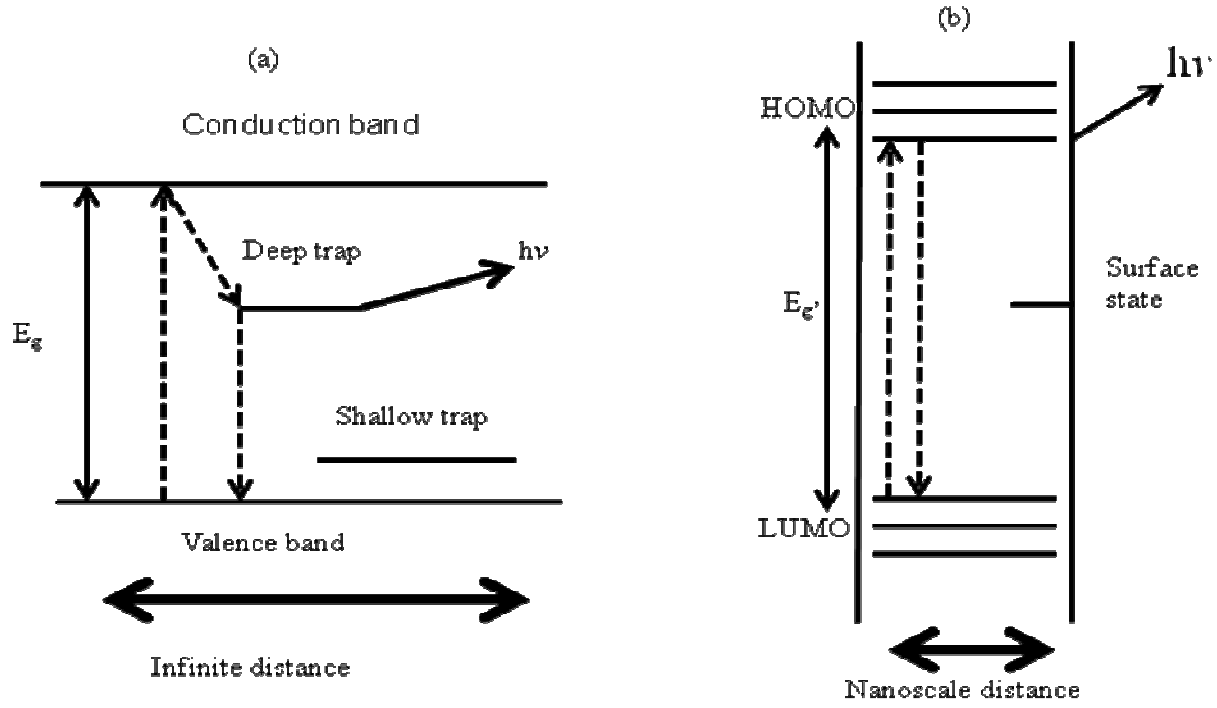

Figure 1.2 The spacial electronic state diagram showing the quantum confinement effect of (a) bulk semiconductors and (b) nanoparticles [12].

The absorption of photons leads to the excitation of an electron from the valence band to the conduction band leaving a hole behind. The electron and hole are taken as charged particles with own effective mass. An electron gives up its energy either in the form of phonons/heat via non-radiative transition or by emitting light in the form of photons via radiative transition as it returns to its lowest state, the valence band. The electron-hole recombination occurs via deep traps and shallow traps in a bulk semiconductor. In a semiconductor nanoparticle, there is a direct recombination of charge carriers.

There have been a lot of attempts aiming at calculating the electronic energy levels in quantum dots. Brus [13] developed the model to calculate the first excitonic state of a semiconductor cluster with radius R using the approximation expression:

$$E_g(R) = E_g(R=\infty) + \frac{h^2\pi^2}{2R^2}\left[\frac{1}{m_e^*} + \frac{1}{m_h^*}\right] - \frac{1.8e^2}{\varepsilon R} \quad \text{..... (1.2)}$$

In this equation $E_g(R)$ is the exciton energy, the first term corresponds to the band gap of the bulk semiconductor, the second term corresponds to the sum of the confinement energies for the electron and the hole and the last term is their Coulombic interaction energy. The effective mass of electron and hole is represented by m_e^* and m_h^* respectively, e represents elementary charge and R is the radius of the spherical nanocrystal. The Coulomb term varies $E_g(R)$ as R, whereas the quantum localization terms vary $E_g(R)$ as R^2. Owing to these relationships, the apparent band gap will always increase for infinitesimally small values of R. The increase in the band gap is observed by the blue shift in the absorption spectra as seen in many semiconducting

nanoparticles. The luminescence spectra of surface passivated nanoparticles have narrow line widths, and exhibit a small Stoke's shift or near band edge emission due to the direct recombination of charge carriers. On the other hand, nanoparticles that show broad emission with a large Stoke's shift are well known to display emission from deep and shallow traps [14].

1.2 Luminescence

Luminescence occurs as a result of stimulation of a material which has previously been exposed to ionization radiation. When stimulation is caused by heating, the luminescence is called thermoluminescence. Optically stimulated luminescence is when the stimulation is by light. The underlying principle of luminescence is that defects in a crystal lattice act as charge traps and recombination centers. Ionization radiation energy can move charge to these traps which are metastable. Subsequent stimulation then de-traps the charges and luminescence is emitted when the charges make a transition to a lower energy state.

The most widely used luminescence in nanotechnology is photoluminescence (PL). This process involves the absorption of photons by a material followed by the emission of photons. Using the principle of quantum mechanics, this can be described as an excitation to a higher energy state and then a return to a lower energy state accompanied by the emission of certain energy in the form of a photon. This can be described using the simple general reaction:

$$A^* \rightarrow A + h\nu \quad \text{..... (1.3)}$$

in which A^* denotes the excited state of a material A, and h and v represents the Planck's constant and the frequency of the photon, respectively. This is one of many forms of luminescence (light emission). The period between absorption and emission is typically infinitesimally short, in the order of nanoseconds, however, this period can be extended into minutes and hours [15-19].

The emission properties of semiconducting nanocrystals depend on the emission colour, colour purity, brightness, quantum yields and stability of the emission [20]. Photoluminescence of nanoparticles depend on the behavior of a semiconductor nanocrystal in which two types of emission bands can be detected, namely the band gap emission and the deep trap emission [21]. The deep trap emission is broad and considerably red shifted from the absorption onset, and this is due to the recombination of charge carriers. In the case of the band gap emission, a slight red-shift is observed with narrow line widths [22,23].

Due to extremely large surface-to-volume atom ratio, or specific surface area in nanoparticles, surface atoms play a prominent role in the emission properties of the nanoparticles, whereas in the case of a bulk material, the bulk atoms are responsible for the emission properties. A typical example is CdSe nanoparticles in which the increase of surface atoms from 20 to 100 % leads to the decrease in particle size from 10 to 1 nm. The surface atoms usually have unsaturated bonds, extra energy and they are more reactive relative to those in the bulk, and hence the nanoparticles are easily transformable from one phase to another with relatively low transformation temperature. In addition, surface atoms in a semiconductor usually allow extra electronic states in the band gap. The decrease in the size of the crystal due to the increase of the percentage of

the surface atoms leads to the formation of more electronic states in the band gap which act as electron and hole trapping centres. The excitation of an electron from the valence band to the conduction band results in the electron-hole pair recombination. When the electron and hole recombination occurs, a photon of light is emitted with an energy equivalent to E_g. There is a high possibility of finding either the exited electron or the hole being trapped by the trap states within the material caused by surface defects, and thus become less available for the radiative recombination. This leads to the quenching of PL which is not desirable for certain applications [24].

The possibility of charge carriers residing in traps is decreased by surface passivation in the bulk semiconductors. Surface modification results in the increase in quantum yields (QYs). Organic shells are extremely efficient in coating the surface of the nanocrystals in the way that they provide electronic passivation. They also prevent agglomeration, control the growth rate of the nanocrystals, its size, shape and solubility [25]. Inorganic materials of a wide band gap also provide good passivation of the surface of the nanocrystals. If the surface of the nanocrystal is coated with wide band gap materials, there is further confinement of the electron-hole pair and surface states are eliminated. The typical example is CdSe nanocrystals which can be passivated with CdS, ZnS or ZnSe to create a core-shell material. If the boundary between the two inorganic materials is perfect, a near unity quantum yield (QY) material may result.

1.3 General methods for the synthesis of semiconducting nanoparticles

There are many routes to synthesize semiconducting nanoparticles. In this dissertation the colloidal and hot injection methods will be briefly reviewed. Recent adaptations of these two

principal routes leading to the so-called 'greener route' to nanostructured materials will also be discussed. An ideal synthetic route should produce nanoparticles that are pure, crystalline, reasonably mono-dispersed and have a surface which is independently derivatized.

1.3.1 Colloidal methods

Colloidal methods rely on the precipitation of nanometer sized particles within a continuous fluid solvent matrix to form a colloidal sol. Generally a finely dispersed system in a high energy state has work to break up the solid, which is equivalent to the free energy required to increase the surface area. The colloidal material will therefore tend to aggregate due to attractive van der Waals forces and lower its energy unless a substantial energy barrier to this process exists. The presence and magnitude of an energy barrier to agglomeration depends on the balance of attractive and repulsive forces between the particles [26].

The synthesis of highly monodispersed nanoparticles was first engineered in the past decades where it was suggested that if the seeds (nuclei) could be made to grow in concert into larger particles, the formation of the monodispersed sols could be favored [27]. The reported routes to the formation of colloidal nanoparticles involved the precipitation of dilute colloidal solution and the retardation of growth soon after nucleation. In early years of this work, the particles were typically monomeric. Later on, nucleation and growth were properly monitored and the particles with dimensions of the order of the nanometers could be reproducibly synthesized as small crystals which are less stable, dissolved, and then recrystallize on larger and more stable crystals. This process is known as Ostwald ripening. Solvent, pH and the passivating agent are chosen such that nanoparticles possess low solubility. The highly monodispersed samples are obtained if

nucleation and growth process are distinctly separated (fast nucleation and slow growth). The colloidal growth stability of those crystals has been improved by using solvents with low dielectric constant or by using stabilizers such as styrene/maleic acid co-polymer [27-31].

The earlier work on colloidal synthesis of nanoparticles of CdS and ZnS was reported by Brus [32], Weller [33] and Henglein [34]. Nanocrystalline CdS was synthesized by mixing the aqueous solutions of $CdSO_4$ and $(NH_4)_2S$ [32]. Altering the nucleation kinetics through the variation of pH resulted in the control of the size of CdS nanoparticles. Nanocrystalline ZnS and CdS were synthesized in methanolic media without surfactants and the agglomeration and/or sedimentation was prevented by the repulsion of the electrostatic double layer [35]. The spectral characterization revealed the blue-shift compared to the bulk material, and structural characterization showed zinc blend structure.

The photophysical properties of the CdS nanoparticles were studied by Henglein, Weller and co-workers in which they performed the analysis of size distribution [33,34]. Based on their analysis, size distribution showed that a certain size with the greatest oscillator strength was favoured, this was in a direct relation with absorption spectrum. This was due to the existence of magic agglomeration numbers in the size distribution of the sample [36]. Magic agglomeration numbers, integral multiples of N of a large number m_o come out of the stability of a certain size or they are due to the kinetics of particle growth.

Selenosulphate and selenourea have recently been identified as sources of selenium for the synthesis of selenide based nanoparticles through reactive solution growth. Typical example for

this preparation is the reaction of Cd^{2+} with selenosulphate via the chemical bath deposition (CBD) of CdSe films [37]. The precipitation of $Cd(OH)_2$ is usually hindered by complexing Cd^{2+} in the CBD processes, and thus controlling the rate of the overall reaction. The quantum dots of CdSe have been produced by the chemical reaction of complexed cadmium salt with sodium selenosulphate ($Na_2Se_2SO_3$) in aqueous alkaline media [38,39]. If Cd^{2+} is not complexed, the formation of a precipitate is usually favored and little formation of film occurs.

Zhong *et al.* reported the synthesis of CdS, ZnS and $Zn_xCd_{1-x}S$ nanocrystals in one-pot method. In this report, less-toxic salts of stearate, acetate, chloride and sulphate were used with elemental sulphur as the sulphide source [40]. The as-synthesized nanoparticles exhibited band edge emission, and the zinc blend phase was obtained at high temperature.

1.3.2 Hot injection routes

The injection of multiple or single molecular precursors into hot high boiling point solvents is a very popular route to synthesize semiconductor nanomaterials. The first reported synthetic method via this route was by Murray *et al.* [41] in which they used a volatile metal alkyl and a chalcogenide source TOPX (tri-*n*-octylphosphine chalcogenide) under anaerobic conditions. They dispersed the metal alkyl precursors in TOP (tri-*n*-octylphosphine) and injected the mixture into hot TOPO (tri-*n*-octylphosphine oxide), a polar coordinating Lewis base solvent at high temperatures (120-300 ºC). After injection there is immediate nucleation followed by the slow growth or annealing which is believed to be directly related to Ostwald ripening process. They used a flocculating solvent to separate the solid particles by centrifugation and dispersed the resulting solid particles in a solvent (e.g. toluene) resulting in the formation of a solution of

optically clear TOPO capped nanoparticles. The coordinating solvent is an important stabilizing agent for the nanocrystalline colloidal dispersions and it plays a major role in passivating the surface of a semiconductor.

The above mentioned route has been used to synthesize and study the optical properties of CdSe nanoparticles. However, the major drawback to the route has been the use of the reagents that are volatile, extremely toxic, explosive, pyrophoric, unstable at high temperatures and relatively expensive [42]. The avoidance of using pyrophoric metal alkyls led to the development of the single source molecular precursor route. O'Brien *et al.* [43-47] made use of the diselenocarbamate of the type M(SeCNRR'), (M = Cd or Zn) as single source precursors for the synthesis of metal chalcogenide nanoparticles. In their work, they discovered that the nanoparticles synthesized using these precursors are stable in air, monodispersed and of good quality [43-47].

There has been many follow up studies on the use of metal complexes to synthesize nanoparticles. The Revaprasadu group synthesized many sulfur containing complexes such as xanthates [48], thiosemicarbazide and thioureas [49-52] to synthesize CdS, PbS and ZnS nanoparticles. Bruce *et al.* [53] used cadmium complexes of N,N-diethyl-N'-benzoylthiourea and N,N-diethyl-N'-benzoylselenourea as single-source precursors for the synthesis of HDA capped CdS and CdSe. Recent work in Revaprasadu's group has shown that heterocyclic dithiocabarmate complexes are very efficient precursors for larger faceted particles of CdS [54]. They obtained particles with a spherical mophology at high precursor concentrations, however,

the shapes of the particles varied from rods, bi-pods and tri-pods as the concentration of the precursor was decreased.

1.3.3 Greener routes

Even though organometallic routes give high quantum yields, it offers some disadvantages such as the use of volatile and highly toxic precursors and high reaction temperatures. In the materials chemistry context, sustainability is a concept that coincides with many of the principles of green chemistry. For materials synthesis, these principles include the use of less toxic precursors, the use of water as a solvent where possible, using the least quantity of reagents, fewer synthetic steps, reducing the amounts of by-products and waste, and using the reaction temperature close to room temperature [55]. Due to above mentioned disadvantages and limitations of the hot precursor injection methods, there has been an increase in the demand for the development of greener routes for synthesizing nanoparticles.

Peng *et al.* [19] have developed a 'greener' synthetic route to CdSe. In their work, the volatile dimethyl cadmium precursor (used in the Murray route) [41] was replaced by non-volatile CdO as a source of cadmium. They also suggested that the use of cadmium acetate, amines and fatty acids as precursors, solvents and capping agents, respectively, could also result in high quality CdSe nanocrystals. Natural solvents such as olive oil have also been used to functionalize CdSe and PbS nanoparticles. This approach eliminates the use of air sensitive, toxic and expensive chemicals such as TOP, TBP and amines thereby making it a cheaper method to synthesize nanoparticles on large scale [55-57]. Taking the advantages of both the organometallic related and inorganic compound related schemes, Yang *et al.* [58] have proposed a new strategy for the

synthesis of high quality related CdSe QDs in paraffin and oleic acid media. They used simple reagents, such as cadmium oxide, selenium powder and sodium sulphide as precursors for Cd, Se and S, respectively. Han *et al.* [59] synthesized small sized (1-3 nm) CdSe quantum dots from $CdCl_2$ solution and Na_2SeSO_3 solution reacted together with mercaptoacetic acid (MAA) as a stabilizing agent.

Oluwafemi *et al.* [60] proposed the greener route to the synthesis of organically capped cadmium selenide nanoparticles. In this synthetic route, simple reagents such as selenium powder and cadmium chloride as sources of selenium and cadmium were used in an aqueous solution. The resulted bulk cadmium selenide was then dispersed in TOP and the mixture was injected into a hot coordinating solvent, TOPO or HDA. The particles showed strong quantum confinement in their spectral region [60]. Oluwafemi *et al.* [61] further synthesized HDA capped CdSe nanoparticle via the same route. In this recent work, the growth kinetics of the nanoparticles under different conditions was studied deeply. The particles showed blue shift as the reaction time was increased indicating strong quantum confinement [61]. Gao *et al.* [62] recently reported the synthesis of cadmium selenide nanoparticles via a mild solution phase synthetic route. They used mild reagents such as selenium powder and anhydrous sodium selenosulphite and $Cd(CH_3COO)_2.2H_2O$ as sources of selenium and cadmium, respectively. The particles obtained via this route showed confinement effect within spectral region. Maseko *et al.* [63] recently reported the influence of cadmium source on the shape of CdSe nanoparticles. They reported highly dispersed nanoparticles which showed quantum confinement in optical spectra with clearly defined absorption edges and exceptionally narrow emission peaks. They studied the effect of changing the source of cadmium and a capping agent on the shape of the nanoparticles.

They concluded that the particles synthesized with $CdCl_2$ and $CdSO_4$ resulted in spherical particles while those synthesized with cadmium carbonate ($CdCO_3$) resulted in tri-pods and bi-pods.

Due to the need of greener methodologies, Revaprasadu and co-workers developed a new, relatively safe and inexpensive route to water soluble CdSe and ZnSe nanoparticles. Simple and mild reagents such as cadmium chloride and selenium powder were used as sources. The particles synthesized were stable in air and soluble in water, they also showed strong confinement in their optical properties when compared to their bulk counterparts [64]. The same method was used to synthesize starch capped CdSe and ascorbic acid capped ZnSe nanoparticles. Cysteine capped Au-CdSe hybrid nanoparticles were also synthesized using this route [65]. Shang *et al.* [66] synthesized triethylamine capped cadmium selenide nanoparticles of highest degree of sensitivity that were able to detect ion pair in aqueous solution. They used environmentally friendly reagents such as cadmium oxide and selenium powder. The particles produced were of highest stability and they showed strong quantum confinement. Kristl *et al.* [67] recently reported the synthesis of cadmium sulphide and cadmium selenide nanoparticles via the sonochemical method. Amongst the advantages offered by this method is that it is relatively simple as compared to other methods because it avoids the use of inert atmosphere, it uses non hazardous precursors and environmentally friendly solvents. The particles obtained via this route were of a cubic phase and it is believed to be the first report for the synthesis of cadmium sulphide and cadmium selenide without an inert atmosphere.

1.4 Surface passivation

The agglomeration of the nanoparticles is due to the existence of the Van der Waals inter-particle attraction which can be compensated by surrounding the nanocrystals with bulky organic shells, which keep the nanocrystals apart from each other. The organic shells can either possess hydrophilic or lipophylic property thereby efficiently stabilizing the colloids in aqueous or non-polar solvents. A wide variety of materials can be used as components of organic shells with the ionic surfactants, coordinating polymers and capping agents being the most commonly used. All these molecules possess polar groups that can be attached to the nanoparticle surface, and a bulk component within the molecule that provides spatial isolation of the nanocrystal from the environment. The capping ligands and surfactants differ in a way they bind to metal atoms at the nanocrystal surface, with capping ligands having the greater binding strength. Usually, a monolayer of molecules of a capping ligand around the nonocrystal is adequate enough to achieve stability against agglomeration, with the possibility of isolating and re-dissolving the nanoparticles. Owing to differences in electronic and binding properties, capping ligands can have a great influence in the optoelectronic and magnetic properties of functional nanocrystalline inorganic materials. Passivating agents also prevent the oxidative diffusion via the surface defects which can lead to corrosion of a material, and they play an important role in controlling the growth and shape of the nanoparticles [68,69].

The properties of advanced functional materials depend mainly in their final morphology. The shapes of the nanocrystals can be classified as zero-dimensional (0D), 1D, 2D and 3D which can be achieved by using different reaction conditions. In order to achieve a desired end use of functional nanomaterials, shape control need to be taken into consideration. The control of

particle shape is a complex process. It requires a fundamental understanding of the interactions between solid state chemistry, interfacial reactions and kinetics, and solution or vapour chemistry. There are two distinct approaches that could be followed in mastering the shape control of the nanocrystals. These include growth directed synthesis typical of precipitation processes and template directed synthesis in which the growth is directed by epitaxy via a pre-existing structure upon which nucleation and growth take place [70]. By using organic ligands or surfactants that bind differently to the crystallographic faces, the shape of nanoparticles can be controlled. At high temperatures, surfactant molecules are dynamically adsorbed to the surface of the growing crystal. The interaction between the organic ligands and particles is dynamic in an 'on' and 'off' or intermittent manner allowing for controlled growth [71]. Good examples of ligands that behave in this manner are long chain amines such as HDA. HDA, a primary amine offers less steric hindrance, high electron donating ability and high capping density as a result of its small stereochemical interference [72]. HDA has been reported to adsorb selectively (with its amine) on the surface of CdS favoring the formation of anisotropic morphology [73].

Several shapes of CdSe nanocrystals have been reported, ranging from rods, teardrops, tetrapods and branched tetrapods [74]. Different shapes of CdSe nanoparticles are obtained via different fundamental strategies. The spherical shapes of CdSe nanocrystals are obtained using single surfactants under thermodynamic conditions because it minimizes surface area [75], whereas the anisotropic nanorods particles are obtained by rapid growth in surfactant mixture under kinetic conditions, where the different surfactants are used to selectively control the growth rates of different faces [76]. Typical materials that exhibit shape changes as the reaction conditions change include CdSe, CdS and PbS due to their wide variation in 1D morphology [8,77].

The growth rate between the different crystallographic directions can be emphasized if the surfactants stabilize a certain surface by selective adhesion. This selective adhesion of surfactants needs to be taken into consideration in the synthesis of CdSe nanorods [74]. A typical example is the injection of dimethylcadmium and TOPSe into a hot surfactant mixture of TOPO and hexylphosphonic acid (HPA) which leads to the modulation of the growth pattern. This is due to the amount of HPA that selectively binds to the surfaces {100} and {110} of the growing crystals. The synthesis carried at low HPA concentration or in the absence of HPA result in the formation of spherical nanoparticles only. However, the significant increase in the HPA concentration leads to the formation of nanorods. This is due to the surface-bond of HPA molecules which play a role in the reduction of the growth along {100} and {110} surfaces (Figure 1.3 a). Surfactants molecues that specifically bind to the {100} and {110} surfaces of a hexagonal structure have preferential growth along the <001> direction, and this type of growth facilitates the rod growth (Figure 1.3 a) [74]. Alternatively, surfactant molecules that bind to the {001} faces of a hexagonal structure prevent growth along the <001> direction thereby leading to the formation of discs shape [78].

Selective adhesion of surfactants can only induce elongation along a specific axis while the compression along other axis is experienced. An example in this regard, is the formation of copper sulfide nanodiscs in the presence of surface selective alkanethiol surfactant [78]. Alkanethiol molecules strongly absorb on the {001} faces of Cu_2S where the formation of 2D nanodiscs can be achieved by lowering the surface energy (Figure 1.3 b). Microscopic mechanism by which the HPA acts upon the different faces has not yet been understood. The modulation of relative growth rates of the different faces could be the mechanism that explains

the effect of HPA on the faces. There are two possible mechanisms that could be assumed in this type of growth. One could be the HPA being protonated or deprotonated which may directly act as a surfactant absorbing on a certain face, for instance the {100} face and to the {110} faces and shutting down the growth on these faces. The alternative could be the highly acidic environment influencing the growth rates by protonation of particular faces [74].

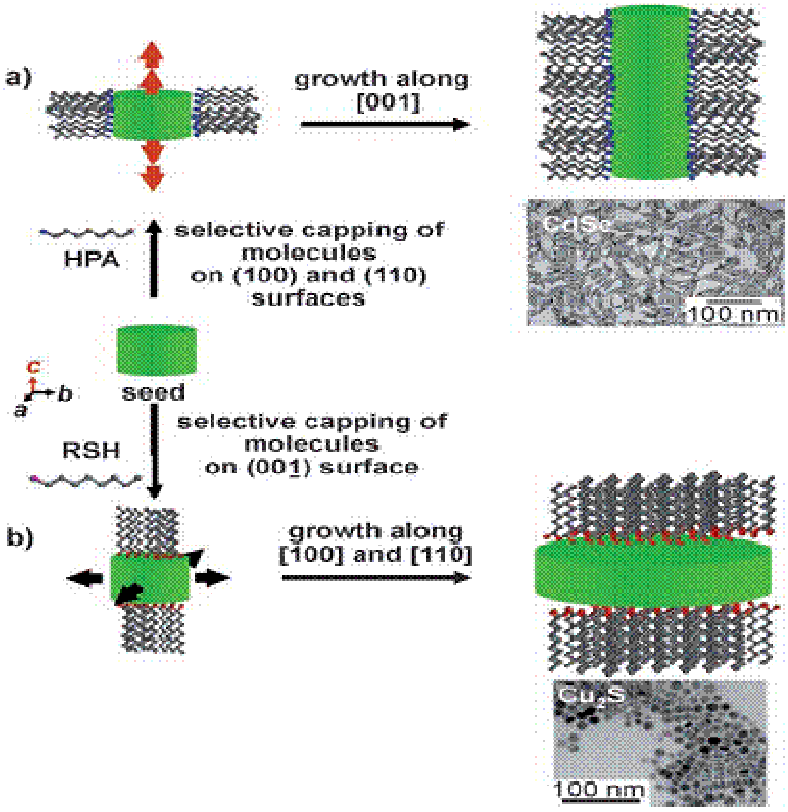

Figure 1.3 Surface modulation effects induced-selective surfactants on either a) anisotropic rod or b) disc growth [79].

1.5 Applications

There are many applications of nanoparticles. However in this work, only the biological applications will be discussed.

1.5.1 Biological applications

Nanocrystalline semiconductors or quantum dots offer several advantages over organic fluorescent dyes that are typically used for biological labeling. A limitation of organic dyes is the loss of fluorescence that occurs when dye molecules react irreversibly with each other or the solvent, producing a non-flourescent material. This process, known as photobleaching, can occur in an aqueous solution on the order of minutes [80,81]. However, photobleaching in quantum dots is diminished as the passivating layer protects particles from external interactions. The passivation layer reduces photo-oxidation of the particle core which can produce free ions (e.g., Cd^{2+}) and eventually, particle dissolution [82]. As a result of reduced photobleaching, quantum dots can exhibit continuous fluorescence for a time period of an order of magnitude greater than organic fluorescent dyes [81]. Furthermore, organic fluorescent dyes typically exhibit fixed, narrow excitation spectra however quantum dots may be excited in a range of wavelengths as determined by their size. Furthermore, the emission bandwidth (e.g., wavelength range of emitted light) for organic dyes can be very large (> 40 nm, often with a tail into red wavelengths) when compared with quantum dots which is very narrow (~20-30 nm), thus creating difficulty in distinguishing individual colours [83]. The narrow band widths result from shrinking and splitting of potential energy bands as the particle size decreases. All of these properties have led to quantum dot applications in diverse biological fields, including biosensing, cellular labelling, and *in vivo* fluorescent detection and therapeutics. Some of these applications in biology or medicine are briefly discussed below.

1.5.1.1 Fluorescent biological labels

The common biological use of quantum dots has been in the fluorescent labeling of cells. For example, they have been used to investigate the motion of biomolecules, detect cell phenotypes and the study of cell migration. In each of these uses, they present several enhancements over systems employing fluorescent dyes. Most importantly, their small size and high resistance to photobleaching, have allowed quantum dots to be used in a number of high throughput systems with real-time monitoring, a feat which is different with dye molecules [84].

The most exciting possibility for quantum dot labels has been their use *in vivo*. Quantum dots have been utilized in a number of *in vivo* procedures that would not be possible with organic fluorescent dyes. Many of these take advantage of the longevity of their fluorescence, as a result of resistance to photobleaching [85-88], while other exploit their electrical properties to deliver therapeutic treatment [89-91]. The majority of nanoparticles used in biological applications have been based on a CdX structure (where X = selenium, tellurium or sulphur). Cadmium is known to interfere with DNA mismatch repair [92], can inhibit certain types of neuronal firing [93] and is also a carcinogen [94]. Therefore, the toxicity of the particles has been a major concern. Surface passivation can significantly reduce the risk of exposure to free cadmium [95], and although the long-term effects of nanoparticle exposure have not yet been investigated, short-term *in vivo* studies do not demonstrate any acute effects [85-91]. One novel use of quantum dots *in vivo* has been to monitor embryogenesis in frogs [85].

Quantum dots have been evident in limited therapeutic contexts. They can be used to image and, even penetrate cancer cells through receptor mediated endocytosis [91]. Particles can be coupled

to therapeutic agents, which are activated in the presence of light excitation. Antibody-conjugated CdSe/ZnS core shell nanocrystals have been used to detect respiratory syncytical viruses [95]. The brightness of the quantum dots enables the virus to be detected in minutes, whereas the previous assay requires four days. The result of this new technology is that, antiviral drugs can be given early in the infection when they are most effective, reducing hospitalization and death. Gold nanoshells conjugated to recognition molecules, can be used to image tumours [96]. When they are optically excited they produce heat, depending on the size of the nanoshell and heat production can be significant enough to kill the attached cells.

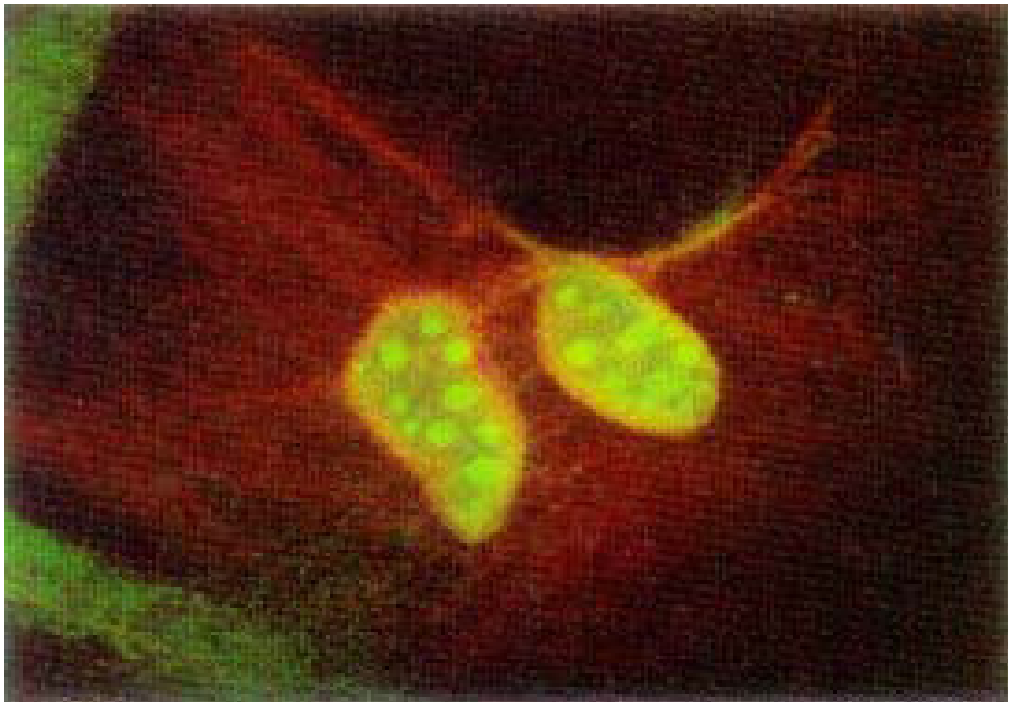

Figure 1.4 Cross section of dual-labeled sample examined with a Bio-Rad 1024 MRC laser-scanning confocal microscope with a 40x oil 1.3 numerical aperture object [83].

In order to demonstrate the use of nanocrystals for biological staining, 3T3 mouse fibroblast cells have been fluorescently labeled using two different sizes of CdSe-CdS core-shell nanocrystals enclosed in a silica shell. In this demonstration, Mouse 3T3 fibron were grown on fibronectin-treated specimens. The specimens were then treated successively with unbiotinylated green nanocrystals and red biotinylated nanocrystals. The specimen stained and fluoresced at two different regions, at 35 nm narrow-pass filter for the green and 585 nm long-pass filter for the red (Figure 1.4) [83].

1.5.1.2 Drug delivery

Nanomedicine incorporates the science and technology of nanometer scale systems. Drug delivery systems are very important in treating, preventing or diagnosing diseases sometimes called smart-drug or theragnostics [97].

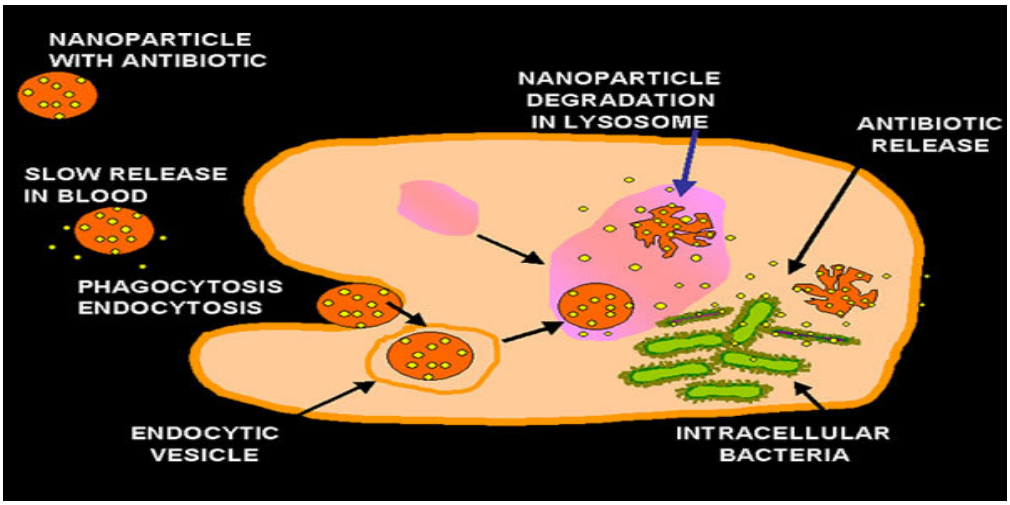

Figure 1.5 Schematic diagram showing drug delivery mechanism of the nanoparticles into the targeted diseased cells [97].

Nanotechnology offers so many advantages over other technologies due to the number of ways that can be used to deliver the drugs into targeted human system. The drug delivery mechanism can be by oral administration, intravenous, inhalation, transdermal and implantation. The uptake of the nanoparticles via oral administration can occur by transcytosis. It has been noted that nanoparticles provide sustainable release of the anti-TB drugs and have considerably enhanced efficiency after oral administration [98]. In this demonstration, three drugs rifampin (RMP), isoniazid (INH) and pyrazinemide (PZA) were coencapsulated in poly(lactide-co-glycodide) (PLG) nanoparticles. It was noted that if the oral dose was given every day, M. tuberculosis infected mice were completely cured after 10 days [98].

The main goal of research in nanomedicine is to achieve specific drug targeting and delivery while reducing the toxicity. The knowledge on drug incorporation and release, formation stability and shelf life, biocompatibility, bio-distribution and targeting and functionality is a key concept in the search for appropriate design of new materials as carriers for drug delivery systems [99]. As shown in Figure 1.5, the antibiotics to be delivered are protected from degradation and transported by the nanoparticles. Since the nanoparticles are small, they easily diffuse through the cell. As they enter the cell, they degrade in the liposome where the antibiotic release takes place. The released antibiotics enter the targeted diseased site.

The direct delivery of the TB drug to the lungs is one of the most effective forms of TB cure. This type of delivery often occurs by inhalation. The advantages offered by this form of delivery include the possibility of reduced systemic toxicity, as well as achieving higher drug concentration at the main site of infection. The use of nanocarriers for pulmonary delivery

renders some difficulties. Their mass median aerodynamic diameter, an important parameter for the particle deposit in lungs is often too small [100]. There have been reports demonstrating the effectiveness of pulmonary drug delivery using nanoparticles [101]. Pigs have been used to investigate the pharmacokinetics and antibacterial effect of the nanoparticle-bound anti-TB drugs. The drugs were administered via the respiratory route. It was found that the respiratory administered drugs cured TB in pigs lungs in fewer days relative to other delivery routes [102]

1.5.1.3 Tissue engineering

Natural bone surface contains features that are in the order of nanometers across. If the artificial bone implant is used, its surface need not to be left smooth because the body will try to reject it because the smooth surface leads to the production of fibrous tissue covering the surface of the implant. Fibrous tissue reduces the bone-implant contact, which may result in loosening of the implant and further inflammation. As an alternative, the bone implants made of nanoparticles have reduced chances of rejection by the body and they stimulate the production of osteoblast. Osteoblasts are the cells responsible for the growth of the bone matrix and are found on the advancing surface of the developing bone [103].

The bone repair using titanium is a widely used technique in orthopaedics and dentistry. Titanium has a high fracture resistance, ductility and weight to strength ratio. However, titanium use in bone repair offers some disadvantages due to its less bioactivity and it does not well support cell adhesion and growth. Apatite coating are known to be bioactive and can bond to the bone. As a result, several techniques have been used to provide apatite coating on titanium. However, these coatings have some limitations because they have thickness non-uniformity,

poor adhesion and low mechanical strength. However, nanometer scale systems can provide a solution to this problem. A biomimetic approach to make nanostructured apatite can act as a replacement for apatite coatings. The nanostructured apatite work well with stimulated body fluids as a result, the formation of a strongly adherent, uniform nanoporous layer occurs. This layer which is in the order of nanometers is stable and bioactive [104].

A real bone is a nanomposite material, composed of hydroxyapatite crystallite in the organic matrix, which is mainly composed of collagen. The bone is a mechanically tough, at the same time plastic that can recover easily from mechanical damage. Actual nano-scale mechanism leading to the understanding of the bone properties is an interesting field of research.

1.5.1.4 Protein detection

Protein functionality needs to be well understood for further progress in human well being. They play a major role in cell's language, machinery and structure. Nanoparticles are used in immunohistochemistry to identify protein-protein interaction. However, there are some limitations in using this technique for multiple, simultaneous detection. Single dye molecule can be well detected using surface enhanced Raman scattering spectroscopy. Nanoparticle can be used in designing sophisticated multifunctional probes. The probes made of nanoparticles are capable of recognizing small molecules, and they can be modified to contain antibodies on the surface to recognize proteins [105]. Cognet *et al.* [106] performed an immunochemistry assay to demonstrate the capabilities of the photothermal interference contrast (PIC) method to image low amounts of immunogold-labeled proteins in cells.

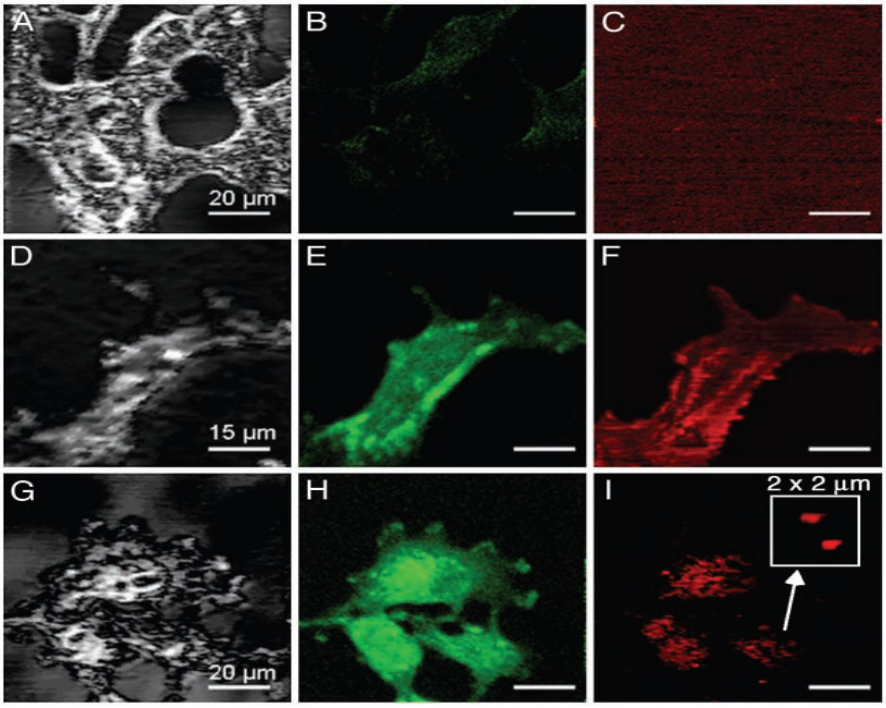

Figure 1.6 Scattering (*A, D*, and *G*), fluorescence (*B, E*, and *H*), and photothermal (*C, F*, and *I*) images recorded on COS7 cells. *A–C* correspond to untransfected cells and *D–I* correspond to cells expressing a membrane protein (mGluR5, a receptor for neurotransmitter) containing a myc tag. All cells were immunolabeled with anti-myc-Alexa568 (10 g/mL) and with anti-IgG 10-nm gold as secondary antibody, for two different concentrations (10 g/ml in *A–F* and 0.5 g/mL in *G–I*). Cells expressing mGluR5 were efficiently labeled with anti-myc-Alexa568 and anti-IgG 10-nm gold. (*I* Inset) Detail of the PIC image revealing individual anti-IgG 10-nm gold imaging. The heating beam intensity is 3 MW/cm^2 [107].

Commercially available protein-conjugated colloid gold nanoparticles are in the order of nanometers (1-100 nm). When electron microscopy is used, metal particles with sizes less than 10 nm are preferred because of their better penetration in cellular organelles [107]. The COS7 cells tranfected with membrane protein were used. Fluorescent images were able to easily

discriminate the cells that contained fluorescent-labeled receptors from untransfected ones (Figure 1.6 B, E and H). The untransfected cells didn't detect any signal on PIC method due to the specificity of gold labeling as shown in Figure 1.6 A-C.

Resolved discrete spots that may be attributed to single nanoparticles can be observed in cell regions with low density of labels as shown in Figure 1.6 *I* inset. Successive recording of the same region leads to identical images display due to the nonphotobleaching feature of the labels.

1.6 Problem

The nanoparticles synthesized via the hot injections routes are generally not suitable for biological applications. There is an increase in a demand for the use of selenide based nanoparticles in a number of fields including biological fields and these materials need to be biocompatible and environmentally friendly. In order for the nanoparticles to be used in biological fields, they need to be synthesized in such a way that they are both organically and aqueous soluble, and hence less toxic.

The synthesis of biocompatible nanoparticles should be via environmentally friendly methodologies which eliminate the use toxic starting materials. Environmentally friendly methodologies involve the use of less toxic starting materials, least number of reagents, few synthetic steps, reduced amount of by-products and wastes, low reaction temperature and if possible, the use of water as a solvent. This study presents the synthesis of selenide based nanoparticles using mild conditions.

1.7 Aims and objectives of the study

1.7.1 Aims

- Synthesis of high quality, monodispersed, crystalline CdSe and ZnSe nanoparticles.
- Investigation of the effect of varying several parameters such as Cd:Se ratio of TEA capped CdSe nanoparticles, pH, capping agent, duration of thermolysis of HDA capped ZnSe, variation of cadmium/zinc source and reaction time on optical, morphological and structural properties of CdSe and ZnSe nanoparticles.

1.7.2 Objectives

- To synthesize water soluble triethanolamine (TEA) and cysteine capped CdSe and ZnSe nanoparticles.

- To investigate the effect of varying the following parameters on the morphology and electronic properties of the CdSe and ZnSe particles:

  (a) Cd:Se ratio of TEA capped CdSe nanoparticles

  (b) capping agent,

  (c) pH

  (d) cadmium or zinc source

  (e) reaction time and

  (f) duration of thermolysis of HDA capped ZnSe

- To study the optical, morphological and structural properties of CdSe and ZnSe nanoparticles.

1.8 References

[1] F. Du, J. Liu, Z. Guo, Journal of Matarials Research 44 **(2008)** 25.

[2] M.A.L. Russo, C. O'Sullivan, B. Rounsefell, P.J. Halley, R. Truss, W.P. Clarke, Journal of Bioresearch Technology 100 **(2008)** 1705.

[3] A. Shidfar, M. Alinejadmofrad, M. Garshasbi, Journal of Optics and Laser Tchnology 41 **(2008)** 280.

[4] C. Dupas, P. Hondy, M. Lahmani, Journal of Nanotechnolgy and Nanophysics 2 **(2006)** 177.

[5] J. Wu, F. Luo, Q. Zhang, M. Gao, Journal of Optics and Laser Technology 41 **(2008)** 360.

[6] N. Sheng, P. Zhu, C. Ma, J. Jiang, Journal Dyes and Pigmens 81 **(2008)** 91.

[7] A. Kumar, K. S. Meenakshi, B.R.V. Narashimhan, S. Srikanth, G. Arthanareeswaran, Journal of Materials Chemistry and Physics 113 **(2008)** 57.

[8] J. Hu, L.S. Li, L.W. Wang, L. Manna, A. Alivisatos, Science 292 **(2001)** 2060.

[9] X. Peng, Advanced Matererials 15 **(2003)** 459.

[10] Z.A. Peng, X.G. Peng, Journal of American Chemical Society 124 **(2002)** 3343.

[11] H. Weller, H.M. Schmidt, U. Koch, A. Fojtik, S. Baral, A. Henglein, W. Kunati, K. Weiss, E. Dieman, Chemical Physics Letters 124 **(1986)** 557.

[12] S.M. Lee, Y.G. Yun, S.N. Cho, J. Cheon, Journal of American Chemical Society 124 **(2002)** 11244.

[13] L.E. Brus, Journal of Chemical Physics 79 **(1983)** 5566.

[14] G. Li, M. Nogami, Journal of Applied Physics 75 **(1994)** 4276.

[15] A. Euteneuer, R. Hellmann, R. Gobel, S. Shevel, V. Vozny, M. Vytrykhivsky, W. Petri, C. J. Klingshirn, Journal of Crystal Growth 1081 **(1998)** 184.

[16] K. Shimakawa, A. Kolobov, S. R. Elliot, Advanced Physics 44 **(1995)** 475.

[17] K. D. Kepler, G. C. Lisensky, M. Patel, L. A. Sigworth, A. B. Ellis, Journal of Physical Chemistry 99 **(1995)** 6011.

[18] C. Donega, S. G. Hickey, S. F. Wuister, D. Vanmaekelbergh, A. Meijerink, Journal of Physical Chemistry B 107 **(2003)** 489.

[19] L. Qu, Z. Peng, X. Peng, Journal of Nanotechnology 1 **(2001)** 333.

[20] L. Qu , X. Peng, Journal of American Chemical Society 124 **(2002)** 2049.

[21] W. Hoheisel, V. L. Colvin, C. S. Johnson, A. P. Alivisatos, Journal of Chemical Physics 101 **(1994)** 8455.

[22] C. F. Landes, S. Link, M. B. Mohammed, B. Nikoobakht, A. EI-Sayed, Pure and Applied Chemistry 14 **(2002)** 1675.

[23] V. N. Soloviev, A. Eichhofer, D. Fenske, U. Banin, Journal of American Chemical Society 122 **(2000)** 2673.

[24] X. Chen, Y. Lou, C. Burda, International Journal of Nanotechnology 1 **(2004)** 105.

[25] X. G. Peng, L. Manna, W. D. Yang, J. Wickham, E. Scher, A. Kadavanich, A. P. Alivisatos, Nature 404 **(2000)** 59.

[26] A. M. Chuah, T. Kuroiwa, I. Kobayashi, M. Nakajima, Journal of Food Hydrocolloids 23 **(2008)** 600.

[27] J. Johnson, V.K. La Mer, Journal of American Chemical Society 69 **(1947)** 1184.

[28] M. Bruchez, J.M. Moronne, S. Weiss, A.P. Alivisatos, Science 281 **(1998)** 2013.

[29] L. Spenhel, H. Hasse, H. Weller, A. Henglein, Journal of American Chemical Society 109 **(1987)** 5649.

[30] L. Spenhel, H. Weller, A. Henglein, Journal of American Chemical Society 109 **(1987)** 6632.

[31] M. L. Steigerwald, L. E. Brus, Annual Reviews of Materials Science 19 **(1989)** 471.

[32] R. Rossetti, J.L. Ellison, J.M. Gibson, L.E. Brus, Journal of Chemical Physics 80 **(1984)** 4464.

[33] H. Weller, Advanced Materials 5 **(1993)** 88.

[34] H. Weller, A. Fojtik, A. Henglen, Chemical Physics Letters 117 **(1985)** 485.

[35] R. Rossetti, J.L. Ellison, J.M. Gibson, L.E. Brus, Journal of Chemical Physics 82 **(1985)** 552.

[36] M.A. Malik, P. O'Brien, Phosphorus, Sulphur and Silicon 180 **(2005)** 687.

[37] G. Hodes, Chemical Solution Deposition of Semiconductor Films, Marcel Dekker: New York, **2002**.

[38] S. Yochelis, G. Hodes, Chemistry of Materials 16 **(2004)** 2740.

[39] P.P. Hankare, V.M. Bhuse, K.M. Garadka, S.D. Delekar, I.S. Mulia, Materials Chemistry and Physics 90 **(1989)** 3463.

[40] X. Zhong, S. Liu, Z. Zhang, L. Li, Z. Wei, W. Knoll, Journal of Materials Chemistry 14 **(2004)** 2790.

[41] C.B. Murray, D.J. Norris, M.G. Bawendi, Journal of American Chemical Society 115 **(1993)** 8706.

[42] P. S. Nair, T. Radhakrihsnan, N. Revaprasadu, G. A. Kolawole, P. O'Brien, Polyhedron 22 **(2003)** 3129.

[43] T. Trindade, P. O'Brien, Advanced Materials 8 **(1996)** 161.

[44] T. Trindade, P. O'Brien, X. Zhang, Chemical Maters 9 **(1997)** 523.

[45] B. Ludolph, M.A. Malik, P. O'Brien, N. Revaprasadu, Chemical Communications **(1998)** 833.

[46] N. Revaprasadu, M.A. Malik, P. O'Brien, M.M. Zulu, G. Wakefield, Journal of Materials Chemistry 8 **(1998)** 1885.

[47] M.A. Malik, N. Revaprasadu, P. O'Brien, Chemical Maters 13 **(2001)** 913.

[48] P.S. Nair, T. Radhakrishnan, N. Revaprasadu, G. Kolawole, P. O'Brien, Journal of Materials Chemistry 12 **(2002)** 2722.

[49] S.N. Mlondo, N.Revaprasadu, P. Christian, P. O'Brien, Polyhedron 28 **(2009)** 2097.

[50] P. S. Nair, T. Radhakrishnan, N. Revaprasadu P. O'Brien, Materilas Science and Technology 21 **(2005)** 237.

[51] M.J. Moloto, N. Revaprasadu, Journal of Materials Chemistry 15 **(2004)** 313.

[52] N. Moloto, N. Revaprasadu, M.J. Moloto, P. O'Brien, M. Helliwell, Polyhedron 26 **(2007)** 3947.

[53] J. C. Bruce, N. Revaprasadu, K. R Koch, New Journal of Chemistry 31 **(2007)** 1647.

[54] T. Mthethwa, V.S.R.R Pullabhotla, P.S. Mdluli, J. Wesley-Smith, N. Revaprasadu, Polyhedron 28 **(2009)** 2977.

[55] C.J. Murphy, Journal of Materials Chemistry 18 **(2008)** 2173.

[56] S. Sapra, A.L. Rogach, J. Feldman, Journal of Materials Chemistry 16 **(2006)** 3391.

[57] J. Aktar, M.A Malik, P.O'Brien, K.G.U Wijayantha, R. Dharmadasa, S.J.O Hardman, D.M Graham, B.F Spencer, S.K Stubbs, W.R Flavell, D.J Binks, F. Sirotto, M El kazzi, M. Silly, Journal of Materials Chemistry 20 **(2010)** 2336.

[58] J. Ge, Y. Li, G. Yang, Chemical Communications 17 **(2002)** 1826.

[59] H. Han, Z. Sheng, J. Liang, Journal of Materials Letters 60 **(2006)** 3782.

[60] S.S. Oluwafemi, N. Revaprasadu, New Journal of Chemistry 10 **(2008)** 1432.

[61] S.O. Oluwafemi, N. Revaprasadu, Physica B 404 **(2009)** 1204.

[62] Y. Gao, Q. Zhang, Q. Gao, Y. Tian, W. Zhou, L. Zheng, S. Zhang, Materials Chemistry and Physics 115 **(2009)** 724.

[63] N.N. Maseko, N. Revaprasadu, V.S.R. Rajasekhar Pullabhotla, R. Karthik, P. O'Brien, Materials Letters 64 **(2010)** 1037.

[64] S.O. Oluwafemi, N. Revaprasadu, A.J. Ramirez, Journal of Crystal Growth 310 **(2008)** 3230.

[65] V.S.R. Rajasekhar Pullabotla, N. Revaprasadu, Mterials Letters 63 **(2009)** 2097.

[66] Z.B. Shang, Y. Wang, W.J. Jin, Talanta 78 **(2009)** 364.

[67] M. Kristl, I. Ban, A. Danc, V. Danc, M. Drofenic, Ultrasonics Sonochemistry 17 **(2010)** 916.

[68] D. Zhou, Y. Li, E.A.H. Hall, C. Abell, D. Klenerman, Nanoscale 3 **(2011)** 201.

[69] S. Satapathy, P.K. Gupta, H. Srivastava, A.K. Srivastava, V.K. Wadhawan, K.B.R. Varma, V.G. Sathe, Journal of Crystal Growth 307 **(2007)** 185.

[70] J.H. Adair, E. Suvaci, Current Option in Colloidal & Interface Science 5 **(2000)** 160.

[71] N. Pradhan, D. Reifsnyder, R.G. Xie, J. Aldana, X.G. Peng, Journal of American Chemical Society 129 (**2007**) 9500.

[72] L. Qu, X. Peng, Journal of American Chemical Society 124 **(2002)** 2049.

[73] Y. Li, X. Li, C. Yang, Y. Li, Chemistry of Materials 13 **(2003)** 2461.

[74] L. Manna, E.C. Scher, A.P. Alivisatos, Journal of American Chemical Society 122 **(2000)** 12700.

[75] X. Peng, J. Wackham, A.P. Alivisatos, Journal of American Chemical Society 120 **(1998)** 5343.

[76] X. Peng, Nature 404 **(2000)** 59.

[77] L. Li, J. Hu, W. Yang, L. Manna, A.P. Alivisatos, Nano Letters 1 (**2001**) 349.

[78] A. Ghezelbash, B.A. Korgel, Langmuir 21 **(2005)** 9451.

[79] Y. Jun, J. Choi, J. Cheon, Angrewandte Chemie International Edition 45 **(2006)** 3414.

[80] M. A. Hines, P. J. Guyot-Sionnest, Journal of Physical Chemistry 100 **(1996)** 468.

[81] W. C. W. Chan, S. Nie, Science 281 **(1998)** 2016.

[82] L. Spanhel, M. Haase, H. Weller and A. Henglein, Journal of American Chemical Society 109 **(1987)** 5649.

[83] M. Bruchez, J. M. Moronne, P. Gin, S. Weiss, A. P. Alivisatos, Science 281 **(1998)** 2013.

[84] L. C. Mattheakis, J. M. Dias, Y. J. Choi, J. Gong, M. P. Bruchez, J. Liu, E. Wang, Analytical Chemistry 327 **(2004)** 200.

[85] B. Dubertret, P. Skourides, D. J. Norris, V. Noireaux, A. H. Brivanlou, A. Libchaber, Science 298 **(2002)** 1759.

[86] D. R. Larson, W. R. Zipfel, R. M. Williams, S. W. Clark, M. P. Bruchez, F. W. Wise, W. W. Webb, Science 300 **(2003)** 1434.

[87] W. C. W. Chan, D. J. Maxwell, X. Gao, R. E. Bailey, M. Han, S. Nie. Current Opinion on Biotechnology 13 **(2000)** 40.

[88] M. E. Akerman, W. C. W. Chan, P. Laakkone, S. N. Bhatia, E. Ruoslahti, Procurement Natural Academic Science 99 **(2002)** 12617.

[89] C. Loo, A. Lin, L. Hirsch, M. H. Lee, J. Barton, N. Halas, J. West, R. Drezek, Technological Cancer Research Treatment 3 **(2004)** 33.

[90] C. Seydel, Science 300 **(2003)** 80.

[91] X. Wu, H. Liu, J. Liu, K. N. Haley, J. A. Treadway, J. P. Larson, N. Ge, F. Peale,

M. P. Bruchez, Natural Biotechnology 21 **(2003)** 41.

[92] A. Hartwig, T. Schwedtle, Toxic Letters 127 **(2002)** 47.

[93] J. B. Lansman, P. Hess, R. W. Tsien, Journal of General Physiochemistry 88 **(1986)** 321.

[94] M. P. Waalkes, Materials Research 533 **(2003)** 107.

[95] A. M. Derfus, W. C. W. Chan, S. N. Bhatia, Nano Letters 4 **(2004)** 11.

591.

[96] E. L. Bentzen, F. House, T. J. Utley, J. E. Crowe, D. W. Wrigth, Nano Letters 5 **(2005)** 591.

[97] D.A. LaVan, T. MacGuire, R. Langer, Natural Biotechnology 21 **(2003)** 1184.

[98] A.T. Florence, Journal of Drug Target 12 **(2004)** 65.

[99] W.H. De Hong, P.J.A. Borm, International Journal of Nanotechnology 3 **(2008)** 133.

[100] S. Gelperian, K. Kisich, M.D. Iseman, L. Heifets, American Journal of Respiratory and Critical Care Medicine 172 **(2005)** 1487.

[101] R. Pandey, G.K. Khuller, Journal of Antimicrobial Chemotherapy 55 **(2005)** 430.

[102] R. Pandey, A. Sharma, A. Zahoor, S. Sharm, G.K. Khula, B.P. Prasad, Journal of Antimicrobial Chemotherapy 52 **(2003)** 981.

[103] L.G. Gutwein, T.J. Webster, American Ceramic Society 26th Annual Meeting Conference Proceedings (**2003**) in press.

[104] J. Ma, H. Wong, L.B. Kong, K.W. Peng, Nanotechnology 14 **(2003)** 619.

[105] Y.C. Cao, R. Jin, J.M. Nam, C.S. Thaxton, C.A. Markin, Journal of American Chemical Institute 125 **(2003)** 14676.

[106] L. Cognet, C. Tardin, D. Boyer, D. Choquet, B. Lounis, PNAS 100 **(2003)** 11350.

[107] M.A. Hayat, Colloidal Gold: Principles, Methods and Applications (Academic, San Diego) **1989**.

Chapter 2

Synthesis of water soluble CdSe and ZnSe nanoparticles

2.0 Introduction

Many methods have been developed to synthesize semiconductor nanoparticles ranging from colloidal to hot injection routes. There are still a few limitations to some of these methods due to the fact that they use sophisticated equipment, volatile solvents, toxic precursors and extremely high temperatures and therefore, they are not environmentally friendly and cost effective [1]. The biocompatibility of semiconducting materials depends on their solubility. The solubility of the functional nanostructures is attained by surface modification, which is generally very time consuming [2]. An alternative direct synthesis in an aqueous medium can also be used. The passivating groups used in these aqueous routes are predominantly thiophenols, thioureas and mercapto acetates. The toxicity of these ligands can have harmful effect in the environment if the synthesis is done on a larger scale [3,4]. It is therefore important to develop greener routes to nanomaterials. These routes should involve the use of less toxic precursors, use of water as a solvent where possible, use of least number of synthetic steps as possible, reducing the amounts of by-products and waste, and using the reaction temperature close to room temperature [1,5,6].

Amongst the II-VI group semiconducting materials, CdSe is undoubtedly the most widely studied because of its major contribution to photovoltaics, biosensors, targeted drug deliveries, fluorescent sensors and solar cells [7-13]. A variety of methods have been reported to synthesize cadmium selenide nanoparticles which include the single source precursor method, aqueous synthesis, electrochemical deposition, chemical bath deposition, spray pyrolysis deposition and chemical vapour deposition techniques [14-25]. Pioneering work on CdSe was done by Murray, Norris and Bawendi [26]. They used dimethyl cadmium (Me_2Cd) as the cadmium source and $(TMS)_2X$ (X = S, Se, Te) or TOPSe as the chalcogen source. These reagents were injected into

tri-n-octyl-phosphine oxide (TOPO), a high boiling point coordinating solvent, at temperatures ranging from 120 to 250 ^{o}C. Due to the reported risks involved in Bawendi's method, Peng *et al.* [27] replaced volatile dimethyl cadmium with CdO to synthesize CdSe nanoparticles. Later, his group showed that cadmium acetate, amines and fatty acids as precursors, solvents and capping agents also give high quality CdSe nanocrystals [28]. CdSe nanocrystals have also been prepared in aqueous solution, but their quantum yields (QY) were very low [29] with quite broad bandwidths (the full width at half maximum, FWHM > 100 nm). In comparison to the organic route synthetic routes for quantum dots, little attention has been paid to aqueous based routes for high quantum yields.

In the search for methodologies to synthesize water soluble nanoparticles, Ge *et al.* [30] proposed a novel method of synthesizing CdSe nanocrystallites in an aqueous solution by an ultrasonic technique. Han *et al.* [31] proposed a method for synthesizing small sized (1-3 nm) CdSe nanoparticles, based on the reaction of $CdCl_2$ and Na_2SeSO_3 solutions reacted together with mercaptoacetic acid (MAA) as a stabilizing agent in the high-intensity ultrasonic horn. They further studied the influence of the initial molar ratio of Cd:Se and reaction time on the size of CdSe nanoparticles.

Cadmium is generally known for its inherent toxicity. Therefore, for safe use in *in-vivo* applications, cadmium containing sources need to be replaced with less toxic labeling materials. Cadmium ions can easily be released in aqueous solutions. This hinders the use of CdSe for biomedical purposes. The natural toxicity of Cd^{2+} has led to the replacement of Cd^{2+} with Zn^{2+}. As one of the wide band gap semiconducting materials, ZnSe, a light yellow solid with a band

gap E_g = 2.7 eV, is potentially a suitable material for short wavelength photoelectronic devices including but not limited to blue laser diodes, light emitting diodes, photodetectors, high density optical storage, full colour displays and biomedical labeling and sensors [32-37]. ZnSe has recently also been found to be a sensitive-type humidity sensor based on a one dimensional ZnSe nanostructure. However, humidity sensors made of ZnSe have poor reproducibility, and hence, finding ways to improve the stability and the reproducibility of humidity sensors based on ZnSe is an interesting field of study [38].

ZnSe nanoparticles have been synthesized via the microwave heating process, which is very cheap and quick [39]. Owing to the advantages offered by water soluble routes, Archana *et al.* [40] synthesized triethanolamine (TEA) capped ZnSe nanoparticles using a simple wet chemical method. Their main goal was to study the properties of the quantum dots such as shape, size, structure, band-gap, absorption and luminescence. Haung *et al.* [41] recently reported the synthesis of water soluble ZnSe nanoparticles via the microwave irradiation technique. This method showed that the properties of the particles are pH dependent, which is typical of water soluble nanoparticles.

For biological related applications, cysteine and triethanolamine are commonly chosen as capping groups. Cysteine is chosen as a biocompatible capping agent because it is an amino acid that can be found in many proteins throughout the body. When it used as a supplement, it is usually in the form of N-acetyl-L-cysteine (NAC). This current work describes the synthesis of water soluble cadmium and zinc selenide nanoparticles. The CdSe and ZnSe particles were capped with water soluble capping groups, cysteine and triethanolamine (TEA). In addition, the

reaction parameters such as reaction time, pH, temperature and the metal source on optical and structural properties of the as-synthesized nanoparticles were investigated.

2.1 Experimental

2.1.1 Chemicals

All chemicals used were obtained from Sigma Aldrich and are, hydrochloric acid (90.0%), ammonia solution (90.0%), selenium powder (99.99%), cadmium chloride (88 %), cadmium carbonate (90 %), zinc chloride (89.0%), zinc carbonate (90.0%), triethanolamine, cysteine (99.99%) and N_2 gas were used as received.

2.1.2 Synthesis of water soluble CdSe and ZnSe nanoparticles

CdSe and ZnSe nanoparticles were synthesized in water soluble capping groups, cysteine and triethanolamine (TEA). The method used is an adaptation of the method previously reported by Oluwafemi and Revaprasadu [42] with slight modifications.

2.1.2.1 Synthesis of cysteine capped CdSe nanoparticles

In this synthetic procedure, cysteine had been chosen as the surface passivating group for CdSe nanoparticles. CdSe nanoparticles were prepared using Se powder as source of selenium. In a typical room temperature reaction, selenium powder (0.32 mmol) was mixed with 20.0 mL of de-ionized water in a three-necked round bottom flask and purged with N_2. This was followed by the addition a solution of sodium borohydrate (0.81 mmol). The complete reduction of selenium powder was confirmed by the formation of clear colourless solution after two hours. An aqueous solution of $CdCl_2$ or $CdCO_3$ (3.2×10^{-4} M) was added into the reduced selenium solution

followed by an immediate addition of cysteine with a mole ratio 1:20-Cd^{2+}:cysteine. The reaction was carried at room temperature and 90 ^{o}C. The pH of the reaction was varied from 4, 7 and 11. Aliquots were withdrawn, at intervals of 1, 3, 5 and 18 h, respectively centrifuged and the isolated product redispersed in de-ionized water, for analysis.

2.1.2.2 Synthesis of TEA-capped cadmium selenide

The methodology explained in section 2.1.2 had been used to synthesize TEA capped CdSe nanoparticles [42]. Briefly, in a typical room temperature reaction, selenium powder (0.32 mmol) was mixed with de-ionised water (20.0 mL) in a three necked round bottom flask. A solution of sodium borohydrate (0.81 mmol) was added into this mixture and the flask was immediately purged with nitrogen gas in order to create an inert atmosphere. After the complete dissolution of selenium (~2-3 h), a $CdCl_2$ (0.32 mmol) solution and a solution of TEA (0.64 mmol) were simultaneously added into the reduced selenium solution. Aliquots were withdrawn, centrifuged and re-dispersed in de-ionized water for analysis. The reaction was investigated with different mole ratios of cadmium to selenium in which the concentration of a capping agent was not varied. The reaction pH was maintained at pH 8.0 by using HCl (0.10 M) and NH_3 (0.10 M) solutions.

2.1.2.3 Synthesis of cysteine capped ZnSe nanoparticles

The nanoparticle was done using a modified version of the methodology reported by Oluwafemi and Revaprasadu [42]. In a typical room temperature reaction, Selenium (Se) powder (0.32 mmol) was mixed with deionised water (20.0 mL) in a three necked flask. Sodium borohydride ($NaBH_4$) (0.81 mmol) was added to reduce selenium powder, and the flask instantly purged with

nitrogen gas to create an inert atmosphere. After 2 h of Se digestion, a clean colourless solution represents the complete reduction of selenium powder. A solution of zinc source ($ZnCl_2$ or $ZnCO_3$) dissolved in de-ionized water (20.0 mL) was added to the reduced selenium solution and water soluble capping agent (cysteine) was added instantly under inert N_2 conditions. The reactions were carried at room temperature and 90 ^oC. The ratio of Zn:Se was kept at 1:1 and that of zinc to a capping group (Zn:TEA or Zn:cysteine) was kept at 1:20. The aliquots were withdrawn at 1, 3, 5, and 18 h intervals and samples were centrifuged to isolate the capped particles.

2.1.2.4 Synthesis of TEA capped ZnSe nanoparticles

In this synthetic procedure, TEA has been chosen as a capping agent. ZnSe nanoparticles have been synthesized by the reduction of selenium powder (0.32 mmol) with sodium borohydrate (0.81 mmol) using de-ionized water as a solvent under inert atmosphere to produce selenide ions. The complete reduction of selenium took about 2 h leading to the formation of clear colourless solution. After 2 h of selenium reduction, simultaneous addition of zinc salt (zinc chloride or zinc carbonate) and a capping agent (TEA) led to the formation of TEA capped ZnSe nanoparticles. The synthesis was carried at room temperature and at 90 ^oC, while the pH of the reaction medium was varied from 4, 7 and 11 using dilute hydrochloric acid and ammonia solutions to control the pH. The ratio of Zn:Se was fixed to 1:1 and that of Zn:TEA to 1:20. The aliquots were withdrawn at 1, 3, 5 and 18 h, respectively. The samples were centrifuged and redispersed in de-ionized water for characterization.

2.1.3 Characterization

The synthesized particles were characterized by UV-Vis, photoluminescence, X-ray diffraction, TEM, HR-TEM and FT-IR techniques.

2.1.3.1 Optical characterization

Perkin Elmer Lambda 25 UV-Vis Spectrophotometer was used to carry out the optical measurements and the samples were placed in cuvettes (1 cm, path length), using deionized water and/or methanol as a reference solvent. A Perkin Elmer LS 55 Lumminiscence Spectrophotometer was used to measure the photoluminescence of the particles. The samples were placed in cuvettes (1 cm path length). The measurements were done at room temperature.

2.1.3.2 TEM and HR-TEM analysis

The transmission electron microscopy (TEM) and high resolution transmission electron microscopy (HR-TEM) images were obtained using a JEOL 1010 and JEOL 2100 respectively. Viewing was done at an accelerating voltage of 100 kV (TEM) and 200 kV (HR-TEM), and images were captured digitally using a Megaview III camera; stored and measured using Soft Imaging Systems iTEM software.

2.1.3.3 X-Ray diffraction

The diffraction patterns were recorded in the high angle 2θ range of 10-80^{o} using a Bruker AXS D8 Advance X-ray diffractometer, equipped with nickel filtered Co K_{α} radiation (λ = 1.5418 Å) at 40 kV, 40 mA and at room temperature. The scan speed and step size were 0.05^{o} min^{-1} and 0.00657 respectively.

2.1.3.4 FT-IR analysis

Bruker FT-IR spectrometer was used for the FT-IR measurements. Solid samples were dried and ground to fine powder and the spectra were recorded using a Tensor 27. Liquid samples were directly measured without further preparative techniques.

2.2 Results and discussion

2.2.1 Cysteine capped CdSe nanoparticles

The synthetic procedure used in this study involves the addition of cadmium salt to freshly prepared aqueous selenium solution. The reaction was carried at room temperature and at 90 ^{o}C and the metal sources used are cadmium chloride and cadmium carbonate. The same synthetic procedure was used to synthesize to ZnSe nanoparticles using different capping agents (TEA and systeine). The reaction representing the formation of cysteine capped-CdSe nanoparticles is shown in Equations 2.1.

$$4\,NaBH_4 + 2\,Se + 7\,H_2O \xrightarrow[N_2,\ R.T.]{2\ h} 2\,NaHSe + Na_2B_4O_7 + 14\,H_2$$

$$NaHSe + CdCl_2/CdCO_3 \xrightarrow[R.T./\ 90\ ^{o}C]{N_2} \text{Cysteine-capped CdSe} + NaCl + HCl$$

Equations 2.1 Equations representing the synthetic route for cysteine-capped CdSe nanoparticles synthesized at room temperature (R.T) and at 90 ^{o}C.

2.2.1.1 Optical properties of cysteine capped CdSe: Effect of pH

The effect of pH on the behavior of absorption and photoluminescence spectra under different pH (4, 7 and 11) was investigated. The nanoparticles synthesized with pH 11 showed unique behavior in its absorption spectrum compared to the nanoparticles synthesized at pH 4 and 7. The nanoparticles synthesized at pH 11 displayed showed two excitonic peaks, one at 225 nm and another at 430 nm. The reason for the formation of two excitonic peaks could be due to the polydispersity of the nanoparticles. The cysteine capped CdSe nanoparticles exhibiting excitonic peak at 225 nm had been previously reported [18].

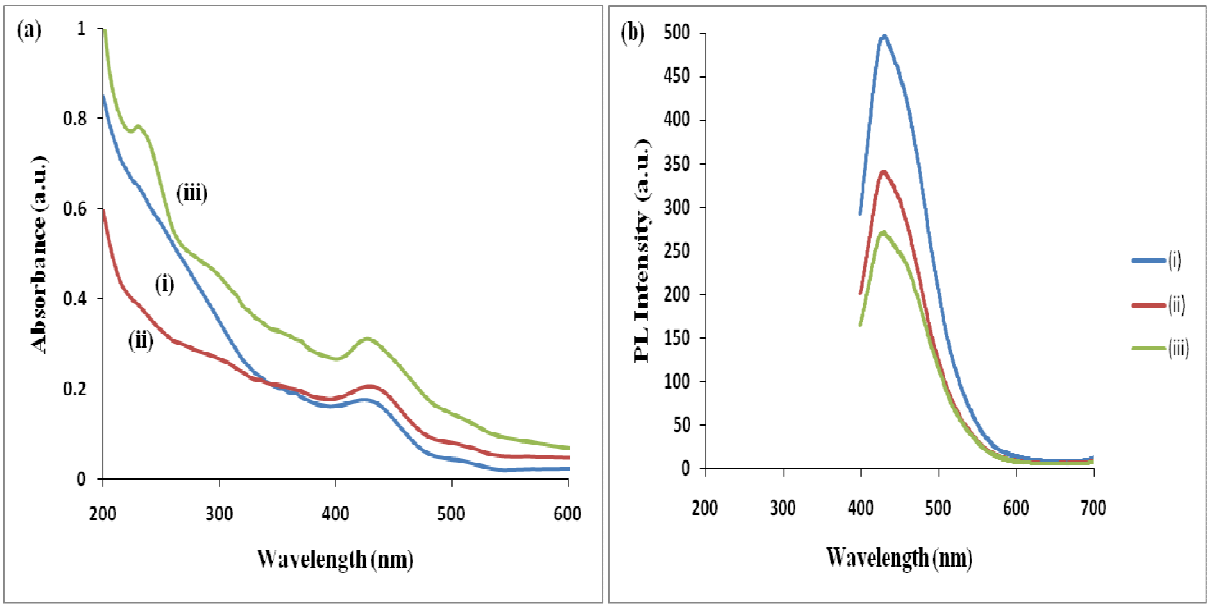

Figure 2.1 (a) Absorption and (b) photoluminescence spectra of cysteine capped CdSe nanoparticles synthesized at (i) pH 4 (ii) pH 7 and (iii) pH 11 using $CdCl_2$ source.

The absorption (Figure 2.1a) and the emission (Figure 2.1b) spectra under all the reaction conditions are blue shifted when compared to their bulk counterparts which is 716 nm. The band

edges of the nanoparticles synthesized under different pH standards have been compared. The nanoparticles obtained at pH 4, displayed a band edge at 490 nm, whereas those synthesized at pH 7 displayed a band edge at 500 nm. A band edge of 530 nm and an excitonic peak at 370 nm was observed when the pH of the solution was further increased to 11. The photoluminescence spectra of the as synthesized CdSe nanoparticles are shown in Figure 2.1b. The nanoparticles synthesized at different pH conditions displayed emission maximum at approximately 435 nm.

2.2.1.2 Optical properties of cysteine capped CdSe: Effect of reaction time

The effect of the reaction time on the optical properties of cysteine capped CdSe nanoparticles was also investigated. This was done by keeping certain reaction parameters constant and varying the reaction time by withdrawing aliquots at pH 11. Figure 2.2 shows the absorption and photoluminescence spectra of cysteine capped CdSe nanoparticles at room temperature at different reaction times. The absorption band edges are blue shifted when compared to their bulk counterparts, an indication of quantum confinement. The absorption band edges for the samples are at 460 nm, 2.66 eV (1 h), 465 nm, 2.63 eV (3 h), 470 nm, 2.60 eV (5 h) and 600 nm, 2.04 eV (18 h). The shift of the absorption band gaps to lower energies as the reaction time increases is attributed to the increase in particle size. The absorption shoulders become narrow as the reaction time decreases indicating the narrowing of particle size distribution.

The emission properties of cysteine capped CdSe nanoparticles were also investigated at different reaction times. The photoluminescence spectra of the as-synthesize cysteine capped CdSe nanoparticles are shown in Figure 2.2b. The as-synthesized cysteine capped CdSe nanoparticle exhibit exceptionally narrow emission peaks, reflecting negligible surface emission

and significant confinement. The emission maximum is observed at 435 nm for samples prepared at shorter reaction times and the sample prepared at longer reaction time of 18 h shows a slight red-shift, with a slight increase in the FWHM as the reaction time increases.

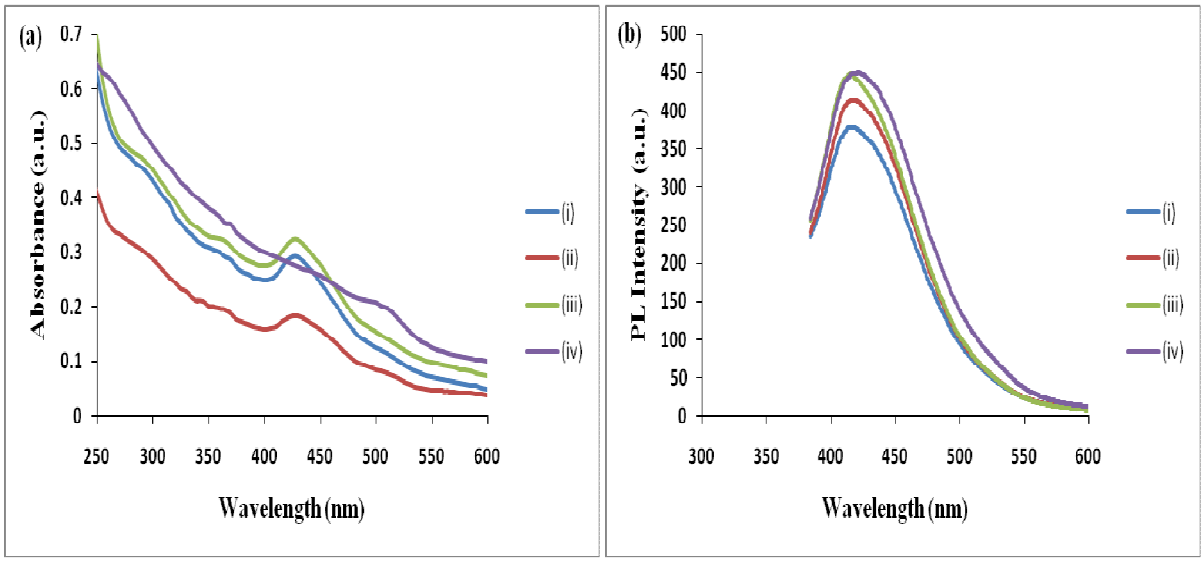

Figure 2.2 (a) Absorption and (b) photoluminescence spectra of cysteine capped CdSe nanoparticles synthesized after reaction times of (i) 1 (ii) 3 (iii) 5 and (iv) 18 h using $CdCl_2$ source.

2.2.1.3 Structural and morphological properties of cysteine capped CdSe nanoparticles: Effect of pH

The structural properties of the as-synthesized cysteine capped CdSe nanoparticles were studied using TEM, XRD, HR-TEM and FT-IR techniques. The TEM images of cysteine capped CdSe nanoparticles are shown in Figure 2.3. The growth mechanism of the nanoparticles was studied at different pH values (4, 7 and 11). The particles are not mono-dispersed but are of aggregated in nature as shown in Fig. 2.3.

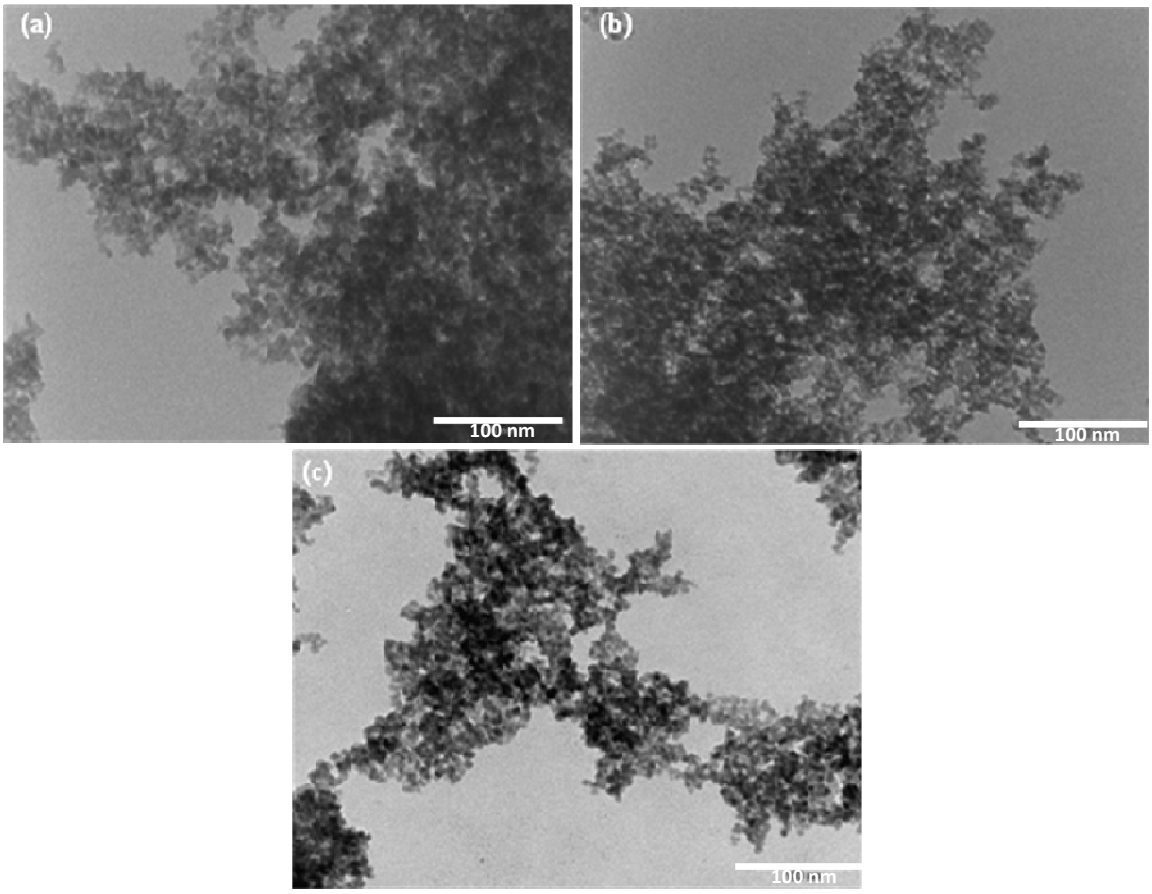

Figure 2.3 TEM images of cysteine capped CdSe nanoparticles synthesized at (a) pH 4 (b) pH 7 and (c) pH 11 using $CdCl_2$ source.

The nanoparticles synthesized at pH 4 (Figure 2.3a) yielded the particles with average particle sizes of 8.42 ± 1.92 nm, whereas those synthesized at pH 7 (Figure 2.3b) had an average particle size of 5.89 ± 1.46 nm. The decrease in particle size is in good agreement with the optical spectra data. All the nanoparticles synthesized under different pH conditions had a spherical morphology. The average particle size of the nanoparticles synthesized at pH 11 was 7.88 ± 2.86 nm.

2.2.1.4 Structural properties of cysteine capped CdSe nanoparticles: Effect of cadmium source

The morphological properties of the nanoparticles involving the use of different cadmium sources ($CdCl_2$ and $CdCO_3$) were investigated. Figure 2.4 shows the TEM images of CdSe nanoparticles synthesized with (a) cadmium carbonate and (b) cadmium chloride as sources at pH 11 after a reaction time of 18 h. It is clear from the images that the nanoparticles synthesized using cadmium carbonate as a source showed particles that are aggregated with an average particle size of 10.49 ± 2.60 nm. This effect may be due to the fact that cadmium carbonate is less soluble than the other cadmium salts and as a result they participate in self capping.

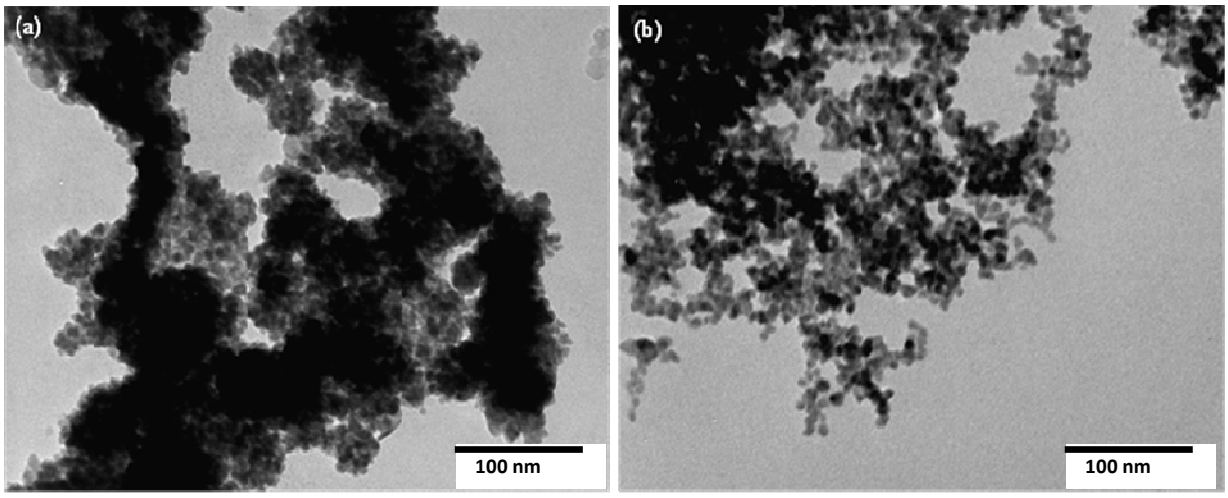

Figure 2.4 TEM images of cysteine capped CdSe nanoparticles synthesized from (a) cadmium carbonate and (b) cadmium chloride sources.

The nanoparticles synthesized from cadmium chloride as a source resulted in the particles that are reasonably monodispersed with an average particle size of 8.49 ± 1.31 nm which is smaller

than that obtained from carbonate source. Both the sources resulted in particles that are spherical in shape.

The crystallographic analysis of cysteine capped CdSe nanoparticles was performed to study its crystal phase structure. The diffraction pattern of the CdSe nanoparticles synthesized from cadmium chloride at pH 7 showed three typical distinct peaks as shown in Figure 2.5. The first peak at 2θ = 25.6º is due to the (111) reflection and the two broad peaks appearing at 2θ = 42.4º and 49.8º correspond to the (220) and (311) reflections, respectively. This can be indexed to the cubic phase of CdSe nanoparticles. The present experimental scheme is a convenient route to acquire highly crystalline cubic structure of CdSe nanoparticles which agree with the results that we have reported recently with TEA capped CdSe nanoparticles [43]. No peaks corresponding to impurities were detected, indicating the high purity of the material.

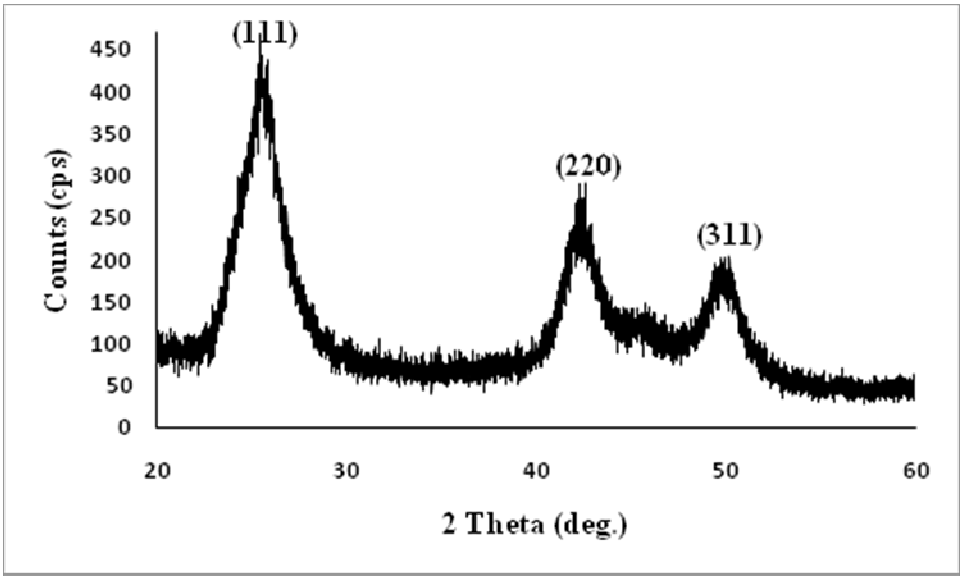

Figure 2.5 XRD pattern of the cysteine capped CdSe nanoparticles synthesized from cadmium chloride source at pH 7.

The crystallinity of the as-synthesized cysteine capped CdSe nanoparticles was further confirmed by HR-TEM studies. The HR-TEM images of cysteine capped CdSe nanoparticles synthesized at different pH values are shown in Figure 2.6. The HR-TEM images showed all the nanoparticles that are of crystalline in nature and the distinct lattice fringes with an interplanar distance of 3.44 Å indexed to the (111) plane of cubic CdSe.

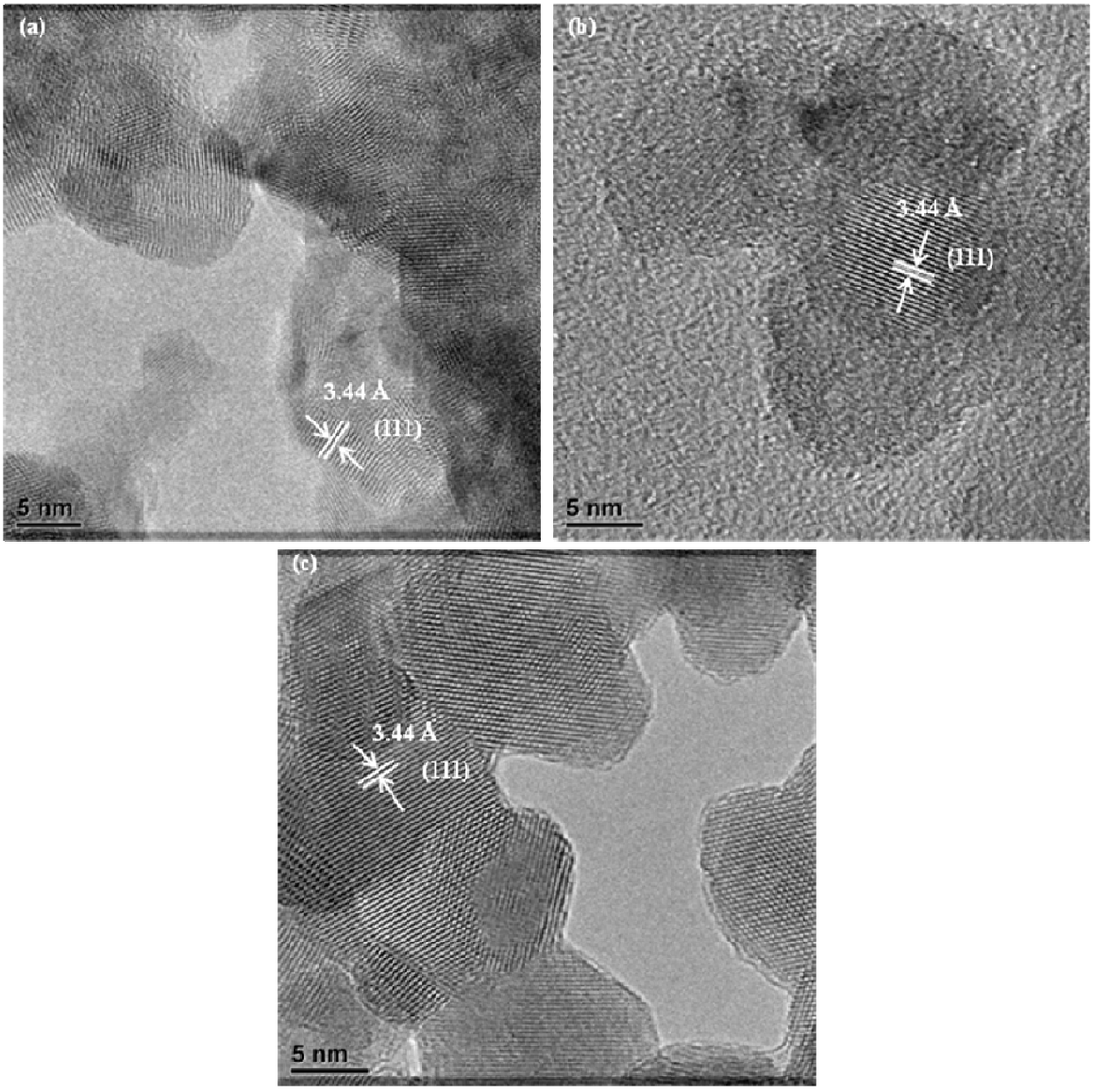

Figure 2.6 HR-TEM images of cysteine capped CdSe nanoparticles synthesized at (a) pH 4 (b) pH 7 and (c) pH 11.

The capping of CdSe nanoparticles by cysteine was further confirmed by FT-IR spectroscopy. The typical spectra of amino acids usually are of carboxylate and primary amine salts. The presence of the $–COO^-$ group was confirmed by the IR absorption observed around 1637 and 1430 cm^{-1} (Figure 2.7). Covalent bonding between thiols and the surface of CdSe hindered the existence of the S-H group vibration at 2550-2670 cm^{-1} on the cysteine capped CdSe nanoparticles. The shift of the carboxylic group stretching frequency from 1717 cm-1 to 1631 cm^{-1} could be due to the change of dipole moment caused by binding of cysteine with high electron density metal surface [44]. These results confirm the capping of CdSe nanoparticles by cysteine.

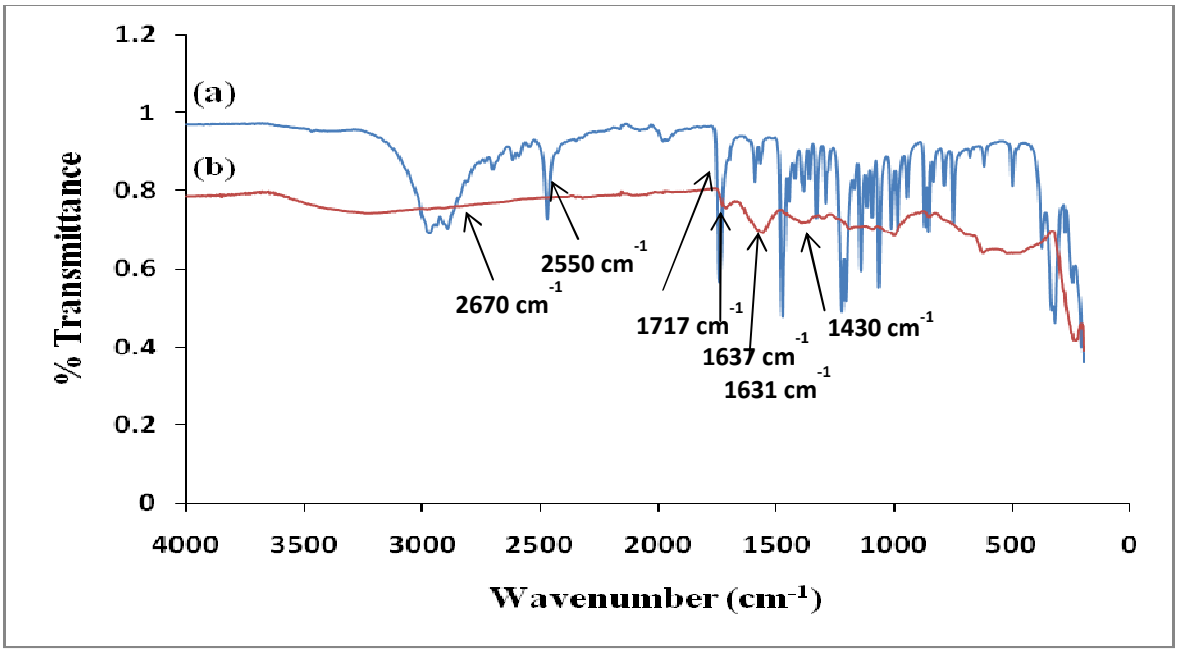

Figure 2.7 FT-IR spectra of (a) cysteine and (b) cysteine capped CdSe nanoparticles synthesized with cadmium chloride source for a room temperature reaction at pH 7 after 3 h.

2.2.2 TEA capped CdSe nanoparticles

Water-soluble amino alcohols such as triethanolamine (TEA) have been used as surface stabilizing agents for nanoparticles. There have been few reports on the synthesis of TEA-capped nanoparticles such as CdSe, PbS, CdS and ZnSe [11,40,45,46]. The CdSe particles are attached to TEA through the amino group. The amino group binds to the Cd atom and the RNH_2^- amino polar group provides the hydrophilicity function. This work presents the synthesis of TEA capped CdSe nanoparticles. The synthesis involves the simultaneous addition of a cadmium source and a capping agent to a freshly prepared aqueous selenium solution at room temperatuture. The mole ratios of Cd:Se were varied from 1:1, 1:4 1:6 to 4:1. The typical reaction showing the step by step synthesis of TEA capped CdSe nanoparticles is shown in Equations 2.2.

$$4\,NaBH_4 + 2\,Se + 7\,H_2O \xrightarrow[N_2,\ R.T.]{2\ h} 2\,NaHSe + Na_2B_4O_7 + 14\,H_2$$

$$NaHSe + ZnCl_2 \xrightarrow[TEA,\ R.T.\ or\ 90\ ^oC]{N_2} TEA\text{-}capped\ ZnSe + NaCl + HCl$$

Equations 2.2 Equations representing the synthetic route for TEA-capped cadmium selenide nanoparticles.

2.2.2.1 Optical properties of TEA capped CdSe nanoparticles: Effect of Cd:Se ratio

UV-Vis and photoluminescence spectroscopy have been used to study the effect of Cd:Se molar concentrations on the optical properties of the as-synthesized CdSe nanoparticles. The absorption and photoluminescence spectra of the TEA capped CdSe nanoparticles with varying Cd:Se mole

ratios are shown in Figure 2.8. The observed absorption spectra are typical for CdSe with distinct excitonic peaks at about 450 nm for all the reaction conditions. The absorption band edge for the CdSe nanoparticles with Cd:Se mole ratios of 1:1, 1:4 1:6 and 4:1 were 518, 516, 500 and 537 nm, respectively. The emission spectra shows narrow emission with the maxima for the CdSe nanoparticles with Cd:Se mole ratios of 1:1, 1:4 1:6 and 4:1 observed at 456, 456, 457 and 455 nm respectively.

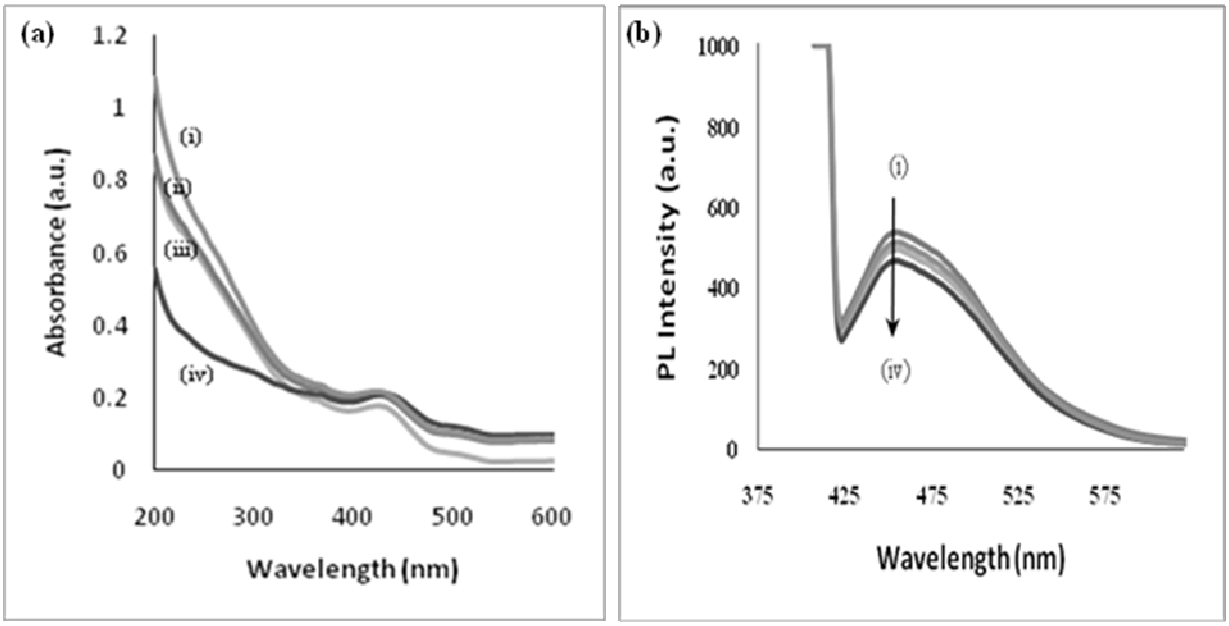

Figure 2.8 (a) Absorption and (b) photoluminescence spectra of CdSe nanoparticles synthesized with (i) 1:1-Cd:Se (ii) 1:4-Cd:Se (iii) 1:6-Cd:Se (iv) 4:1-Cd:Se and 1:20-Cd:TEA mole ratio.

2.2.2.2 Structural properties of TEA capped CdSe nanoparticles: Effect of Cd:Se ratio

Transmission electron microscopy (TEM) was used to determine the particle size and morphology of the TEA capped CdSe nanoparticles. In order to study the effect of the Cd to Se concentration on the particle size, the reaction was monitored by varying the mole ratio of Cd:Se and keeping Cd:TEA mole ratio constant at 1:20, reaction time ~18 h and at a pH of 8.0.

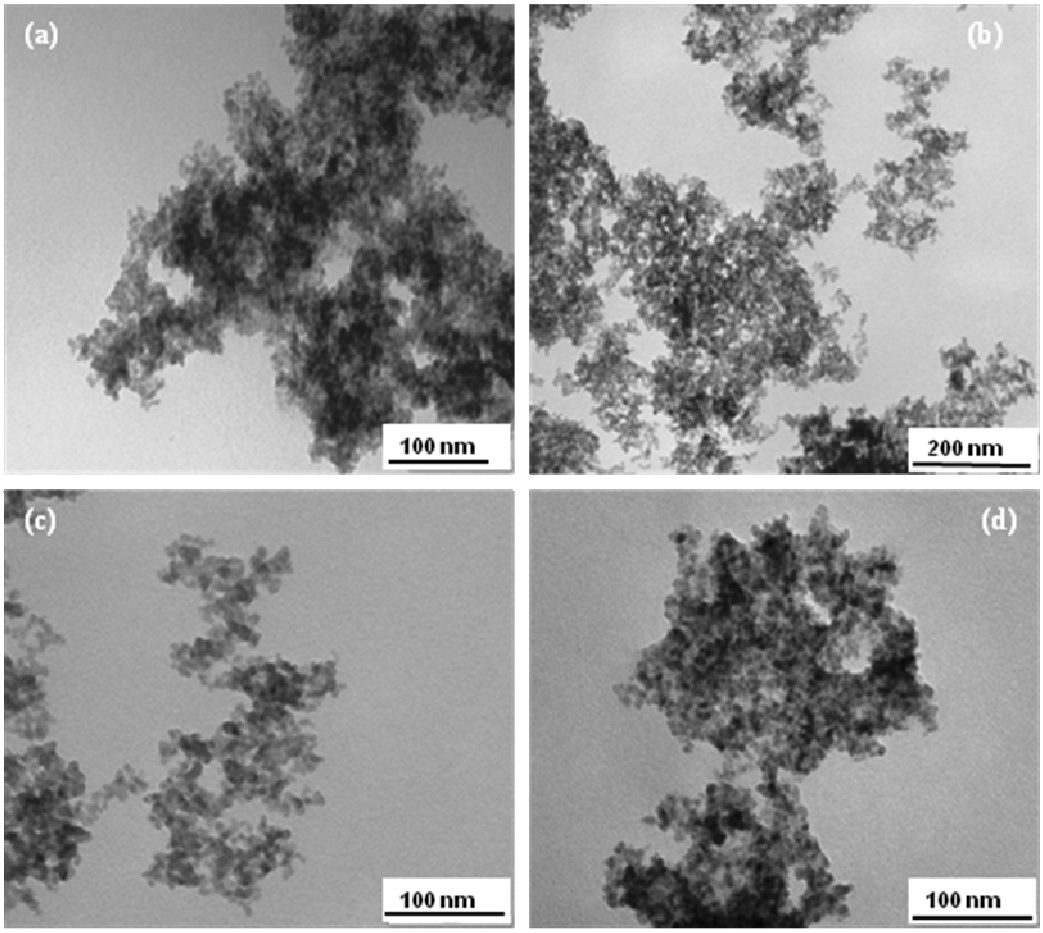

Figure 2.9 TEM images of CdSe nanoparticles synthesised with (a) 1:1-Cd:Se (b) 1:4-Cd:Se (c) 1:6-Cd:Se and (d) 4:1-Cd:Se and 1:20-Cd:TEA mole ratios.

Figure 2.9 shows the TEM images for the CdSe nanoparticles synthesized at different Cd:Se mole ratios. All images show well defined particles within the matrix of the capping group. With the Cd:Se mole ratio at 1:1, the average size of the particles observed was 9.95 ± 1.45 nm ranging from 8-19 nm (Figure 2.9a). When the ratio of Cd:Se was increased to 1:4 (Figure 2.9b), the average particle size increased to 13.50 ± 1.90 nm. Whereas, with the 1:6-Cd:Se ratio the average particle size was found to be 9.47 ± 0.84 nm (Figure 2.9c). The 4:1-Cd:Se mole ratio resulted particles with an average size of 9.53 ± 1.42 nm (Figure 2.9d). The variation of selenium

concentration had induced a slight change in the particles size, however, the 1:4-CdSe concentration produced the particles that are predominantly larger as compared to other mole ratio variations. There is also very little variation of particle shape with change in mole ratio of the starting materials.

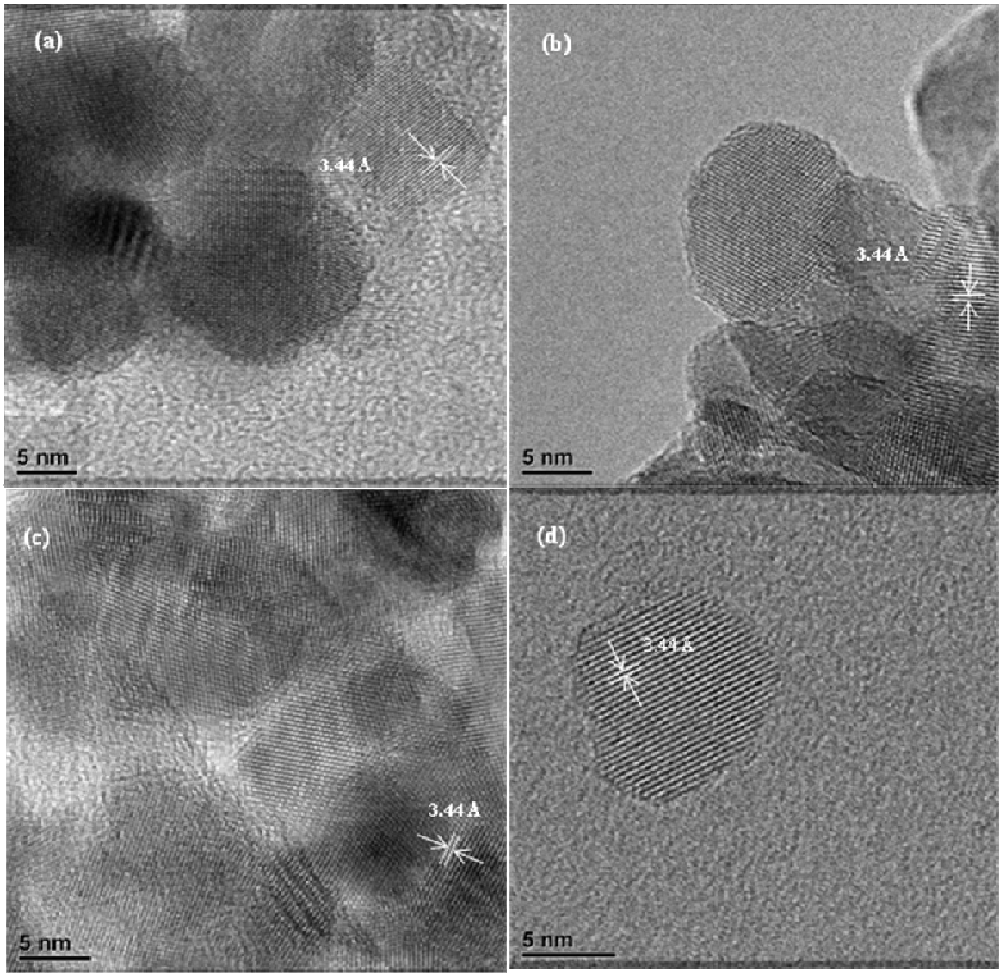

Figure 2.10 HR-TEM image of the CdSe nanoparticles synthesised with (a) 1:1-Cd:Se, (b) 1:4-Cd:Se and (c) 4:1-Cd:Se and 1:20-Cd:TEA mole ratios.

The HR-TEM images show particles with distinct lattice fringes (Figure 2.10). From the HR-TEM images, it is clear that the crystalline particles are surrounded by the triethanolamine

matrix. The lattice spacing of 3.44 Å visible in all images can be indexed to the (111) plane of cubic CdSe.

2.2.2.3 Structural properties of TEA capped CdSe nanoparticles: Effect of reaction time

In order to study the effect of the reaction time on the growth of CdSe nanoparticles, parameters such as Cd:Se and Cd:TEA mole ratios were kept constant at 1:1, 1:20, respectively, and the pH of the solution was kept at 8.0. The effect of the reaction time on the growth of the nanoparticles was monitored by varying the duration of the reaction involving 1:1-Cd:Se and 1:20-Cd:TEA mole ratios at a pH of 8.0. When the reaction time was 10 min, the average particle size was 8.04 ± 1.18 nm (Figure 2.11a), and when the reaction time was increased to 25 min (Figure 2.11b) and 3 h (Figure 2.11c), resulted in the average particle size of 7.62 ± 1.29 nm and 8.84 ± 1.37 nm, whereas with 18 h reaction, the average particle size observed was 8.33 ± 1.06 nm (Figure 2.11d). This trend shows that with the increase in the duration of reaction from 10 min to 18 h, the average size of the particles become smaller. This decrease in particle size could be due to digestive ripening, a process whereby particles are broken into smaller fragments [47]. Factors such as type of ligands, solvents and surfactants have been identified as the driving force for this mode of growth.

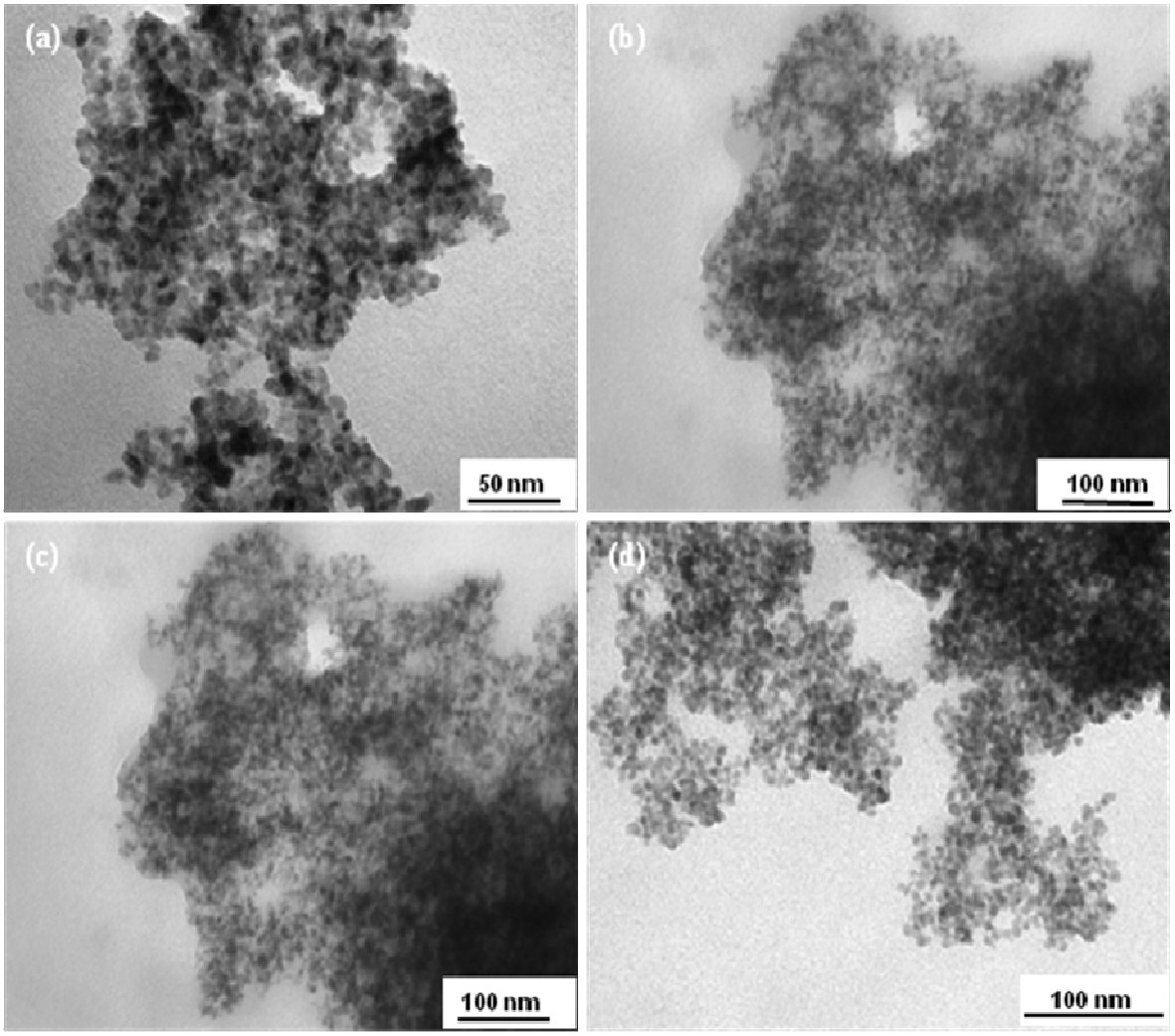

Figure 2.11 TEM images of CdSe nanoparticles synthesised with 1:1-Cd:Se and 1:20-Cd:TEA mole ratios (a) for 10 min (b) 25 min (c) 3 h and (d) for 18 h reaction at pH 8.

The crystallographic study of the as synthesized TEA capped CdSe nanoparticles was performed using the XRD technique. From the XRD pattern (Figure 2.12), three typical distinct peaks can be distinguished. The first peak at $2\theta = 25.6^{\circ}$ is due to the (111) reflection and the two broad peaks appearing at $2\theta = 42.4^{\circ}$ and 49.8° results from the (220) and (311) reflections, respectively. The present experimental scheme is a convenient route to acquire highly crystalline cubic

structure of CdSe nanoparticles which agree with the results that have previously been reported [31] and no peaks corresponding to impurities were detected, indicating the high purity of the product.

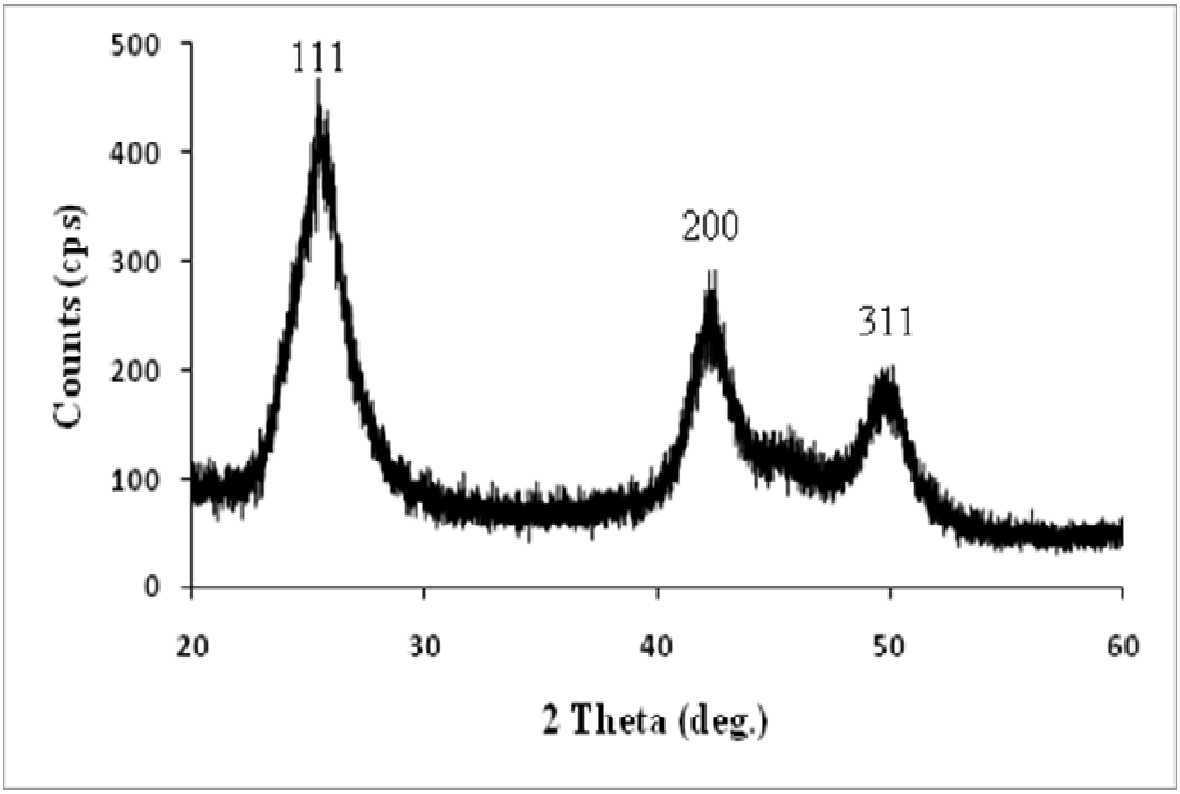

Figure 2.12 XRD pattern of the CdSe nanoparticles synthesised with 1:1-Cd:Se and 1:20-Cd:TEA mole ratios for 18 h reaction at pH 8.

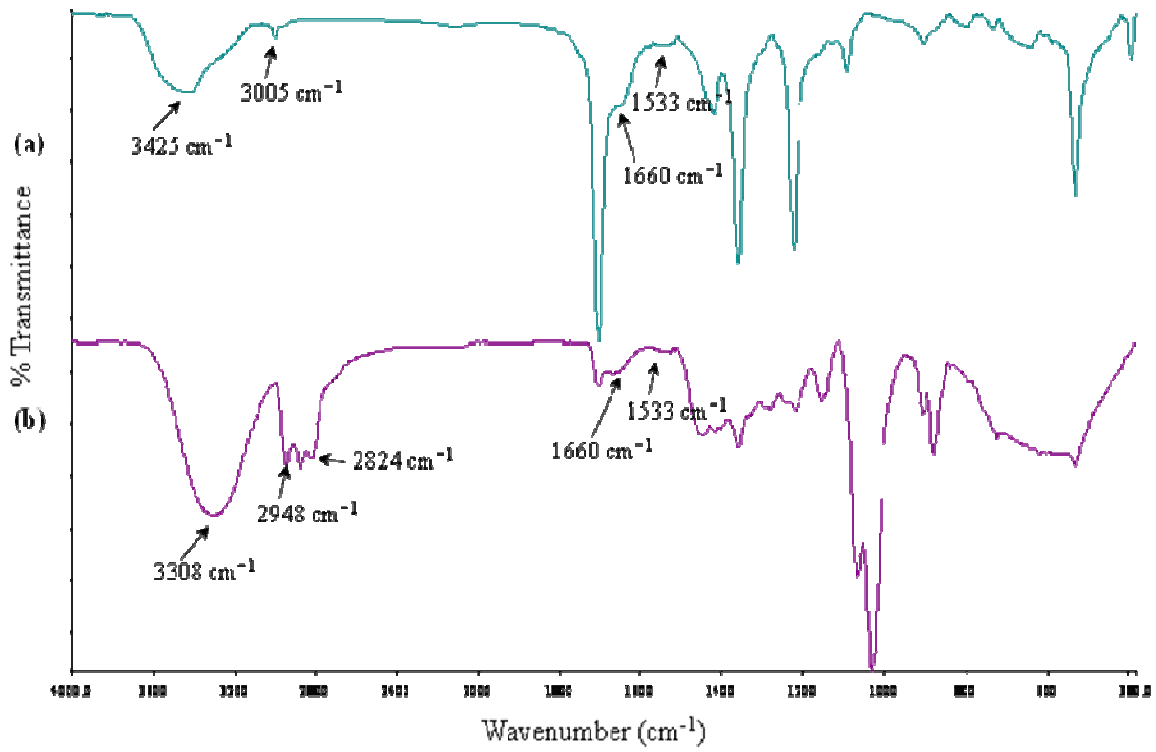

Figure 2.13 FT-IR spectra of (a) TEA capped CdSe nanoparticles and (b) TEA.

In orders to confirm the capping efficiency of the ligand, the FT-IR analysis were performed. The FT-IR spectra of TEA capped CdSe nanoparticles and that of TEA are shown in Figure 2.13. The FT-IR results reveal that the CdSe particles are coordinated to the TEA ligand. The peak observed at 1360 cm^{-1}, the multiplet at around 2824 - 2948 cm^{-1}, and the peak around 3005 cm^{-1} can be attributed to C–H stretching. The broad bands around 3308 cm^{-1}, 3425 cm^{-1} and shoulder at around 1660 cm^{-1} could be due to the –OH stretching [31,48]. The NH stretching can be seen at around 3420-3440 cm^{-1} and NH bending at 1533 cm^{-1}.

2.2.3 Cysteine capped ZnSe nanoparticles

Water soluble ZnSe were under similar reaction conditions to the cadmium based nanoparticles. Zinc chloride and zinc carbonate were used as the metal sources.

2.2.3.1 Optical properties of cysteine capped ZnSe nanoparticles: Effect of pH

The optical properties of cysteine capped ZnSe nanoparticles were studied at different pH and reaction times. The absorption and the photoluminescence spectra of an aqueous solution of cysteine capped ZnSe nanoparticles at different pH (4, 7 and 11) after 1 h reaction time are shown in Figures 2.14- 2.16. The particles showed clearly defined excitonic peaks at 365 nm (Figure 2.14), 372 nm (Figure 2.15) and 400 nm (Figure 2.16) respectively, evidence for the formation of particles with sizes in the order of the nanometer range indicating strong quantum confinement. The pH 11 sample shows a more pronounced excitonic peak. The absorption band gap is observed at 410 nm (pH 4), 440 nm (pH 7) and 418 (pH 11). The PL maxima for all samples are observed at approximately 425 nm.

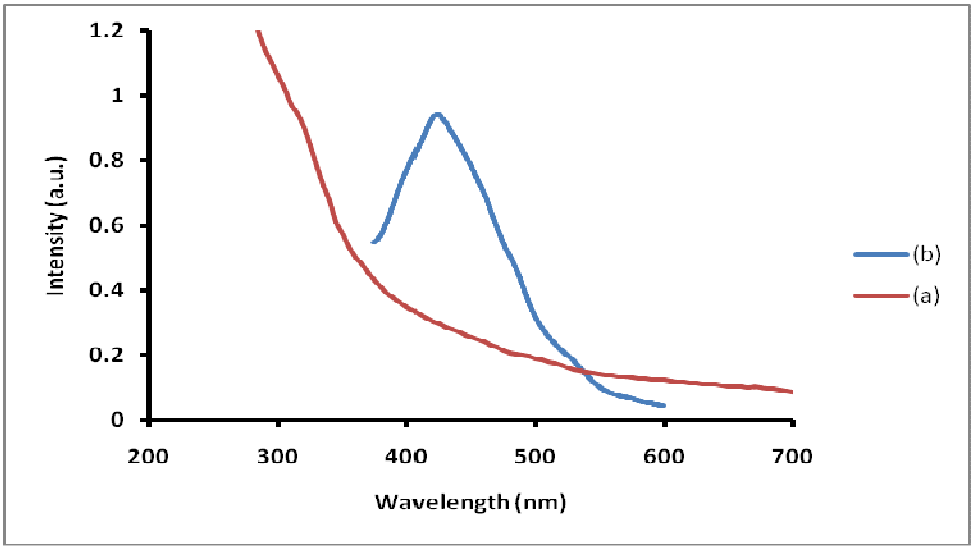

Figure 2.14 (a) Absorption and (b) photoluminescence spectra of cysteine capped ZnSe nanoparticles synthesized at pH 4.

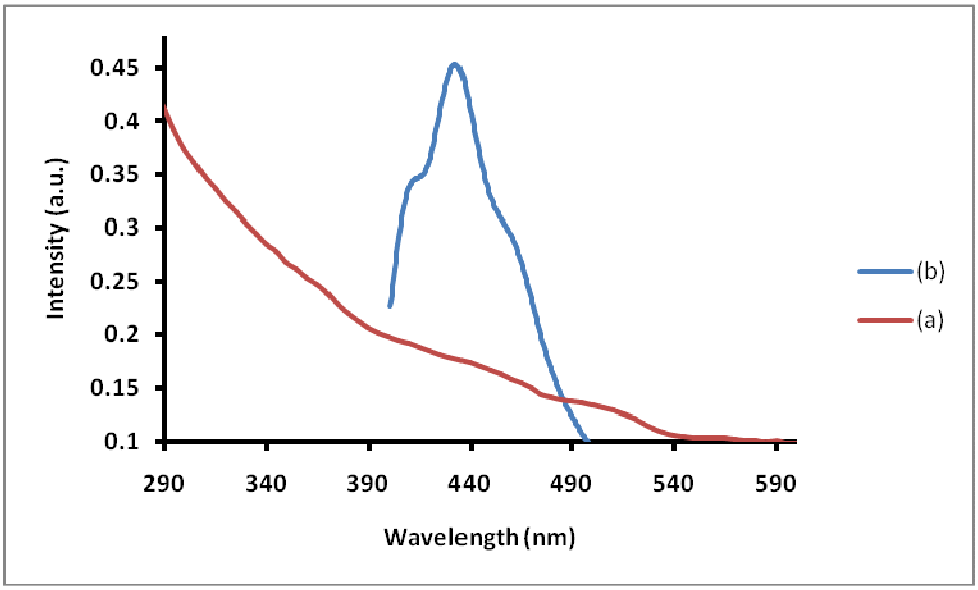

Figure 2.15 (a) Absorption and (b) photoluminescence spectra of cysteine capped ZnSe nanoparticles synthesized at pH 7.

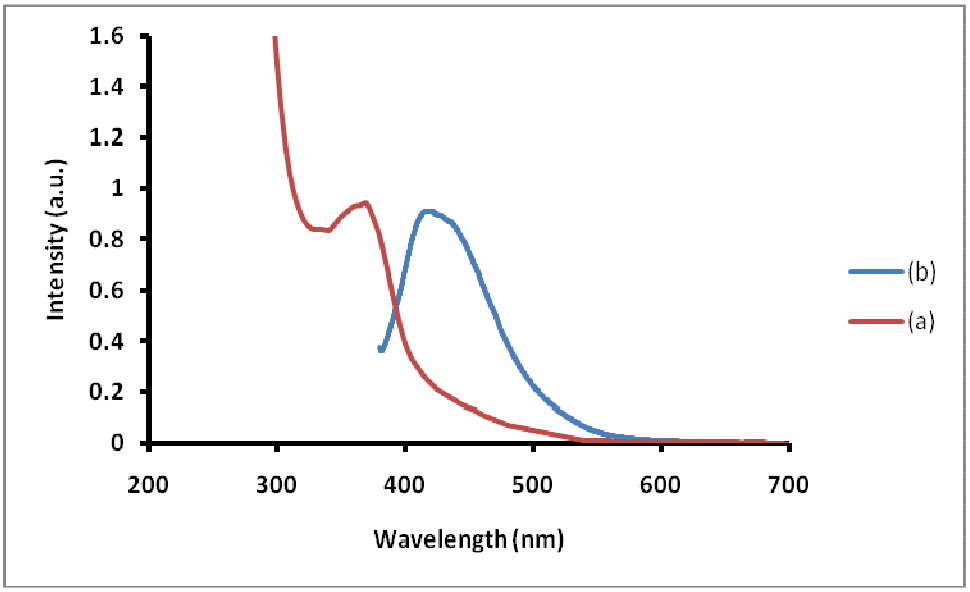

Figure 2.16 (a) Absorption and (b) photoluminescence spectra of cysteine capped ZnSe nanoparticles synthesized at pH 11.

2.2.3.2 Effect of the reaction time on optical properties

The reaction at pH 11 was repeated with samples collected at different reaction times (1, 3, 5 and 18 h). The absorption spectra are shown in Figure 2.17. In relation to the bulk band gap of ZnSe, the absorption band-edges showed a blue shift in relation to their bulk counterparts indicating quantum confinement. The particles synthesized under the reaction time of 1 and 3 h exhibit sharp pronounced excitonic peaks which indicate that the as-synthesized particles are mono-dispersed. The ZnSe nanoparticles synthesized after 18 h did not show any excitonic features. With an increase in the reaction time, the band gaps varied from 410 nm (for 1 h), 415 nm (for 3 h), 440 nm (for 5 h) and 500 nm (for 18 h) confirming an increase in the particle size with an increase in reaction times.

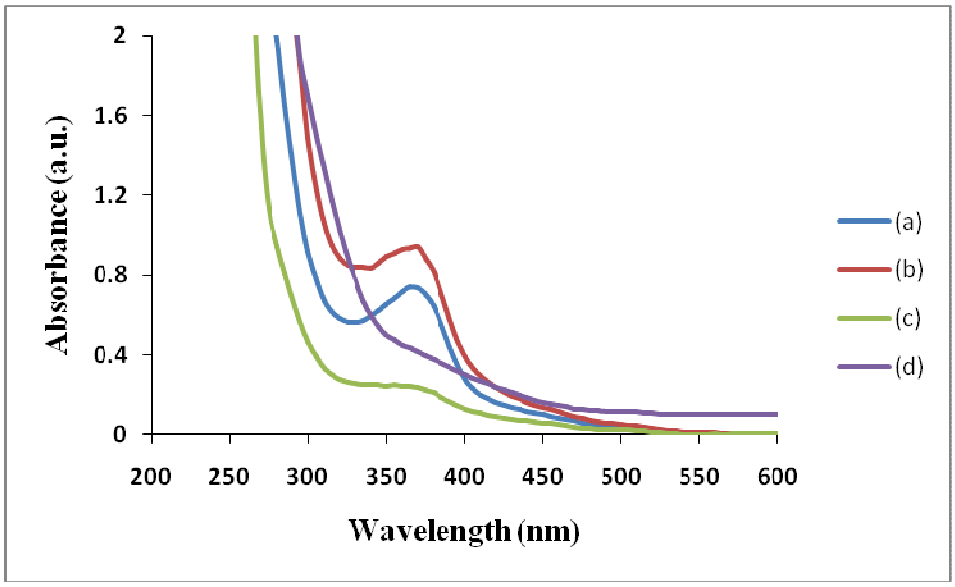

Figure 2.17 Absorption spectra of cysteine capped zinc selenide nanoparticle synthesized using zinc chloride source for (a) 1 (b) 3 (c) 5 and (d) 18 h reaction time at pH 11 and room temperature.

2.2.3.3 Optical properties of cysteine capped ZnSe nanoparticles: Effect of zinc source

The effect of the zinc source on the optical properties of the as-synthesized cysteine capped ZnSe nanoparticles was investigated. Zinc carbonate was used as the alternate zinc source. The absorption and photoluminescence spectra of the cysteine capped ZnSe nanoparticles synthesized with zinc chloride and with zinc carbonate are shown in Figure 2.18. In both cases, the reaction was carried at room temperature and at pH 7 for 1 h. The reaction studies using zinc chloride source resulted in a band gap of 380 nm (Figure 2.18a-i) while zinc carbonate source yielded a band gap of 520 nm (Figure 2.18a-ii).

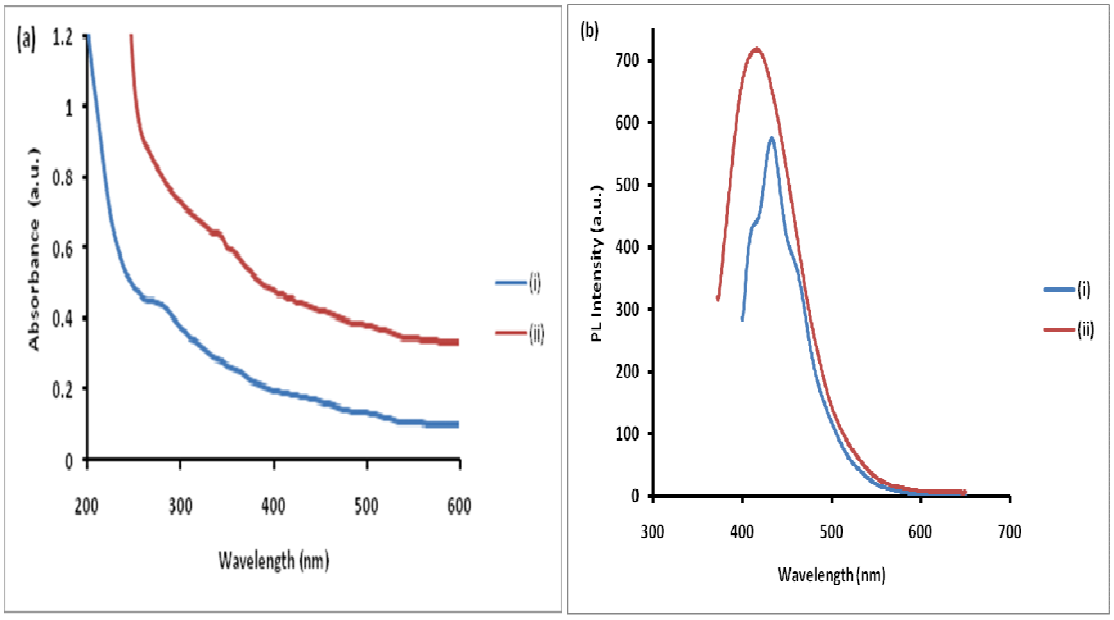

Figure 2.18 (a) Absorption and (b) photoluminescence spectra of cysteine capped ZnSe nanoparticles synthesized at pH 7 and room temperature with (i) zinc chloride and (ii) zinc carbonate sources after 1 h.

The emission maximum for the zinc chloride sample (Figure 2.18b-i) appeared at about 433 nm and that of zinc carbonate sample (2.18b-ii) appeared at 420 nm, in which the zinc chloride source resulted in narrow emission as compared to that obtained using the zinc carbonate source. The shift of the optical band gap of the nanoparticles synthesized using zinc chloride as compared to that synthesized with zinc carbonate is due to the reduction of particle size. The narrow emission of the nanoparticles synthesized with zinc chloride results from the narrowing of particle size distribution.

2.2.3.4 Structural properties of cysteine capped ZnSe nanoparticles: Effect of pH

The TEM images of cysteine capped ZnSe nanoparticles at different pH values (4, 7 and 11) for 3 h reaction time are shown in Figure 2.19. It was extremely difficult to estimate the size of the particles of ZnSe synthesized at pH 4 (Figure 2.19a). This effect could be caused by the large ratio of the uncoordinated thiol groups to the particles, which resulted in the aggregation of ZnSe nanoparticles. The nanoparticles synthesized at pH 7 (Figure 2.19b) are small, nearly mono-dispersed and are of close to spherical morphology. At pH 11, the ZnSe nanoparticles aggregated to form clusters or microspheres with an average size of 148.42 ± 11.99 nm. In correlation with the optical properties, it was noticeable that with the increase of the pH of the solution the size of the particles became smaller as shown in Figure 2.19b for pH 7 (6.8 ± 1.62 nm) and Figure 2.19c for pH 11 (average particle size - 3.79 ± 0.80 nm).

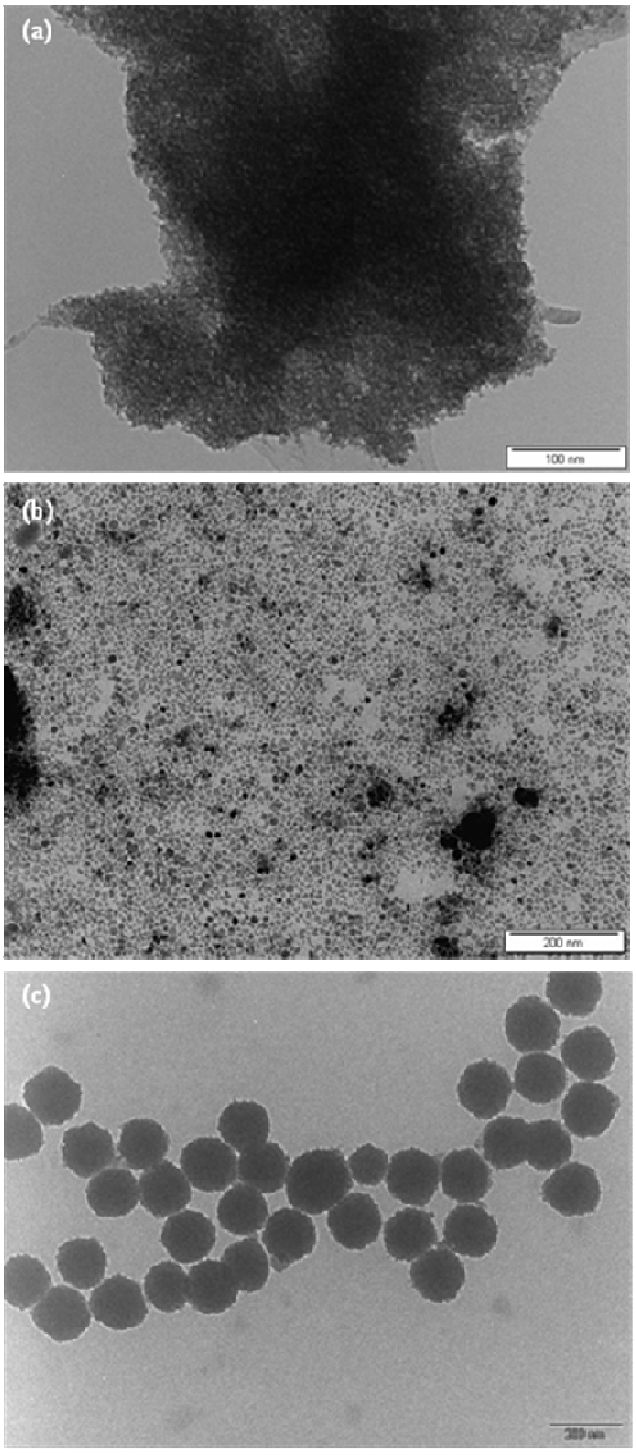

Figure 2.19 TEM images of cysteine capped ZnSe naparticles synthesized at (a) pH 4 (b) pH 7 and (c) pH 11.

2.2.3.5 Structural properties of cysteine capped ZnSe nanoparticles: Effect of reaction time

The effect of the reaction time on the morphology of the as-synthesized ZnSe nanoparticles has been studied. The TEM images of cysteine capped ZnSe nanoparticles at different reaction times (1, 3, 4 and 18 h) synthesized from zinc chloride at pH 11 at room temperature are shown in Figure 2.20.

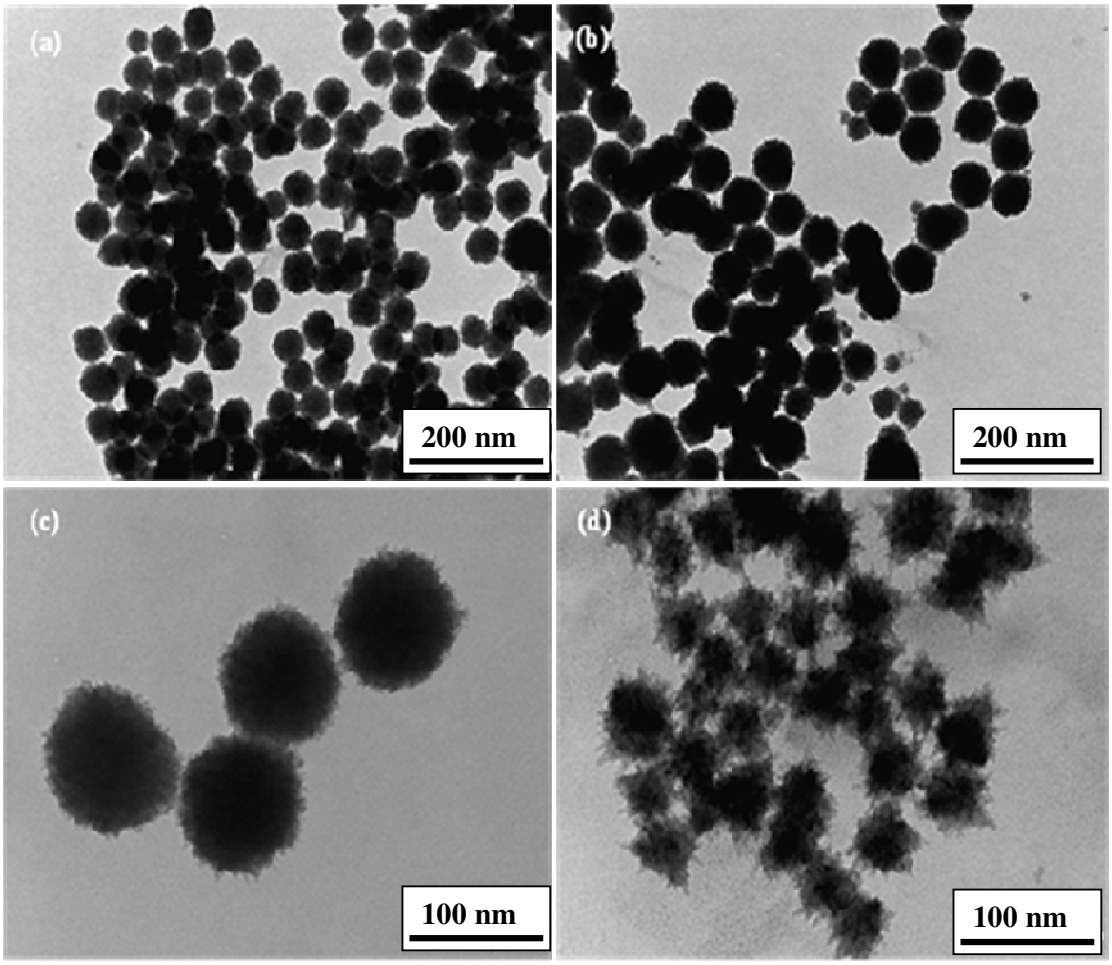

Figure 2.20 TEM images of cysteine capped zinc selenide nanoparticle synthesized after (a) 1 (b) 3 (c) 5 and (d) 18 h.

The nanoparticles synthesized at this pH led to the formation of clusters which varied in diameter as the reaction time was increased. As the reaction time was increased, the diameter of clusters increases as shown in Figure 2.20 from 1h (103.23 ± 6.76 nm), 3 h (123.12 ± 6.66 nm) to 5 h (132.32 ± 10.75 nm). The shape of the nanoclusters synthesized after 18 h reaction time is not regular compared to the nanoclusters synthesized under reaction time less than 18 h which resulted in spherical clusters. The theoretical study of colloidal semiconductors shows that the pH and reaction time have the major effect in control of cluster sizes [49]. It has been experimentally proven that the correlation between the cluster sizes and the band gaps exists. As the size of the cluster increases due to the increase in the reaction time, the band gaps in the absorption spectra shift to lower energies.

2.2.3.6 Structural properties of cysteine capped ZnSe nanoparticles: Effect of zinc source

The TEM images of cysteine capped ZnSe nanoparticles synthesized using zinc chloride (Figure 2.21a) and zinc carbonate at pH 7 are shown in Figure 2.21. The particles obtained from the zinc chloride source are well defined, monodispersed and spheroidal in shape with an average diameter of 6.79 ± 1.66 nm (Figure 2.21a). The zinc carbonate source produced aggregated nanoparticles in the capping matrx making the particle size difficult to determine.

The crystallinity of the as-synthesized cysteine capped nanoparticles was studied with HR-TEM. The HR-TEM images of cysteine capped ZnSe nanoparticles synthesized from the chloride source are shown in Figure 2.22 for (a) pH 7 and (b) pH 11. The existence of lattice planes reveals that the particles are crystalline. The lattice spacing of about 3.42 ± 0.19 Å

(Figure 2.22a) and 3.36 ± 0.20 Å (Figure 2.22b) corresponds to the (111) plane of cubic ZnSe.

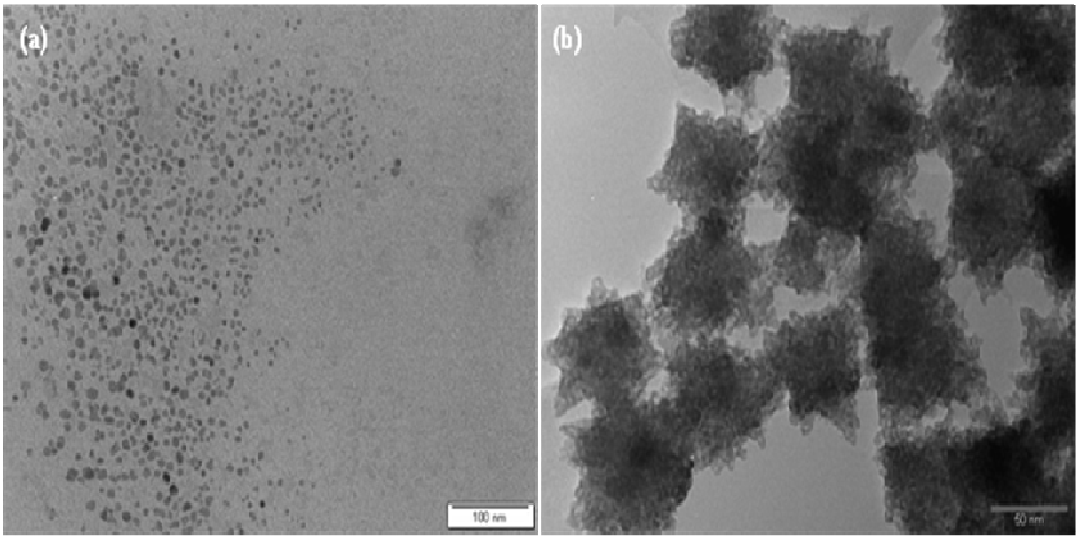

Figure 2.21 TEM images of cysteine capped ZnSe synthesized with (a) zinc chloride (b) zinc carbonate sources.

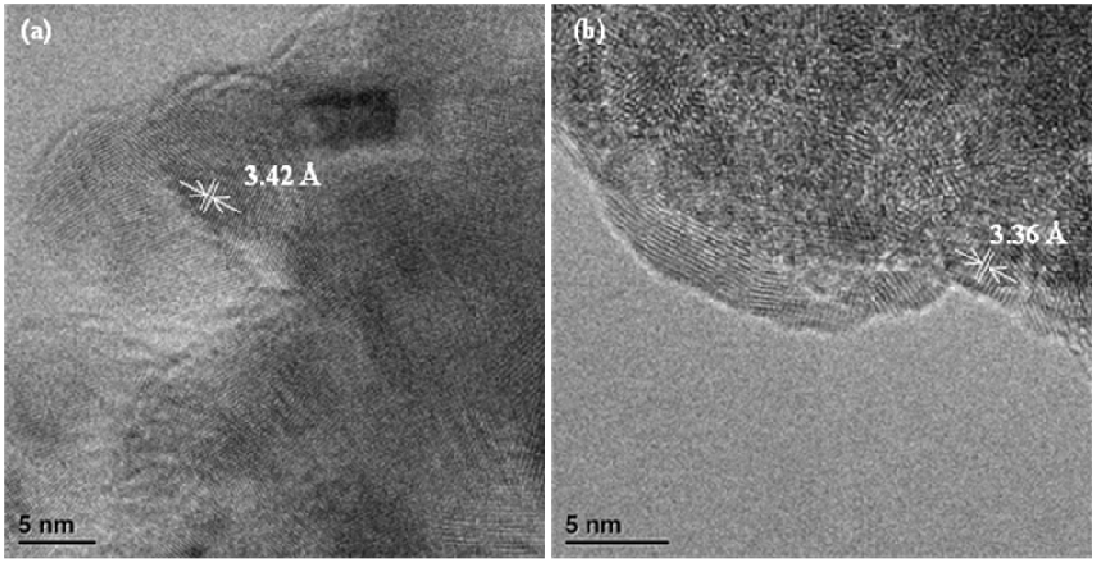

Figure 2.22 HR-TEM images of cysteine capped ZnSe nanoparticles synthesized at (a) pH 7 and (b) pH 11.

The crystallinity of the particles was further confirmed by the powder XRD technique. From the XRD pattern (Figure 2.23), three distinct peaks can be observed. The first peak at $2\theta = 26.4^{o}$ is due to the (111) reflection and the two broad peaks appearing at $2\theta = 43.2^{o}$ and 50.2^{o} result from the (220) and (311) reflections, respectively, and therefore the pattern can be indexed to cubic ZnSe.

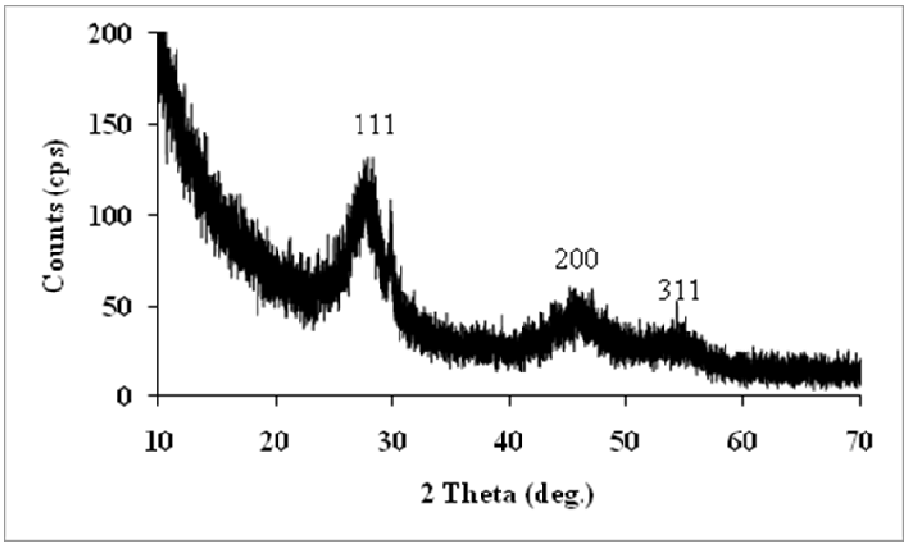

Figure 2.23 XRD pattern of cysteine capped ZnSe nanoparticles synthesized from the zinc chloride source at a room temperature reaction at pH 7.

FT-IR spectroscopy was used to investigate the surface morphology of the nanoparticles in order to confirm the capping of the ZnSe nanoparticles by cysteine. Usually, amino acids exist as zwitterions (internal salts) and exhibit typical spectra of both carboxylate and primary amine salts. Amino acids of this type show NH^{3+} stretch (very broad), N-H bend (asymmetric/symmetric) and COO^{-} (carboxylate ion) stretch (asymmetric/symmetric) as characteristic vibrations [50].

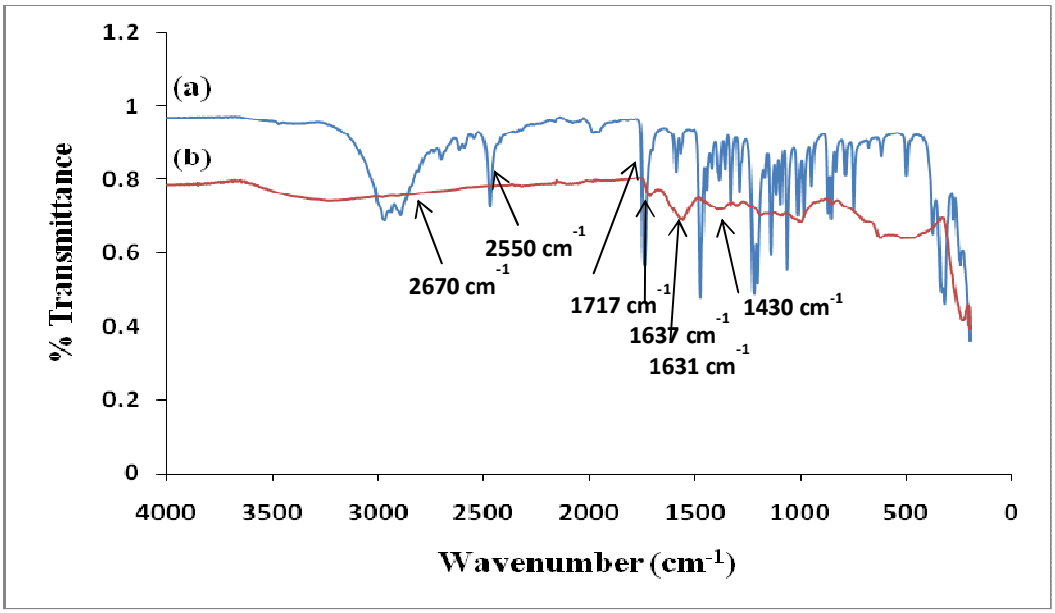

Figure 2.24 FT-IR spectra of (a) cysteine and (b) cysteine capped ZnSe nanoparticles synthesized using zinc chloride at pH 7.

The FT-IR absorption observed around 1637 and 1430 cm^{-1} indicates the presence of the $-COO^-$ group (Figure 2.24). The evidence for the de-protonation of S-H group vibration at 2550-2670 cm^{-1}would tend to suggest that the interaction of cysteine with the ZnSe is most probably electrostatic rather than covalent; i.e. the surface of ZnSe probably carries a net positive charge. The shift of the carboxylic group stretching frequency from 1717 cm^{-1} to 1631 cm^{-1} could be due to the change of dipole moment caused by binding of cysteine with high electron density metal surface [44]. These results confirm the presence of typical amino acid.

2.2.4 TEA capped ZnSe nanoparticles

Water soluble triethanolamine (TEA) capped ZnSe were synthesized under similar reaction conditions to the csyteine capped nanoparticles.

2.2.4.1 Optical properties of TEA capped ZnSe nanoparticles: Effect of pH

The optical properties of TEA capped ZnSe nanoparticles were studied at different pH values (4, 7 and 11). The absorption and the photoluminescence spectra of an aqueous solution of TEA capped ZnSe nanoparticles at different pH are shown in Figure 2.25. With an exception of the synthesis carried at pH 4 (Figure 2.25a-i), the particles showed clearly defined absorption peaks at 415 nm (pH 7, Figure 2.25a-ii) and at 409 nm (pH 11, Figure 2.25a-iii).

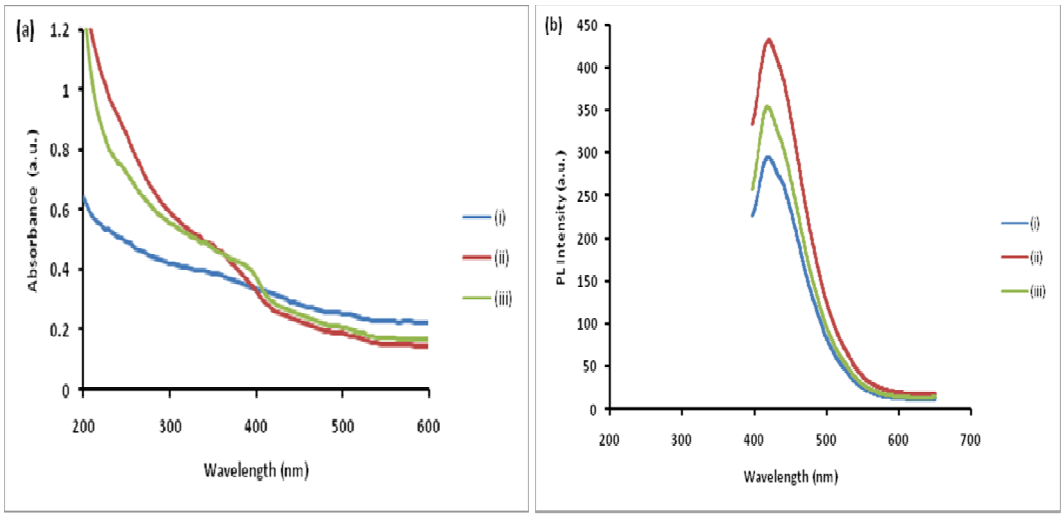

Figure 2.25 (a) Absorption and (b) photoluminescence spectra of TEA capped ZnSe nanoparticles synthesized at (i) pH 4, (ii) pH 7 and (ii) pH 11 using $ZnCl_2$ source.

The absorption band gap obtained using a direct band gap method is 500 nm (2.48 eV) for ZnSe nanoparticles synthesized at pH 4 (Figure 2.25a-i). For the particles synthesized at pH 7, the band gap is at 470 nm (Figure 2.25a-ii) and 460 nm for the reaction at pH 11 (Figure 2.25a-iii). The absorption spectra indicate clearly that the absorption peaks shifted to higher energies as the pH of the solution was increased from 4 to 11. The as-synthesized ZnSe

nanoparticles photoluminescence spectra are as shown in Figure 2.25b. The emission maximum is at approximately 420 nm.

2.2.4.2 Structural properties of TEA capped ZnSe nanoparticles: Effect of pH

The TEM images synthesized at different pH (4, 7 and 11) are shown in Figure 2.26. All the images show well defined particles within the matrix of the capping group. The particles synthesized at pH 4, had the average size of the particles of 6.37 ± 0.88 nm (Figure 2.26a). As the pH of the solution was increased from 4 to 11, the average particle size decreased. When the pH was 7, the average size of the particles was 5.10 ± 0.58 nm (Figure 2.26b), whereas pH 11 (Figure 2.26c) resulted an average particle size of 4.88 ± 0.22 nm. It is clear from the images that the morphology and shape of the particles is pH dependent, in which the acidic medium yielded larger particles while the basic medium produced smaller particles.

The particles of similar sizes have been previously reported by Jiao *et al.* [51]. The crystallinity of the particles was confirmed with HR-TEM images shown in Figure 2.26, and the images show the particles with distinct lattice fringes. The particles are surrounded by the triethanolamine matrix. The lattice spacing of 3.44 Å visible in all images can be indexed to the (111) plane of a cubic phase ZnSe nanoparticles.

The crystallinity of the particles was confirmed by XRD. From the XRD pattern (Figure 2.27), three distinct peaks can be observed. The first peak at $2\theta = 26.4^{o}$ is due to the (111) reflection and the two broad peaks appearing at $2\theta = 43.2^{o}$ and 50.2^{o} results from the (220) and (311) reflections, respectively. The peaks can be assigned to the cubic phase of ZnSe.

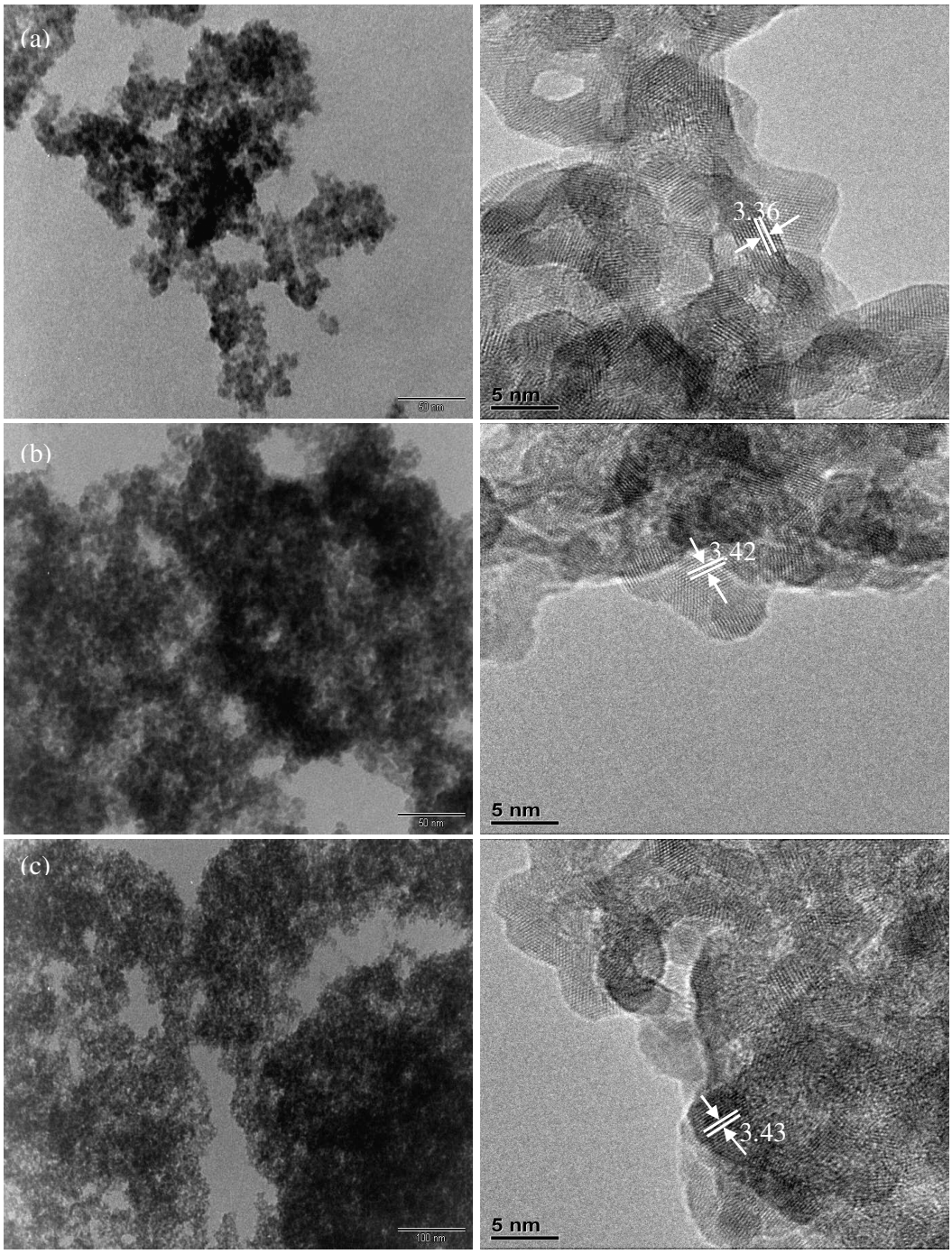

Figure 2.26 TEM images of TEA capped ZnSe nanoparticle and their corresponding HR-TEM images synthesized at pH (a) 4 (b) 7 and (c) 11.

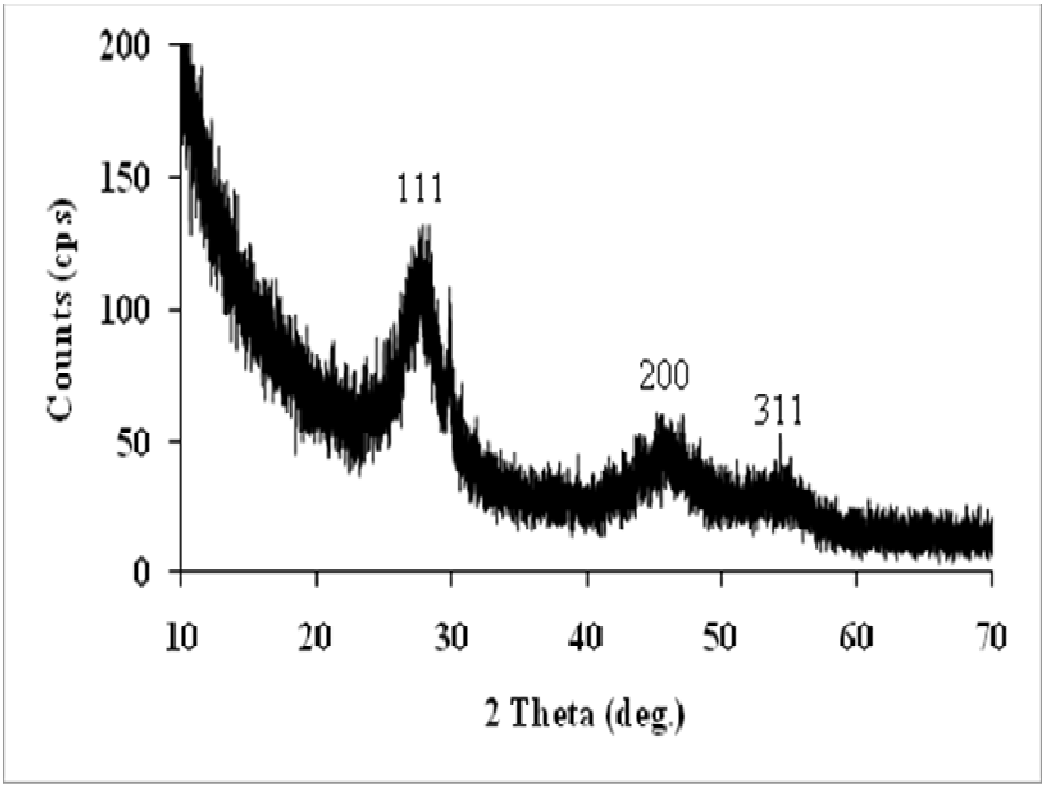

Figure 2.27 XRD pattern of TEA capped ZnSe nanoparticles synthesized with zinc chloride source at a room temperature reaction at pH 7.

The surface morphology of the nanoparticles was studied using FT-IR spectroscopy. The FT-IR spectra of TEA capped ZnSe are shown in Figure 2.28 indicating the presence of TEA capped ZnSe nanoparticles. The strong band at 3308 cm^{-1} corresponds to O-H group vibrations. Usually, the C-N stretching and the C-H bonding vibrations appear in the range of 1000-1180 cm^{-1} and 1400-1300 cm^{-1}, respectively [52].

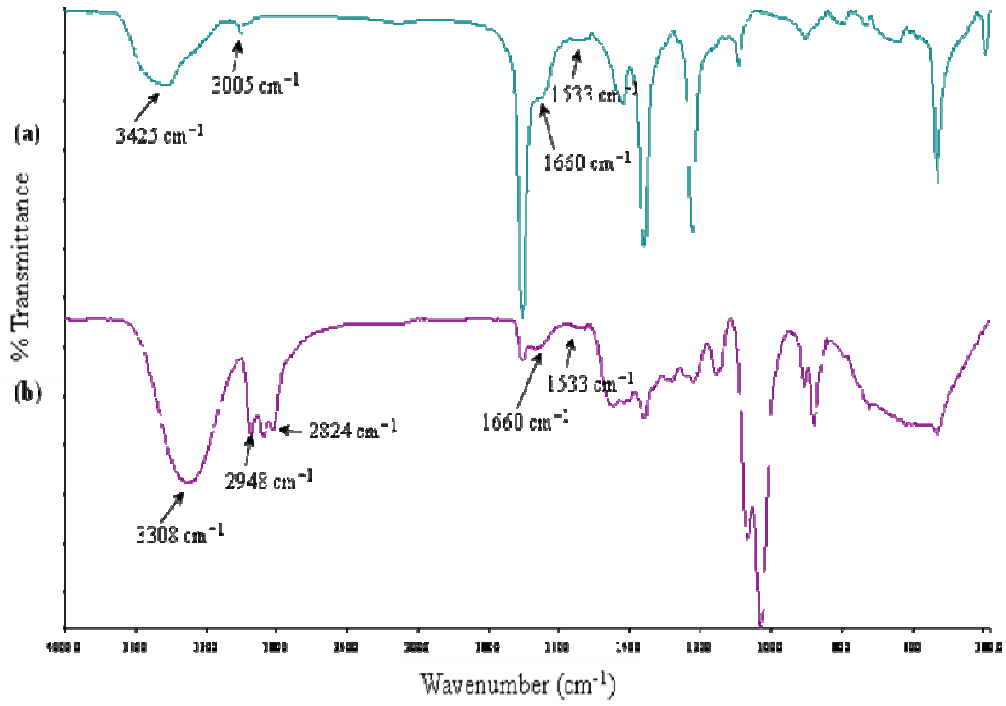

Figure 2.28 FT-IR spectra of (a) TEA and (b) TEA capped ZnSe nanoparticles.

In this current work, the C-N stretching appears at 1092 cm^{-1} and the C-H bonding vibrations appear at 1379 cm^{-1}. The band at 1590 cm^{-1} could be due to the N-H bending. The existence of the major functional groups of TEA confirms the effective bonding of the TEA molecules with the vacancy shell of Zn^{2+} in ZnSe nanostructures.

2.3 Conclusion

CdSe and ZnSe nanoparticles have been synthesized in two water soluble capping groups, cysteine and triethanolamine (TEA). The method employed is a simple one pot synthesis which involves the addition of the metal salt and capping group to a freshly prepared solution of reduced selenium. The effect of the reaction parameters such as pH, reaction time, concentration, reactant ratio and temperature on the optical properties and morphology of cysteine and TEA capped CdSe and ZnSe nanoparticles was investigated. The cysteine capped CdSe nanoparticles showed blue shifted absorption spectra for the reactions carried out at pH 4, 7 and 11. There was a slight shift in the absorption band gap to higher energy with increase in pH. Distinct excitonic peaks were visible in the absorption spectra. There were no differences in the position and shape of the emission maxima at the various pH. The pH of the reaction did not have a profound effect on the particle morphology. The particles were spherical in shape ranging in sizes from 5-8 nm. Aliquots of samples were drawn for the reaction at pH 11 to monitor the growth with reaction time. The optical absorption band gap was shifted to lower energies as the reaction time increases from 1 to 18 h. The effect of the cadmium source was investigated by using cadmium carbonate as an alternate cadmium source. Aggregated particles were observed in TEM image when the carbonate source was used. The XRD pattern confirmed the cubic phase of CdSe. The HR-TEM images showed well defined particles with distinct lattice fringes.

The effect of the Cd:Se ratio (1:1; 1:4; 1:6; 4:1) was studied in the synthesis of the TEA capped CdSe nanoparticles. The variation in mole ratio seemed to have no effect on the optical properties. The TEM images also confirmed this whereby speherical particles were obtained at all ratios. The XRD study confirmed the presence of cubic CdSe.

The cysteine capped ZnSe nanoparticles were also synthesized at different pH. There was not much difference in the position of the band gap however the sample synthesized at pH 11 showed a more pronounced excitonic peak. The TEM images showed that the particles syntehsized at pH 7 had regular morphology with the appearance of close to spherical particles. The particles synthesized at pH 11 were large clusters or microspheres. The zinc carbonate source produced agglomerated particles whose size was difficult to determine. The XRD pattern was indexed to the cubic phase. The TEA capped ZnSe were also synthesized at pH of 4,7 and 11. The sample at pH 4 did not show a clearly defined absorption peak. The TEM images show spherical nanoparticles in the 4-6 nm size range, surrounded by the capping matrix. The HR-TEM images show particles with distinct lattice fringes.

2.4 References

[1] Y. Mao, T. Park, F. Zhang, H. Zhou, S.S. Wong, Small 3 **(2007)** 1122.

[2] O.S. Oluwafemi, O.O. Ayedemi, Materials Letters 64 **(2010)** 2310.

[3] J.H. Lie, C.L. Ren, X.Y. Liu, Z.D. Hu, D.S. Xue, Materials Science and Engineeering A 458 **(2007)** 319.

[4] Q.L. Wei, S.Z. Kang, J. Mu, Colloidal Surface A 247 **(2004)** 125.

[5] C.J. Murphy, Journal of Materials Chemistry **(2008)** 2173.

[6] J.A. Dahi, B.L.S. Maddux, J.E. Hutchison, Chemistry Reviews **(2007)** 2228.

[7] H. Sengul, T.L. Theis, Journal of Cleaner Production xxx **(2010)** 1.

[8] P.A. Chate, P.P. Hankare, D.J. Sathe, Journal of Alloys and Compounds 505 **(2010)** 140.

[9] H. Han, P. Ju, S. Ai, Sensors and Actuators B 149 **(2010)** 98.

[10] B. Mishra, B.B. Patel, S. Tiwari, Nanomedicine: Nanotechnology, Biology and Medicine 6 **(2010)** 9.

[11] Z.B. Shang, Y. Wang, W.J. Jin, Talanta 78 **(2009)** 364.

[12] J. Chen, Y. Gao, C. Guo, G. Wu, Y. Chen, B. Lin, Spectrochimica Acta Part A 69 **(2008)** 572.

[13] K.W. Boer, Energy Conversion and Management xxx **(2010)** xxx-xxx or article in press.

[14] T. Mthethwa, V.S.R.R. Pullabhotla, P.S. Mdluli, J. Wesley-Smith, N. Revaprasadu, Polyhedron 28 **(2009)** 2977.

[15] B. Ludolph, M.A. Malik, P. O'Brien, N. Revaprasadu, Chemical Communications **(1998)** 1849.

[16] G. Kedarnath, S. Dey, V.K. Jain, G.K. Dey, B. Varghese, Polyhedron 25 **(2006)** 2383.

[17] Y. Xia, C. Zhu, Materials Letters 62 **(2008)** 2103.

[18] S.O. Oluwafemi, N. Revaprasadu, A.J. Ramirez, Journal of Crystal Growth 310 **(2008)** 3230.

[19] Y. Gao, Q. Zhang, Q. Gao, Y. Tian, W. Zhou, L. Zheng, S. Zheng, Materials Chemistry and Physics 115 **(2009)** 724.

[20] C. Sheng, X. Zhang, H. Li, Materials Science and Engineering B 84 **(2001)** 265.

[21] C.D. Lokhande, E. Lee, K. Jung, O. Joo, Materials Chemistry and Physics 91 **(2005)** 200.

[22] M. Kristl, I. Ban, A. Danc, V. Danc, M. Drofenic, Ultrasonics Sonochemistry 17 **(2010)** 916.

[23] A.A. Yadav, M.A. Barote, E.U. Masumdar, Materials Chemistry and Physics 121 **(2010)** 53.

[24] T.S. Shyju, S. Anandhi, R. Indirajith, R. Gopalakrishnan, Journal of Alloys and Compounds 506 **(2010)** 892.

[25] B. Pejova, A. Tanusevski, I. Grozdanov, Journal of Solid State Chemistry 172 **(2003)** 381.

[26] C.B. Murray, D.J. Norris, M.G. Bawendi, Journal of American Chemical Society 115 (**1993)** 8706.

[27] Z.A. Qu, X.U. Peng, Peng, Journal of Nanotechnology 1 **(2001)** 333.

[28] Z.A. Peng, X.G. Peng, Journal of American Chemical Society 124 **(2002)** 3343.

[29] C. Zhou, H. Shen , Y. Guo , L. Xud, J. Niu, Z. Zhang , Z. Du ,J. Chen, L.S. Li, Journal of Colloidal and Interface Science 344 **(2010)** 279.

[30] J. Ge, Y. Li, G. Yang, Chemical Communication 17 **(2002)** 1826.

[31] H. Han , Z. Sheng, J. Liang, Materials Letters 60 **(2006)** 3782.

[32] M.A. Haase, J. Qiu, J.M. DePuydt, H. Cheng, Applied Physics Letters 59 **(1991)** 1272.

[33] J. Wang, D.C. Hutchings, A. Miller, E.W. Vanstryland, K.R. Welford, I.T. Murhead, K.L. Lewis, Journal of Applied Physics 73 **(1993)** 4746.

[34] M. Kazes, D.Y. Lewis, Y. Ebenstein, T. Mokari, U. Banin, Advanced Materials 14 **(2002)** 317.

[35] N. Kouklin, L. Menon, A.Z. Wong, D.W. Thompson, J.A. Woollam, P.F. Williams, Applied Physics Letters 79 **(2001)** 4423.

[36] C.C. Kim, S. Sivananthan, Physics Reviews B 53 **(1996)** 1475.

[37] G.F. Neumark, R.M. Park, J.M. Depuydt, Physics Today 47 **(1994)** 26.

[38] W. Yan, C. Hu, Y. Xi, B. Wan, X. He, M. Zhang, Y. Zhang, Materials Research Bulletin 44 **(2009)** 1205.

[39] M. Shakir, S.K. Kushwaha, K.K. Maurya, G. Bhagavannarayana, M.A. Wahab, Solid State Communications 149 **(2009)** 2047.

[40] J. Archana, M. Navaneethan, S. Ponnusamy, Y. Hayakawa, C. Muthamizhchelvan, Materials Letters 63 **(2009)** 1931.

[41] L. Huang, H. Han, Materials Letters 64 **(2010)** 1099.

[42] S.O. Oluwafeni, N. Revaprasadu, Physica B 404 **(2009)** 1204.

[43] N.N. Dlamini, Rajasekharp V.S.R Pullabotla, N. Revaprasadu, Materials Letters 65 **(2011)** 1283.

[44] A. Santosh, B.K.C. Remant, N. Dharmaraj, N. Battarai, C.H. Kim, H.Y. Kim, Spectrochimica Acta Part A 63 **(2006)** 160.

[45] K.J.E. Bowen, V.L. Colvin, A.P. Alivisatos, Journal Physical Chemistry 98 **(1994)** 4109.

[46] M. El-Kemary, H. El-Shamy, M.M. Mosaad, Materials Chemistry and Physics 118 **(2009)** 81.

[47] X.M. Lin, C.M. Sorensen, K.J. Klabunde, Journal of Nanoparticle Research 2 **(2000)** 157.

[48] M.K. Naskar, Journal of Colloid and Interface Science 297 **(2006)** 271.

[49] S.H. Tolbert, A.B. Herhold, C.S. Johnson, A.P. Alivisatos, Physics Review Letters 73 (**1994)** 3266.

[50] D.L. Pavia, G.M. Lampman, G.S. Kriz, Introduction to Spectroscopy, third ed, USA, **2001**.

[51] J. Jiao, D. Yu, Z. Wang, K. Tang, X. Sun, Materials Letters 61 **(2007)** 1541.

[52] M.K. Naskar, A. Patra, M. Chatterjee, Journal of Colloidal Interface Science 297 **(2006)** 271.

Chapter 3

Synthesis of HDA capped ZnSe nanoparticles

3.0 Introduction

The natural toxicity of cadmium may limit the use of cadmium based nanoparticles in *in-vivo* applications, therefore there is a search for substituting cadmium with less toxic labeling materials. There are many drawbacks caused by the high toxicity of Cd^{2+} ions in biological applications which can easily be released in aqueous solutions. Due to these drawbacks, there had been many reports of the use of doped and undoped ZnSe nanoparticles in the place of cadmium. In addition, ZnSe nanoparticles have a wide band gap (E_g = 2.7 eV) which is not observed in other II-IV semiconducting materials and they also show potential applications in short wavelength electrochemical devices. These devices include blue laser diodes [1-3], photodetectors, light emitting diodes [4], high density optical storage [5], full color displays and biomedical labeling and sensors [6]. ZnSe has also recently been found to be a sensitive-type humidity sensor based on a one dimensional ZnSe nanostructure [7].

There have been many reports for the synthesis of ZnSe nanoparticles. Revaprasadu *et al*. [8] reported the synthesis of well defined, isolated tri-n-octylphosphine oxide capped ZnSe nanoparticles using the single source molecular precursor method. Gong *et al*. [9] used a hydrothermal method to synthesize ZnSe powders. The particles synthesized were of good quality. However, the long soaking period in the autoclave made the Gong's [9] method not as cost effective with regards to energy consumption. Other methods that have been developed to synthesize ZnSe nanoparticles include the chemical bath deposition [10], molecular beam epitaxy deposition [11], low temperature synthesis [12,13], molecular precursor deposition [14], microwave irradiation [15], reverse micelles soft templates [16], hydrothermal synthesis [17] and chemical vapor deposition method [18].

In this study we report the synthesis of organically capped ZnSe nanoparticles. The synthetic route used in this study is an adaptation of the previously reported procedure by the Revaprasadu group for cadmium based chalcogenides nanoparticles [19,20]. The effect of the reaction time, temperature and the metal sources on the morphological and optical properties of ZnSe nanoparticles is being investigated. Hexadecylamine (HDA), zinc chloride and zinc carbonate have been chosen as capping agent and sources respectively.

3.1 Experimental

3.1.1 Materials and reagents

Zinc chloride ($ZnCl_2$), zinc carbonate ($ZnCO_3$), sodium borohydride ($NaBH_4$), de-ionized water (HPLC grade), trioctylphosphine (TOP) and hexadecylamine (HDA) were purchased from Aldrich and the selenium powder from Merck. All the chemicals were of analytical grade and used as purchased.

3.1.2 Synthesis of HDA capped ZnSe nanoparticles

HDA capped ZnSe nanoparticles were synthesized by modifying the method by Oluwafemi and Revaprasadu [21,22]. Briefly, in a typical room temperature reaction, selenium (Se) powder (0.32 mmol) was mixed with deionised water in a three necked flask. Sodium borohydride ($NaBH_4$) solution (0.81 mmol) was added into this mixture which dissolves suddenly, and the flask instantly purged with nitrogen gas to create an inert atmosphere. After 2 h of Se digestion, a clear colourless solution represents the complete reduction of selenium powder. The zinc salt dissolved in de-ionized water (1:1-Zn:Se) was added to the reduced selenium solution and the mixture was allowed to react for about 30 min. under stirring. The bulk ZnSe formed was then

flocculated with methanol, centrifuged and dispersed in TOP. The resulting mixture was then injected into a hot coordinating solvent (HDA). The synthesis was carried at different temperatures (190, 230 and 270 ^{o}C). In each reaction temperature, the aliquots were withdrawn at different reaction times, flocculated with methanol, centrifuged and re-dispersed in toluene for further analysis. The reactions were studied at different reaction times (5, 15, 30 min., 1 and 2 h) and temperatures.

3.1.3 Characterization

The as synthesized particles were characterized by UV-Vis and photoluminescence spectroscopy, Powder X-ray diffraction (XRD), TEM and HRTEM techniques as described in the previous chapter (Section 2.1.3, Page no. 43-44).

3.2 Results and discussion

3.2.1 Optical properties of HDA capped ZnSe nanoparticles: Effect of reaction time and temperature

The absorption spectra (Figure 3.1a) of the nanoparticles synthesized at 190 ^{o}C after 30 min. reaction time show the absorption edge (410 nm) shifted to higher energies compared to the bulk band gap of ZnSe (460 nm). The photoluminescence spectra (Figure 3.1b) shows a narrow emission curve with emission maxima at 424 nm.

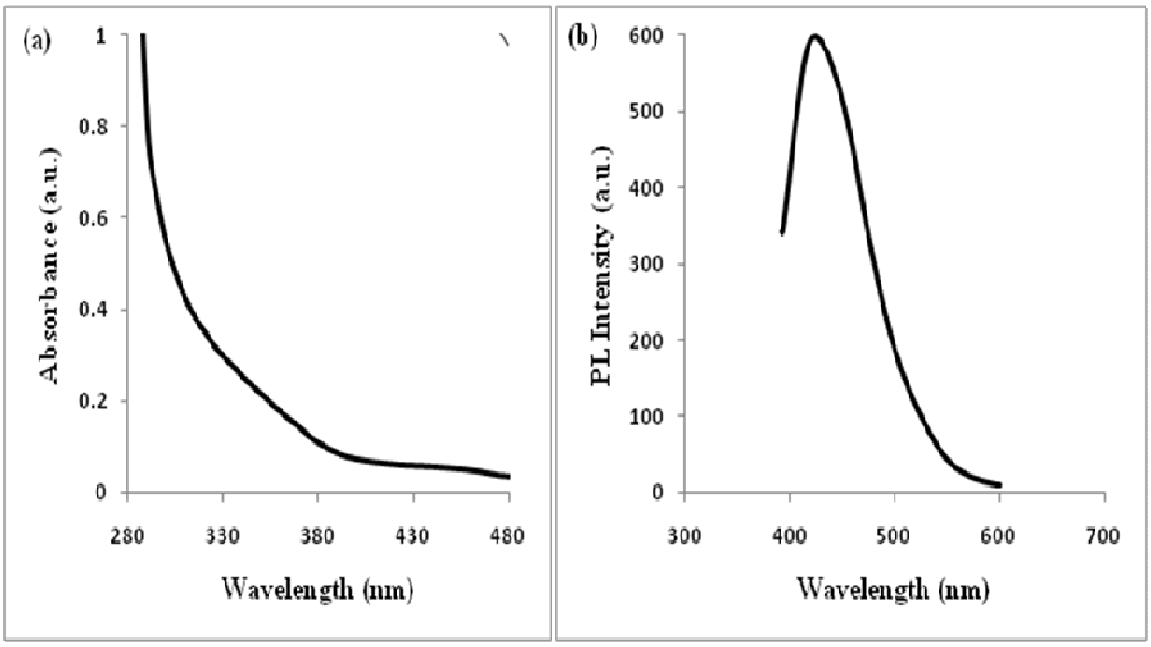

Figure 3.1 (a) Absorption and (b) Photoluminescence spectra of HDA capped ZnSe nanoparticles synthesized at 190 ^{o}C after 30 min. reaction time.

The absorption and photoluminescence spectra of HDA capped ZnSe nanoparticles synthesized at 230 ^{o}C after various reaction times are shown in Figure 3.2. The absorption band edge is far blue shifted indicating strong quantum confinement. The optical absorption band gap of 390 nm was observed for 5 and 15 min. reactions. Whereas, the reactions carried for 30 min. and 1 h resulted in the band gap of 385 nm. There is a distinct absorption shoulder for all samples. In comparison to the report by Revaprasadu *et al.* [8], the as-synthesized ZnSe nanoparticles showed strong quantum confinement confirmed by relatively large shift of the band gaps to higher energies and exceptionally narrow band edge emission appearing at approximately 420 nm. The noticeable shift of the band gaps to higher energies as the reaction time increases is associated with a decrease in particle size.

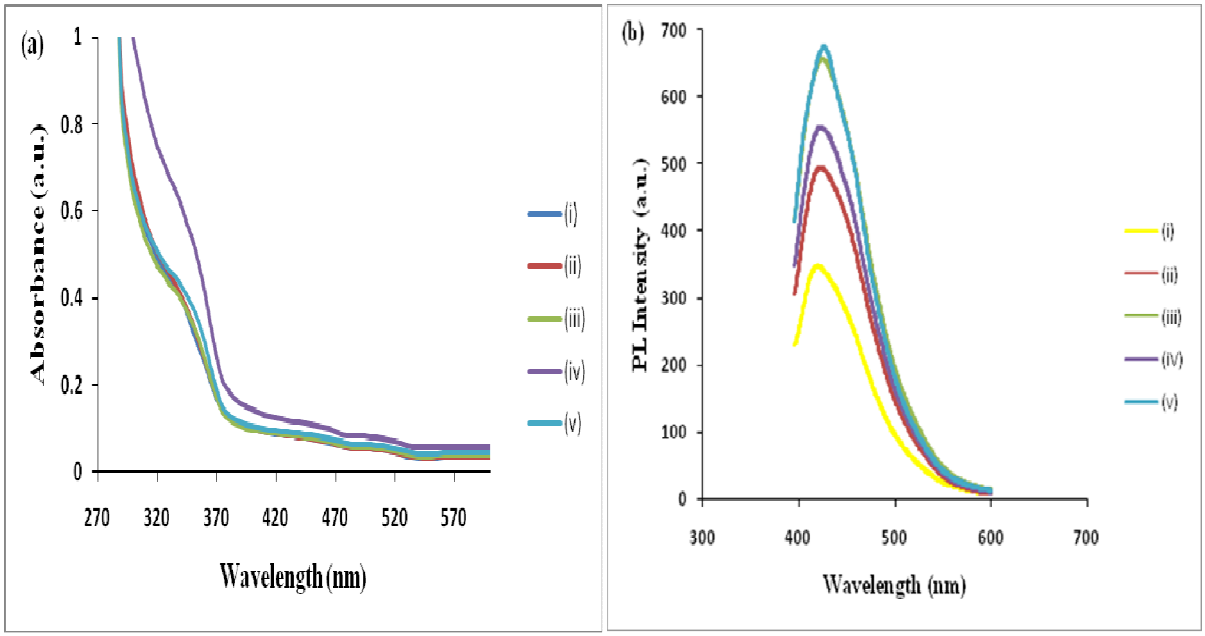

Figure 3.2 (a) Absorption and (b) photoluminescence spectra of HDA capped ZnSe nanoparticles for (i) 5 (ii) 15 (iii) 30 min. (iv) 1 and (v) 2 h reaction time synthesized at 230 ^{o}C.

The optical studies of a reaction carried at 270 ^{o}C were also investigated. The absorption band gap was observed at 400 nm (Figure 3.3a). The emission maximum was observed at 425 nm (Figure 3.3b). The exceptionally narrow emission spectrum is due to HAD which suppresses the growth rate and the particle size when used as capping group, and it also improves the quantum efficiency by effectively passivating the surface defects [24,25].

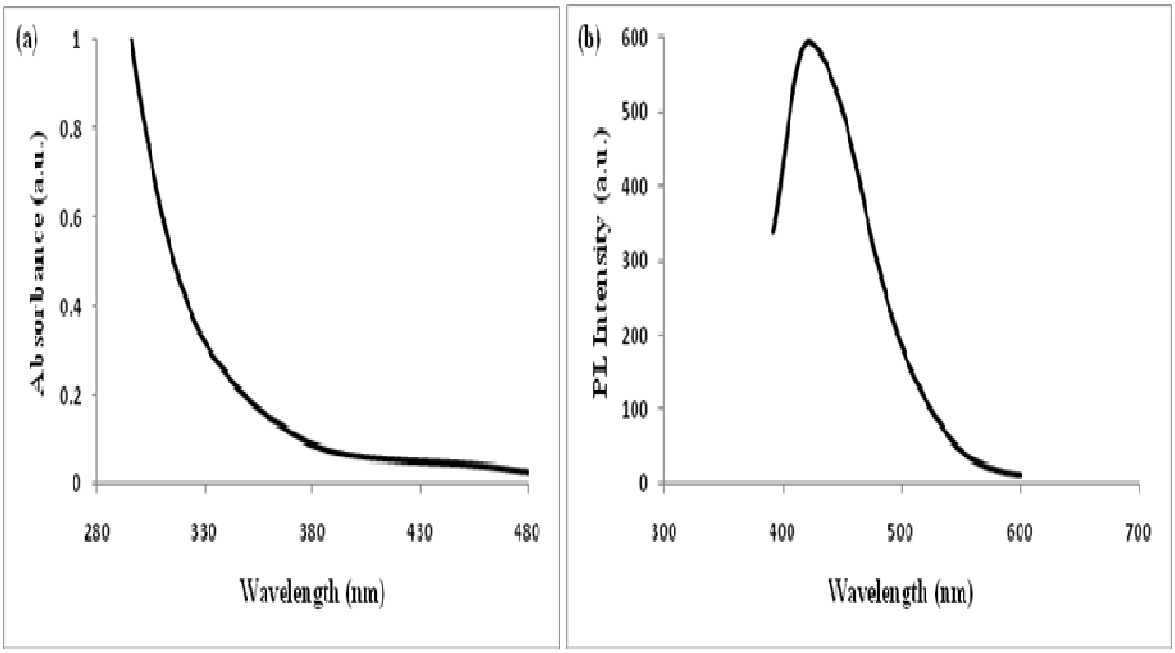

Figure 3.3 (a) Absorption and (b) photoluminescence spectra of HDA capped ZnSe nanoparticles synthesized at 270 ºC after 30 min. reaction time.

3.2.2 Structural properties of HDA capped ZnSe nanoparticles

The XRD pattern of the HDA capped ZnSe nanoparticles synthesized at 230 ^{o}C is shown in Figure 3.4. The pattern can be assigned to the hexagonal phase of ZnSe with the (100), (002), (110), (103) and (112) planes of the wurtzite being clearly observed. The broadening of the diffraction peaks confirms the nanocrystalline nature of the particles. The stronger and narrow peak for (002) planes show that the nanoparticles are elongated along the c-axis.

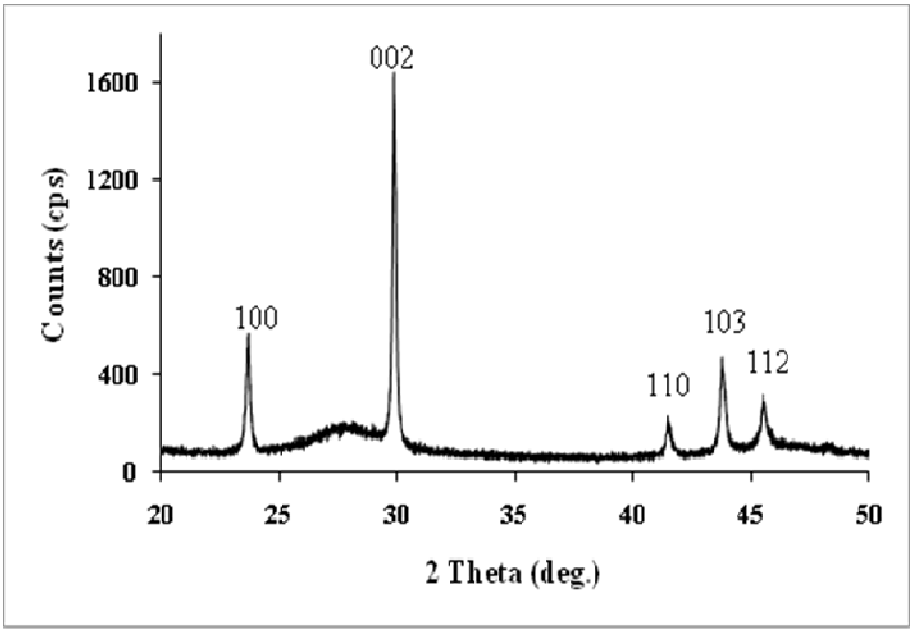

Figure 3.4 XRD pattern of HDA capped ZnSe nanoparticles synthesized at 230 ^{o}C.

The effect of the reaction time on the morphological properties of ZnSe nanoparticles was studied using the reaction synthesized at 230 ^{o}C. Figure 3.4 shows the TEM images of HDA capped ZnSe nanoparticles after 1 h (Figure 3.5a) and 2 h (Figure 3.5b) reaction time. The average particle size of the HDA capped ZnSe nanoparticles for the 1 h reaction was 7.73 ± 2.22 nm (Figure 3.5a), while that of 2 h reaction was 7.17 ± 1.70 nm (Figure 3.5b). This observation shows that as the thermolysis reaction time increases, the average particle size of the nanoparticles becomes smaller.

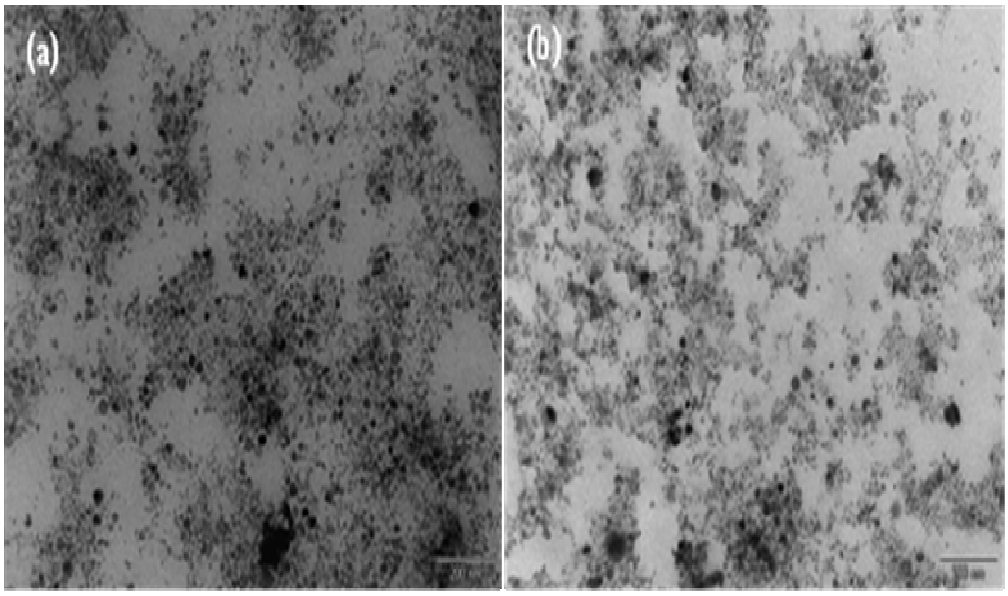

Figure 3.5 TEM images of HDA capped ZnSe nanoparticles synthesized at 230 ^{o}C after (a) 1 and (b) 2 h reaction times.

The effect of the reaction temperature was also studied using transmission electron microscopy. This was done by fixing the reaction time at 1 h and varying the temperature from 190, 230 and 270 ^{o}C. The TEM images of HDA capped ZnSe nanoparticles synthesized at different temperatures are shown in Figure 3.6. ZnSe nanoparticles synthesized at 190 ^{o}C (Figure 3.6a) were nearly spherical in shape but the size could not be estimated. The nanoparticles synthesized at 230 ^{o}C (Figure 3.6b) are well defined, reasonably monodispersed and spherical in shape. This is in good agreement with absorption spectra which showed distinct excitonic peaks with band gaps shifted to higher energies. This reaction temperature resulted in average particle size of 7.73 ± 0.09 nm. The synthesis carried out at 270 ^{o}C resulted in spherical, highly monodispersed particles with an average particle size of 7.14 ± 0.01 nm.

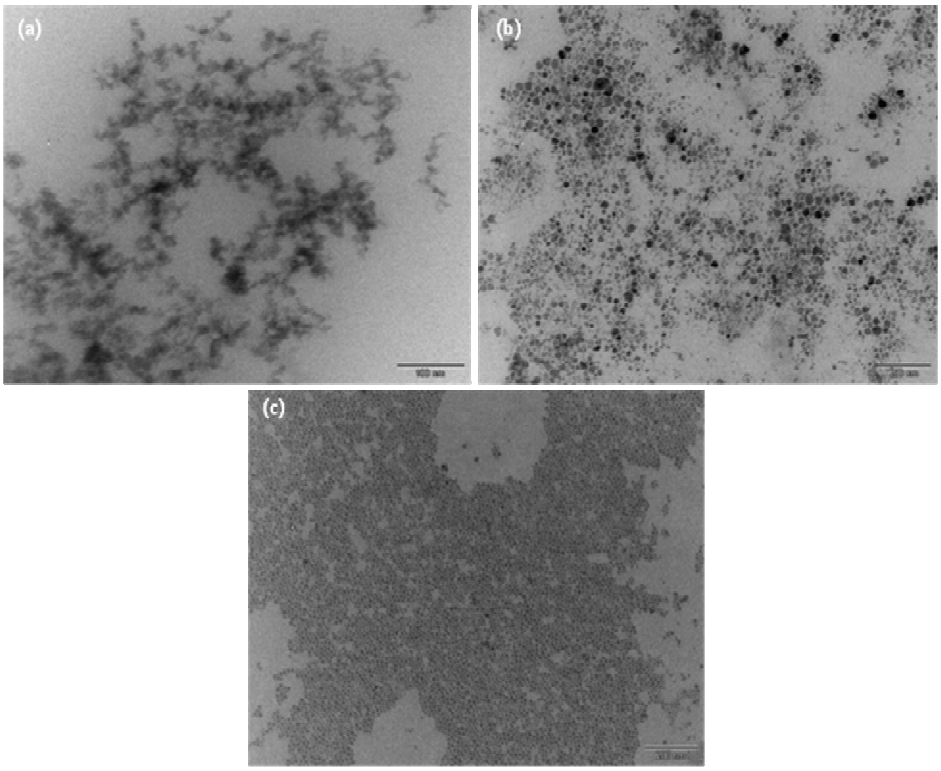

Figure 3.6 TEM images of HDA capped ZnSe nanoparticles synthesized at (a) 190 (b) 230 and (b) 270 ^{o}C after 1h reaction time.

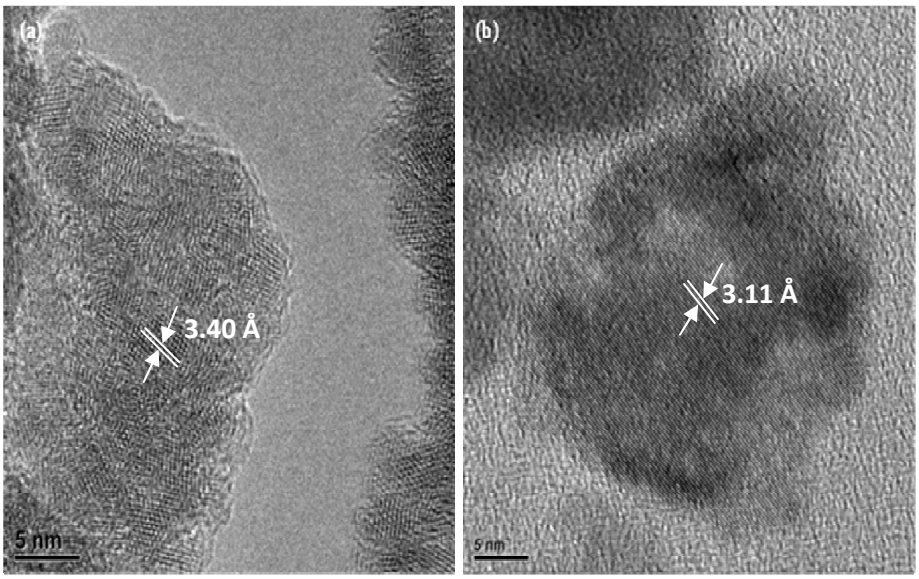

Figure 3.7 HR-TEM images of HDA capped ZnSe nanoparticles synthesized at (a) 190 and (b) 230 ^{o}C after 1 h reaction time.

The crystallinity of the as-synthesized HDA capped ZnSe nanoparticles was confirmed by HR-TEM. The HR-TEM images are shown in Figure 3.7. The images reveal that the particles are well defined, crystalline with clearly visible lattice fringes.

The use of different metal sources plays an important role in the final morphology of the nanoparticles. In order to investigate this effect, zinc carbonate was used as an alternate zinc source at 230 ^{o}C. The TEM images of HDA capped ZnSe nanoparticles synthesized from the carbonate and chloride sources are shown in Figure 3.8a and Figure 3.8b respectively.

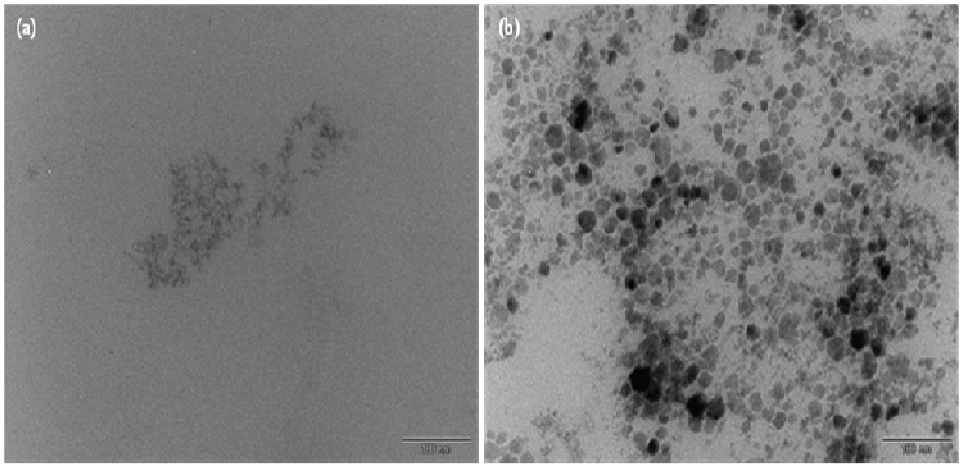

Figure 3.8 TEM images of HDA capped ZnSe nanoparticles synthesized at 230 ^{o}C using (a) zinc carbonate and (b) zinc chloride.

The nanoparticles synthesized with $ZnCO_3$ source were aggregated and not well defined. The chloride source produced monodispersed ZnSe nanoparticles which are spherical in shape with an average diameter of 7.73 ± 2.22 nm.

3.3 Conclusion

Hexadecylamine (HDA) capped ZnSe nanoparticles have been synthesized by a non-organometallic route. The effect of reaction time, temperature and zinc source on the optical and morphological properties of the ZnSe particles was studied. The particles synthesized at all reaction temperatures (190, 230 and 270 ºC) displayed absorption band edges which were blue shifted from the bulk ZnSe. The effect of the reaction time was investigated for thereaction at 230 ºC. There was an increase in the band gap as the reaction proceeded with time, an indication of the increase in particle size. The emission spectra of the as-synthesized HDA capped ZnSe nanoparticles at all reaction conditions show close to band gap emission. The XRD studies confirm the presence of hexagonal ZnSe. The TEM images of the particles synthesized at all temperatures show close to monodispersed particles with average particle size of *ca* 7.5 nm. The HRTEM images show crystalline particles with lattice fringes.

3.4 Future Work

This study describes the successful synthesis of water soluble cysteine capped and TEA capped ZnSe nanoparticles using a simple route. The results of the study has opened the way for further work on the use of these water soluble nanoparticles in applications such as biological imaging. The toxicity of the particles can also be studied and compared with other semiconductor materials such as CdSe and CdTe.

The work on the hexadecylamine capped ZnSe can also be extended. Other primary amines such as oleylamine, decylamine and dodecylamine can be used as capping groups.

3.5 References

[1] M.A. Haase, J. Qiu, J.M. DePuydt, H. Cheng, Applied Physics Letters 59 **(1991)** 1272.

[2] J. Wang, D.C. Hutchings, A. Miller, E.W. Vanstryland, K.R. Welford, I.T. Murhead, K.L. Lewis, Journal of Applied Physics 73 **(1993)** 4746.

[3] G.F. Neumark, R.M. Park, J.M. Depuydt, Physics Today 47 **(1994)** 26.

[4] N. Kouklin, L. Menon, A.Z. Wong, D.W. Thompson, J.A. Woollam, P.F. Williams, Applied Physics Letters 79 **(2001)** 4423.

[5] C.C. Kim, S. Sivananthan, Physics Reviews B 53 **(1996)** 1475.

[6] M. Kazes, D.Y. Lewis, Y. Ebenstein, T. Mokari, U. Banin, Advanced Materials 14 **(2002)** 317.

[7] W. Yan, C. Hu, Y. Xi, B. Wan, X. He, M. Zhang, Y. Zhang, Materials Research Bulletin 44 **(2009)** 1205.

[8] N. Revaprasadu, M.A. Malik, P. O'Brien, M.M. Zulu, G. Wakefield, Journal of Materials Chemistry 8 **(1998)** 1885.

[9] H. Gong, H. Haung, L. Ding, M. Wang, K. Liu, Journal of Crystal Growth 288 **(2006)** 96.

[10] R.B. Kale, C.B. Lokhande, Applied Surface Sciences 252 **(2005)** 929.

[11] C. Haung, H. Weng, Y. Jiang, H. Ueng, Vacuum 83 **(2009)** 313-318.

[12] A.C. Deshpande, S.B. Singh, M.K. Abyaneh, R. Pasricha, S.K. Kulkarni, Materials Letters 62 **(2008)** 3803.

[13] C. Cheng, Y. Chen, Materials Chemistry and Physics 115 **(2009)** 158.

[14] M. Chen, L. Gao, Materials Chemistry and Physics 91 **(2005)** 437.

[15] L. Haung, H. Han, Materials Letters 64 **(2010)** 1099.

[16] L. Li, W. Qing-Sheng, D. Ya-Ping, W. Pei-Mng, Materials Letters 59 **(2005)** 1623.

[17] H. Gaong, H. Haung, M. Wang, K. Liu, Ceramics International 33 **(2007)** 1381.

[18] H. Li, W. Jie, Journal of Crystal Growth 257 **(2003)** 110.

[19] N.N. Maseko, N. Revaprasadu, V.S.R. Rajasekhar Pullabhotla, R. Karthik, P. O'Brien, Materials Letters 64 **(2010)** 1037.

[20] N. Mntungwa, V.S.R. Rajasekhar Pullabhotla, N. Revaprasadu, Materials Chemistry and Physics 126 **(2011)** 500.

[21] S.O. Oluwafeni, N. Revaprasadu, Journal of Physica B, 404 **(2009)** 1204.

[22] S.O. Oluwafeni, Journal of Colloidal and Surface B: Biointerfaces, 73 **(2009)** 382.

[23] J.I Pankove, Optical Processes in Semiconductors, Dover Publications, Incl., New York **1970**.

[24] L. Qu, X. Peng, Journal of American Chemical Society 124 **(2002)** 2049.

[25] D.V. Talapin, A.L. Ragoch, A. Kornowski, M. Haase, H. Weller, Nano Letters 1 **(2001)** 207.

[26] A.C. Rastogi, in Physics of Semiconductor devices, edited by V. Kumar, S.K. Agarwal Narosa Publishing house, **(1998)**, p. 56.

Chapter 4

Summary and conclusions

4.0 Summary and conclusions

The successful synthesis of water soluble CdSe and ZnSe nanoparticles is discussed in chapter two. The nanoparticles have been synthesized using cysteine and triethanolamine (TEA) as capping groups via one pot synthesis method, which involves the addition of the metal salt and capping group to a freshly prepared solution of reduced selenium.

The effect of the reaction parameters such as pH, reaction time, capping agent, reactant ratio, variation of Cd/Zn srouces and temperature on the optical properties and morphology of cysteine and TEA capped CdSe and ZnSe nanoparticles were investigated. The cysteine capped CdSe nanoparticles showed blue shifted absorption spectra for the reactions carried out at pH 4,7 and 11. There was a slight shift in the absorption band gap to higher energy with the increase in pH. Distinct excitonic peaks were visible in the absorption spectra. The emission and absorption spectra for the reactions carried at shorter reaction times were blue-shifted and the samples synthesized at longer reaction time (18 h) showed a slight red-shift. The as-synthesized particles were spherical in shape ranging in sizes from 5-8 nm. Cadmium carbonate salt as the cadmium source resulted in aggregated particles showed by TEM images. The cubic phase of CdSe was confirmed from the XRD pattern with well-defined particles and distinct lattice fringes with lattice spacing (111) was revealed by HR-TEM images. The variation of the Cd:Se ratio (1:1; 1:4; 1:6; 4:1) in the synthesis of the TEA capped CdSe nanoparticles didn't alter the optical and structural properties of the particles.

The cysteine capped ZnSe nanoparticles were also synthesized at different pH. The XRD pattern confirmed the cubic phase of ZnSe. The effect of pH variation on the TEA capped ZnSe

nanoparticles synthesised at pH 4 did not show a clearly defined absorption peak. The TEM images show spherical nanoparticles in the range of 4-6 nm, which are surrounded by the capping matrix and also the distinct lattice fringes were observed in the HR-TEM images. The TEM studies showed that the particles syntehsized at pH 7 had a regular morphology with the appearance of spheroidal particles. There was not much difference in the position of the band gap however the sample synthesized at pH 11 showed a more pronounced excitonic peak. The particles synthesized at pH 11 were large microsphere clusters.

Chapter three describes the synthesis of hexadecylamine (HDA) capped ZnSe nanoparticles via a non-organometallic route with variation in the reaction parameters such as reaction time, temperature and zinc source on the optical and morphological properties of the ZnSe particles. The particles showed blue shift in their absorption spectra for all reaction temperatures (190, 230 and 270 ºC) when compared with the bulk ZnSe. The effect of reaction time was also investigated for the reactions carried at 230 ^{o}C. The band gap was noticed to increase as the reaction time increases, indicating the increase in particle size. The absorption and emission spectra of the as-synthesized HDA capped ZnSe nanoparticles showed blue-shit at all reaction conditions. The XRD studies confirm the presence of hexagonal phase of the ZnSe nanoparticles. The TEM images of the particles synthesized at all temperatures show close to monodispersed particles with average particle size of *ca* 7.5 nm. The HRTEM images also confirm the crystallinity of the ZnSe nanoparticles with distinct lattice fringes.